

NAVAL POSTGRADUATE SCHOOL MONTEREY, CALIFORNIA



THESIS

CORRELATION OF EXPERIMENTAL AND FINITE ELEMENT MODAL ANALYSIS OF THE PHALANX M61A1 CLOSE-IN WEAPON SYSTEM

by

Carlos S. Guzman

John C. Gaffe

December, 1995

Thesis Advisor:

Steven R. Baker

Co-Advisor:

Michael R. Hatch

Approved for public release; distribution is unlimited.

DTIC QUALITY INSPECTED 1

19960401 056

REPORT DOCUMENTATION PAGE			Form Approved OMB No. 0704-0188	
Public reporting burden for this collection of information is estimated to average 1 hour per response, including the time for reviewing instruction, searching existing data sources, gathering and maintaining the data needed, and completing and reviewing the collection of information. Send comments regarding this burden estimate or any other aspect of this collection of information, including suggestions for reducing this burden, to Washington Headquarters Services, Directorate for Information Operations and Reports, 1215 Jefferson Davis Highway, Suite 1204, Arlington, VA 22202-4302, and to the Office of Management and Budget, Paperwork Reduction Project (0704-0188) Washington DC 20503.				
1. AGENCY USE ONLY (Leave blank)		2. REPORT DATE December 95		3. REPORT TYPE AND DATES COVERED Master's Thesis
4. TITLE AND SUBTITLE CORRELATION OF EXPERIMENTAL AND FINITE ELEMENT MODAL ANALYSIS OF THE PHALANX M61A1 CLOSE-IN WEAPON SYSTEM			5. FUNDING NUMBERS	
6. AUTHOR(S) Carlos S. Guzman, LT USN John C. Gaffe, LT USN				
7. PERFORMING ORGANIZATION NAME(S) AND ADDRESS(ES) Naval Postgraduate School Monterey CA 93943-5000			8. PERFORMING ORGANIZATION REPORT NUMBER	
9. SPONSORING/MONITORING AGENCY NAME(S) AND ADDRESS(ES)			10. SPONSORING/MONITORING AGENCY REPORT NUMBER	
11. SUPPLEMENTARY NOTES The views expressed in this thesis are those of the author and do not reflect the official policy or position of the Department of Defense or the U.S. Government.				
12a. DISTRIBUTION/AVAILABILITY STATEMENT Approved for public release; distribution is unlimited.			12b. DISTRIBUTION CODE	
13. ABSTRACT (maximum 200 words) The M61A1 gatling gun is the principal component of the PHALANX Close-In Weapons System (CIWS), which provides U.S. Navy surface ships with a final defense against anti-ship cruise missiles. The objectives of this study are to provide an experimental set of modal parameters and to validate a new finite-element model (FEM) of the gun. Swept sine frequency response measurements on an actual PHALANX gun were conducted in the laboratory to obtain a complete set of modal parameters (frequency, amplitude, mode shapes). The finite-element model was correlated using the experimental modal frequencies as a reference. This result was obtained by adjusting stiffnesses in the three bearing assemblies within the gun: ball-bearing, needle bearing and ball joint. The investigation was conducted with and without the production muzzle restraint currently used in the fleet. Good agreement between the measured and computed FEM modal parameters was found for the first three modes in both the horizontal and vertical directions for the 5 to 125 Hz frequency range of interest. With the production muzzle restraint installed, agreement between the experimental and finite-element results was poor. It is suspected that "play" in the actual restraint mounting system is present, which is not modeled by the FEM. Recommendations are made for follow-on studies.				
14. SUBJECT TERMS Modal Analysis, Star, Finite-Element Model, ANSYS, PHALANX			15. NUMBER OF PAGES 135	
			16. PRICE CODE	
17. SECURITY CLASSIFICATION OF REPORT Unclassified	18. SECURITY CLASSIFICATION OF THIS PAGE Unclassified	19. SECURITY CLASSIFICATION OF ABSTRACT Unclassified	20. LIMITATION OF ABSTRACT UL	

NSN 7540-01-280-5500

Standard Form 298 (Rev. 2-89)
Prescribed by ANSI Std. Z39-18 298-102

Approved for public release; distribution is unlimited.

**CORRELATION OF EXPERIMENTAL AND FINITE ELEMENT MODAL ANALYSIS
OF THE PHALANX M61A1 CLOSE-IN WEAPON SYSTEM**

Carlos S. Guzman
Lieutenant, United States Navy
B.S., Purdue University, 1988

John C. Gaffe
Lieutenant, United States Navy
B.S., Citadel, 1987

Submitted in partial fulfillment
of the requirements for the degree of

MASTER OF SCIENCE IN APPLIED PHYSICS

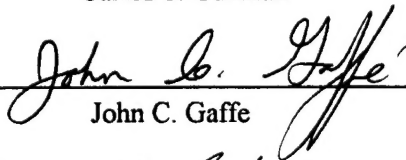
from the

**NAVAL POSTGRADUATE SCHOOL
December 1995**

Authors:



Carlos S. Guzman

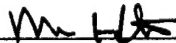


John C. Gaffe

Approved by:



Steven R. Baker, Thesis Advisor



Mike Hatch, Co-Advisor



William B. Colson, Chairman
Department of Physics

ABSTRACT

The M61A1 gatling gun is the principal component of the PHALANX Close-In Weapons System (CIWS), which provides U.S. Navy surface ships with a final defense against anti-ship cruise missiles. The objectives of this study are to provide an experimental set of modal parameters and to validate a new finite-element model (FEM) of the gun. Swept sine frequency response measurements on an actual PHALANX gun were conducted in the laboratory to obtain a complete set of modal parameters (frequency, amplitude, mode shapes). The finite-element model was correlated using the experimental modal frequencies as a reference. This result was obtained by adjusting stiffnesses in the three bearing assemblies within the gun: ball-bearing, needle bearing and ball joint. The investigation was conducted with and without the production muzzle restraint currently used in the fleet. Good agreement between the measured and computed FEM modal parameters was found for the first three modes in both the horizontal and vertical directions for the 5 to 125 Hz frequency range of interest. With the production muzzle restraint installed, agreement between the experimental and finite-element results was poor. It is suspected that "play" in the actual restraint mounting system is present, which is not modeled by the FEM.

Recommendations are made for follow-on studies.

TABLE OF CONTENTS

I. INTRODUCTION	1
II. DESCRIPTION OF EXPERIMENTAL SETUP	5
A. MODAL ANALYSIS	5
B. PHALANX GUN EXPERIMENTAL TEST CONFIGURATIONS	5
C. SHAKER EXCITATION	8
D. ACCELEROMETER LOCATIONS	10
E. FREQUENCY RESPONSE MEASUREMENTS	12
III. FINITE ELEMENT MODEL OVERVIEW	15
A. FINITE ELEMENT CONSTRUCTION	15
1. Model Creation and Overview	15
2. Element Types and Construction Materials	17
a. Element Types	17
b. Construction Materials	17
B. COMPLETED MODEL	17
1. Unrestrained Gun	17
2. Gun With Muzzle Restraint	23
C. ANSYS POST-RUN ANALYSIS	24
1. Modal Analysis and Animation	24
2. Harmonic Analysis	25
IV. EXPERIMENTAL RESULTS	27
A. INTRODUCTION	27
B. LINEARITY RESPONSE TESTING	28
C. FREQUENCY RESPONSE FUNCTION RECORDING.	30
1. Configuration 1	30
2. Configurations 2 and 3	30
D. MODAL PARAMETERS EXTRACTED BY STARMODAL	33

E. MODAL SHAPES OBTAINED BY STARMODAL	34
V. FINITE ELEMENT MODEL CORRELATION	37
A. INTRODUCTION	37
B. PRELIMINARY MODIFICATIONS	37
C. INVESTIGATIONS OF CRITICAL STIFFNESSES: UNRESTRAINED GUN	38
1. Stiffness Modifications by Trial and Error Using Y Bending Mode Frequencies	38
2. Stiffness Modifications: Matrix Method Using Y Bending Mode Frequencies	41
3. Anisotropy of Ball Joint Assembly; Further Stiffness Modifications by Trial and Error Using Z Bending Mode Frequencies	43
4. Final Stiffness Values and Resulting Modal Frequencies	44
D. HARMONIC RESPONSE: UNRESTRAINED GUN	48
E. MODAL BEHAVIOR: RESTRAINED GUN	50
VI. CONCLUSIONS	53
A. SUMMARY	53
B. SUGGESTIONS FOR FOLLOW-ON INVESTIGATIONS	54
APPENDIX A. STARMODAL ANALYSIS SYSTEM	55
A. STARMODAL SOFTWARE	55
B. STARMODAL DATA PROCESSING	55
APPENDIX B. ANALYZER INPUT AND MEASUREMENT STATES	59
APPENDIX C. FREQUENCY RESPONSE FUNCTIONS AND MODAL SHAPES FOR CONFIGURATION 1, Y-DIRECTION	61
APPENDIX D. FREQUENCY RESPONSE FUNCTIONS AND MODAL SHAPES FOR CONFIGURATION 2, Y-DIRECTION	67
APPENDIX E. FREQUENCY RESPONSE FUNCTIONS AND MODAL SHAPES FOR CONFIGURATION 2, Z-DIRECTION	75

APPENDIX F. FREQUENCY RESPONSE FUNCTIONS AND MODAL SHAPES FOR CONFIGURATION 3, Y-DIRECTION	83
APPENDIX G. FREQUENCY RESPONSE FUNCTIONS AND MODAL SHAPES FOR CONFIGURATION 3, Z-DIRECTION	93
APPENDIX H. BRUEL AND KJAER TYPE 8001 IMPEDANCE HEAD CALIBRATION CHART	101
APPENDIX I. PCB J353B04 ACCELEROMETER CALIBRATION CERTIFICATE . . .	103
APPENDIX J. LIST OF ELEMENTS, MATERIALS AND REAL CONSTANTS FOR M61A1 ANSYS FINITE ELEMENT MODEL	105
LIST OF REFERENCES	105
APPENDIX K. ANSYS HARMONIC RESPONSE TRANSFER FUNCTION PLOTS FOR Y AND Z DIRECTIONS	107
LIST OF REFERENCES	115
INITIAL DISTRIBUTION LIST	117

LIST OF FIGURES

1-1.	PHALANX Weapon Group	1
2-1.	PHALANX Gun Major Components	6
2-2.	PHALANX Gun Set-Up With Muzzle Restraint	6
2-3.	Load Inducing Set-Up	7
2-4.	Shaker Assembly for Horizontal Direction, Y-Axis	8
2-5.	Accelerometer Locations for Configurations (1), 2, and 3, Back View	11
2-6.	Accelerometer Locations for Configuration 3, Front View	11
2-7.	Accelerometer Locations for Configuration (1) and 2, Front View	12
2-8.	Displacement FRF for Configuration 1, Accelerometer Location 8	14
3-1.	Composite Model Gun	16
3-2.	Element Types Used for M61A1 Finite Element Modeling	18
3-3.	Rotor Solid Elements	19
3-4.	Stub Rotor Assembly	19
3-5.	Rotor/Stub Assembly	20
3-6.	Rear View of Rotor/Stub Rotor Assembly	20
3-7.	Complete Gun Body and Rotor Assembly	21
3-8.	Rear of Gun Body Showing Ball Joint	21
3-9.	Mid-Barrel Clamp	22
3-10.	Barrels with Mid-Barrel and Muzzle Clamps	22
3-11.	Muzzle Restraint Assembly	23
3-12.	Restrained M61A1 PHALANX Gun	24
4-1.	FRF's Recorded With (Top) and Without (Bottom) Gun Axial Load	28
4-2.	Frequency vs Force Level	29
4-3.	FRF's Recorded for Configuration 2, Z-Direction, Accelerometer Location 1-3	31
4-4.	FRF's Recorded for Configuration 2, Z-Direction, Accelerometer Locations 4-7	32
4-5.	FRF's Recorded for Configuration 2, Z-Direction, Accelerometer Locations 8-9	33
4-6.	Configuration 2, First Z-Mode: 20.25 Hz	34
4-7.	Configuration 2, Second Z-Mode: 69.68 Hz	35
4-8.	Configuration 2, Third Z-Mode: 109.64 Hz	35
5-1.	Stiffness Effects of 1st (Top) and 2nd (Bottom) Y-Mode	40
5-2.	1st Y Mode: 13.62 Hz	45
5-3.	2nd Y Mode: 51.77 Hz	45
5-4.	3rd Y Mode: 91.57 Hz	46
5-5.	1st Z Mode: 18.71 Hz	46
5-6.	2nd Z Mode: 77.54 Hz	47
5-7.	3rd Z Mode: 114.53 Hz	47
5-8.	Actual M61A1 Gun Body Assembly	48
5-9.	Horizontal (Y) FEM (top) and FRF Harmonic Response (bottom)	49
5-10.	Vertical (Z) FEM (top) and FRF Harmonic Response (bottom)	50
B-1.	Measurement State for H-P Analyzer During Data Collection	60

B-2.	Input State for H-P Analyzer During Data Collection	60
C-1.	FRF's Recorded for Configuration 1, Y-Direction, Accelerometer Locations 1-4 . . .	62
C-2.	FRF's Recorded for Configuration 1, Y-Direction, Accelerometer Locations 5-8 . . .	63
C-3.	Configuration 1, Geometry	64
C-4.	Configuration 1, First Y-Mode: 11.09 Hz	64
C-5.	Configuration 1, Second Y-Mode: 16.69 Hz	65
C-6.	Configuration 1, Third Y-Mode: 28.69 Hz	65
D-1.	FRF's Recorded for Configuration 2, Y-Direction, Accelerometer Locations 1-4 . . .	68
D-2.	FRF's Recorded for Configuration 2, Y-Direction, Accelerometer Locations 5-8 . . .	69
D-3.	FRF's Recorded for Configuration 2, Y-Direction, Accelerometer Location 9	70
D-4.	Configuration 2, Geometry	71
D-5.	Configuration 2, First Y-Mode: 14.73 Hz	71
D-6.	Configuration 2, Second Y-Mode: 48.61 Hz	72
D-7.	Configuration 2, Third Y-Mode: 97.37 Hz	72
E-1.	FRF's Recorded for Configuration 2, Z-Direction, Accelerometer Locations 1-4 . . .	76
E-2.	FRF's Recorded for Configuration 2, Z-Direction, Accelerometer Locations 5-8 . . .	77
E-3.	FRF's Recorded for Configuration 2, Z-Direction, Accelerometer Location 9	78
E-4.	Configuration 2, First Z-Mode: 20.25 Hz	79
E-5.	Configuration 2, Second Z-Mode: 69.68 Hz	79
E-6.	Configuration 2, Third Z-Mode: 109.64 Hz	80
F-1.	FRF's Recorded for Configuration 3, Y-Direction, Accelerometer Locations 1-4 . . .	84
F-2.	FRF's Recorded for Configuration 3, Y-Direction, Accelerometer Locations 5-8 . . .	85
F-3.	FRF's Recorded for Configuration 3, Y-Direction, Accelerometer Locations 9-11 . . .	86
F-4.	Configuration 3, Geometry	87
F-5.	Configuration 3, First Y-Mode: 16.44 Hz	87
F-6.	Configuration 3, Second Y-Mode: 41.74 Hz	88
F-7.	Configuration 3, Third Y-Mode: 71.43 Hz	88
F-8.	Configuration 3, Fourth Y-Mode: 103.31 Hz	89
G-1.	FRF's Recorded for Configuration 3, Z-Direction, Accelerometer Locations 1-4 . . .	94
G-2.	FRF's Recorded for Configuration 3, Z-Direction, Accelerometer Locations 5-8 . . .	95
G-3.	FRF's Recorded for Configuration 3, Z-Direction, Accelerometer Locations 9-11 . . .	96
G-4.	Configuration 3, First Z-Mode: 28.24 Hz	97
G-5.	Configuration 3, Second Z-Mode: 44.69 Hz	97
G-6.	Configuration 3, Third Z-Mode: 76.87 Hz	98
G-7.	Configuration 3, Fourth Z-Mode: 101.36 Hz	98
K-1.	FEM Measurement Points	108
K-2.	Y, Barrel-Tip Response	108
K-3.	Y, Rear-of Muzzle-Clamp Response	109
K-4.	Y, Mid-Barrel Response	109
K-5.	Y, Mid-Barrel-Clamp Response	110
K-6.	Y, Rear-of-Barrel Response	110
K-7.	Z, Barrel-Tip Response	111
K-8.	Z, Rear-of Muzzle-Clamp Response	111

K-9. Z, Mid-Barrel Response	112
K-10. Z, Mid-Barrel-Clamp Response	112
K-11. Z, Rear-of-Barrel Response	113

LIST OF TABLES

3-1.	Element Types and Usages in ANSYS Finite Element Model	26
4-1.	Frequencies for Each Mode in Hz for Varying Force Levels	29
4-2.	Modal Frequencies and Percent of Critical Damping for Each Configuration	33
5-1.	Reduced Bearing Stiffness Cases (klb/in.)	39
5-2.	Modal Frequencies for Stiffness Cases	39
5-3.	Final Bearing Stiffnesses	40
5-4.	Comparison of Extrapolated Stiffnesses With Original Values	43
5-5.	Modal Frequencies for Final Bearing Stiffnesses	44
5-6.	Comparison of FEM and Experimental Restrained Gun Vertical Modes	51
6-1.	Comparison of Experimental and Finite-Element Results (Unrestrained)	54
A-1.	Major Steps of Parameter Identification in STAR	56
C-1.	Amplitudes and Phases Computed by STARModal for Configuration 1, Y-Direction	66
D-1.	Amplitudes and Phases Computed by STARModal for Configuration 2, Y-Direction	73
E-1.	Amplitudes and Phases Computed by STARModal for Configuration 2, Z-Direction	81
F-1.	Amplitudes and Phases Computed by STARModal for Configuration 3, Y-Direction	90
G-1.	Amplitudes and Phases Computed by STARModal for Configuration 3, Z-Direction	99

I. INTRODUCTION

The PHALANX Close-In Weapons System (CIWS) is used extensively in the fleet as a "last-ditch" defense against anti-ship cruise missiles. Currently installed versions use the 20mm M61A1, six-barrel "gatling gun", which dates from the Vietnam era [Ref 1]. Figure 1-1 shows the major components of the CIWS. In the two decades since the inception of the PHALANX system, marked improvements have been made in the all of the major subsystems (fire control radar and software, signal processing, etc.) with the exception of the gun and its attachment points.

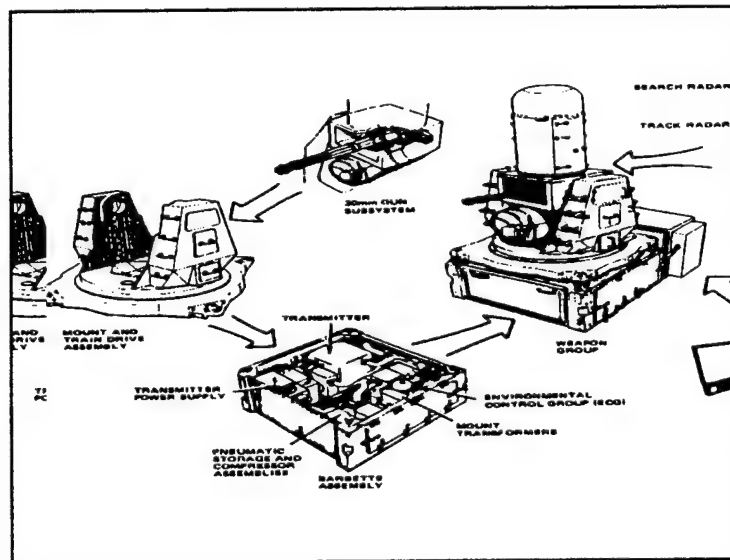


Figure 1-1. PHALANX Weapon Group.

PHALANX systems in use today are limited in their effectiveness to destroy incoming missiles at long ranges (in excess of 1000 yards) due to "**dispersion**" or angular spread of the projectiles as they leave the barrel tips [Ref 2]. Dispersion is attributed to transverse gun barrel displacement caused by the forces exerted by expanding propellant gases and projectile movement

through a barrel during firing, thereby exciting natural vibrational modes. The frequencies and degree of excitation of these modes are dependent upon such factors as the location and stiffness of the gun's attachment and support points, material constants, etc. The U.S. Navy would like to achieve an average dispersion of less than 1 milliradian. A 3 mm lateral displacement at the barrel tip results in an angular dispersion of approximately 2 milliradians. Recent proposed solutions to the dispersion problem have included the addition of a "muzzle restraint" to suppress lateral barrel-tip displacement. An exhaustive discussion of dispersion theory and the PHALANX gun may be found in Reference [2].

The study described in this thesis focuses on three key objectives. The first objective is the collection of a comprehensive data set on the multi-axis modal behavior of the laboratory M61A1 gun. The second objective is the validation of the new modal data set against the modal frequencies and shapes generated by a new finite-element model of the PHALANX gun developed by an independent consultant, Michael R. Hatch, in 1993. The final objective is the modification and optimization of the finite-element model to reflect the actual modal frequencies and mode shapes found in testing the laboratory gun. Agreement between the computer model and physical data is necessary to provide a realistic simulation which may be used to study proposed improvements and enhancements and rapidly and economically assess gun performance and behavior.

The remainder of this thesis is organized as follows. Chapter II discusses the experimental set-up used to analyze the horizontal and vertical vibrational modes of a gun in the laboratory. Only the lower-order modes, which contribute most to the dispersion problem, are considered.

Chapter III provides a detailed description of the finite-element model used to simulate the structural dynamics of the gun. The types of elements used, material constants and structural degrees of freedom for major attachment points of the gun are discussed. Cases of the gun with and without the muzzle restraint are considered.

In Chapter IV, the vibration data collected from the laboratory gun is presented for three experimental configurations: (1) gun and its enclosure alone, i.e., with no additional weights added to the gun enclosure, (2) gun and its enclosure with weight added to the gun enclosure to suppress vibration of the enclosure, (3) configuration (2) with the addition of the production muzzle restraint. In addition, the regimes of linear and non-linear vibration behavior of the gun are explored.

In Chapter V, the effects of changing various parameters in the finite-element model are discussed. Results of several attempts to correlate the finite-element model results with the data from Chapter IV are presented, including modal frequencies and shapes, modal types and transfer-function (harmonic analysis) graphs.

Chapter VI includes conclusions and recommendations suggested by the experimental and theoretical results. These include suggested improvements to the finite-element model to improve its realism and possible methods to obtain better correlation between the computed and measured vibration response of the gun with the muzzle restraint installed. In addition, possible follow-on study opportunities are discussed.

This investigation was useful in determining and implementing a realistic model of the M61A1 gun. Additionally, valuable data was collected from the actual gun and muzzle restraint assembly which will serve as a ready reference for future design changes and enhancements to

the PHALANX system. In summary, the information gained in this study will greatly improve the understanding of the gun's behavior and allow the use of a low-cost computer simulation to address progressive changes.

II. DESCRIPTION OF EXPERIMENTAL SET UP

A. MODAL ANALYSIS

Most noise and vibration problems are related to resonance phenomena, where the operational forces excite one or more of the modes of vibration. [Ref 3] Modes of vibration which lie within the frequency range of the operational dynamic forces present potential problems, such as undesired dispersion in the case of the PHALANX gun. A general discussion of vibration analysis may be found in Reference [3].

An important property of modes is that any forced or free dynamic response of a structure can be described by the response of a discrete set of modes. The modal parameters are: modal frequency, modal damping, and mode shape (eigenfunction). Modal parameters of all the modes within the frequency range of interest constitute a complete dynamical description of the structure. Hence the modes of vibration represent the inherent dynamical properties of a structure.

Modal analysis is the process of determining all the modal parameters, which are then sufficient for formulating a mathematical dynamical model. [Ref 4] The ultimate goals in this study are to experimentally determine these parameters for the PHALANX gun and to use these data to correlate with a finite-element computer model of the gun.

B. PHALANX GUN EXPERIMENTAL TEST CONFIGURATIONS

Swept sine frequency response measurements were conducted on an actual PHALANX gun in the laboratory located in the basement of Spanagel Hall, Naval Postgraduate School. For practical reasons, only the gun (without drive components or ammunition feed guides), gun cradle structure, and gun pallet (see Figure 2-1) were assembled and set on three cork and rubber

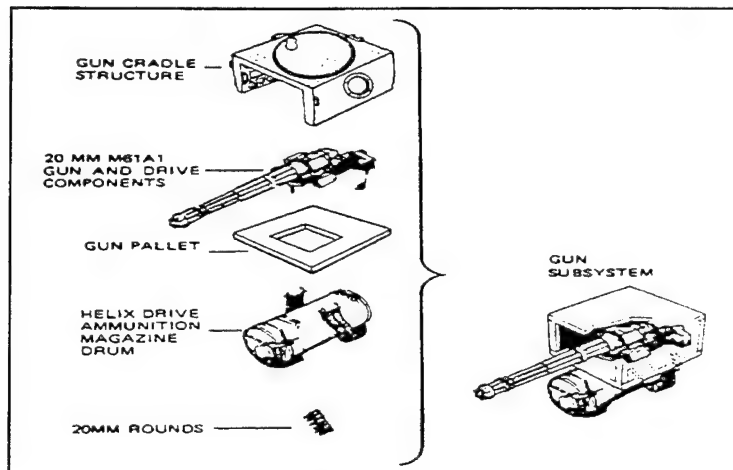


Figure 2-1. PHALANX Gun Major Components.

dampers on the laboratory floor (see Figure 2-2). Two of the dampers were placed under the forward part of the gun pallet just inside the clevises that anchor the legs of the muzzle restraint. The third was centered at the rear of the gun pallet. These dampers were placed so that there was no rocking of the gun pallet about any axis.

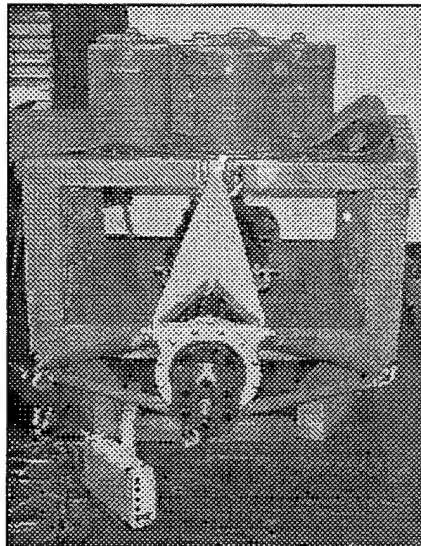


Figure 2-2. PHALANX Gun Set-Up With Muzzle Restraint.

Based on the results obtained in prior investigations [Ref 5] only three configurations of this assembly were tested. These were primarily distinguished by the use of lead weights on top of the gun cradle structure and the use of the muzzle restraint. For all three configurations, the gun's barrel assembly was placed under a static axial load similar to that experienced when a bullet is fired.

The load on the barrels was applied by an aluminum ball large enough to lodge in the forward hole in the center of the stub rotor (see Figure 2-3). The ball was pulled back by an eyebolt screwed through the center of the ball. A high tensile strength chain attached to the eyebolt was threaded through the center of the gun and connected to another eyebolt bolted through a crossbar braced across the back of the gun cradle structure. Care was taken to ensure that the only contact with the gun itself was where the ball pulled back on the stub rotor [Ref 5]. The chain was tensioned to provide a setback of $\frac{3}{8}$ inch, measured at the recoil adapters.

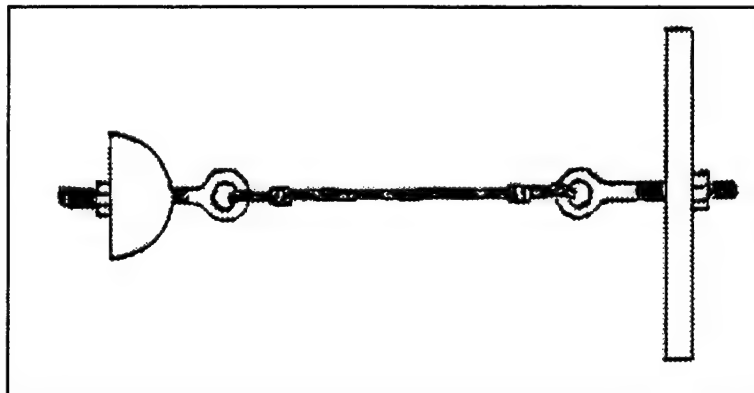


Figure 2-3. Load Inducing Set-Up.

The tested configurations were as follows:

1. topmost barrel at 12 o'clock position (top dead center), barrels axially loaded, no lead weights on top of gun cradle, and no muzzle restraint;
2. topmost barrel at 12 o'clock position, barrels axially loaded, approximately 1200 pounds of lead weights on top of gun cradle, and no muzzle restraint;
3. topmost barrel at 12 o'clock position, barrels axially loaded, lead weights on top of gun cradle, and muzzle restraint attached.

Vibration measurements for configuration 1 were only made in the horizontal direction (Y-axis), while both horizontal (Y-axis) and vertical (Z-axis) vibration measurements were made for configurations 2 and 3.

C. SHAKER EXCITATION

Dynamic force was applied to the muzzle end of the gun using an Acoustics Power Source Perma-Dyne model 120S shaker and amplifier system. [Ref 6] The shaker was placed directly on the floor for the vertical (Z-axis) measurements; for horizontal (Y-axis) measurements it was suspended from a laboratory crane (see Figure 2-4).

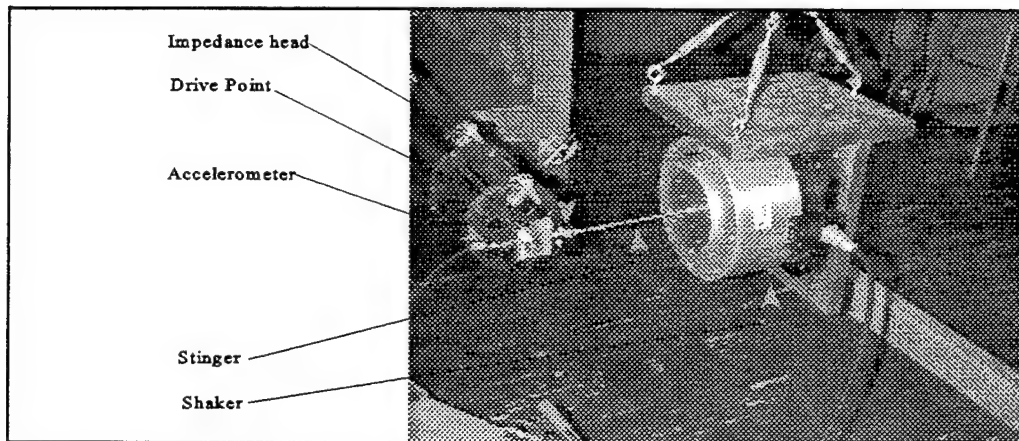


Figure 2-4. Shaker Assembly for Horizontal Direction, Y-Axis.

A stinger assembly consisting of a 213mm long, 10-32 threaded rod, locking nuts, and a Bruel and Kjaer model 8001 impedance head [Ref 7] mounted on the shaker. The stinger serves to isolate the shaker from the structure, reduces added mass, and causes the force to be transmitted axially along the stinger, controlling the direction of the applied force more precisely [Ref 3]. The calibration sheet for the impedance head is given in Appendix H. The impedance head, used to measure the force to the driving point, is attached to a rectangular, aluminum plate (7mm x 48mm x 53mm) in a standard drive configuration. In the center of the plate is a hole that was fitted over an expanding aluminum cylinder that was inserted into the hollow center of the locking lug which secures the muzzle clamp onto the end of the barrels [Ref 5]. The output of the impedance head's force gauge was amplified using an ENDEVCO model 2775A signal conditioner [Ref 8].

Excitation applied to the amplifier input consisted of a swept sinusoidal signal stepped from 5 to 50 Hz in 0.11 Hz increments for configuration 1 and from 5 to 125 Hz in 0.30 Hz increments for configurations 2 and 3 (121 Hz span divided by the 401 points per sweep, as set on the analyzer). The drive signal was supplied by a Hewlett-Packard 35665A 2-channel signal analyzer. The voltage applied was varied using the *autolevel* feature of the analyzer; in this mode the signal output level is automatically adjusted so as to keep the amplitude of one input channel within a specified range [Ref 9]. The reference input channel selected was channel 1 (force) in order to keep the force level at the impedance head constant. The drive signal was amplified by an Acoustics Power Systems model 114 power amplifier [Ref 6], which has a fixed gain, operated in the voltage mode. The lower frequency limit of 5 Hz was chosen as there were no structural resonances below this frequency. Removing the 0 to 5 Hz portion of the sweep reduced the

measurement time significantly [Ref 5]. The upper frequency limit was chosen to observe the first three or four resonant peaks in the forced response of the gun, and so to provide an adequate set of data from which to extract modal parameters to compare with the finite element model results. The measurement and input states of the analyzer are given in Appendix B.

D. ACCELEROMETER LOCATIONS

The acceleration response to the force applied by the shaker was measured with a PCB model 353B44 accelerometer [Ref 10]. The accelerometer was sequentially mounted on cubes clamped to the gun barrel and to studs which had been cemented with epoxy to selected gun body locations. The cubes were machined and mounted so their faces (accelerometer mounting surfaces) were perpendicular to the three directions: horizontal (Y), vertical (Z), and axial (X). The response signal was amplified using a PCB model 482A17 preamplifier [Ref 10]. The calibration sheet for the accelerometer is given in Appendix I.

Eight accelerometer locations along the barrel and gun body were chosen for configuration 1. One more accelerometer location, on the back end of the gun cradle, where the ball joint joins the base of the gun cradle, was added to configuration 2, for a total of nine accelerometer locations. Another two accelerometer locations on the muzzle restraint, were added for configuration 3, for a total of eleven accelerometers. Figure 2-5 shows a back view of the accelerometer mount locations used in configurations 1, 2, and 3. Figure 2-6 shows a front view of accelerometer mount locations used in configuration 3. Figure 2-7 shows a front view of accelerometer mount locations in configurations 1 and 2.

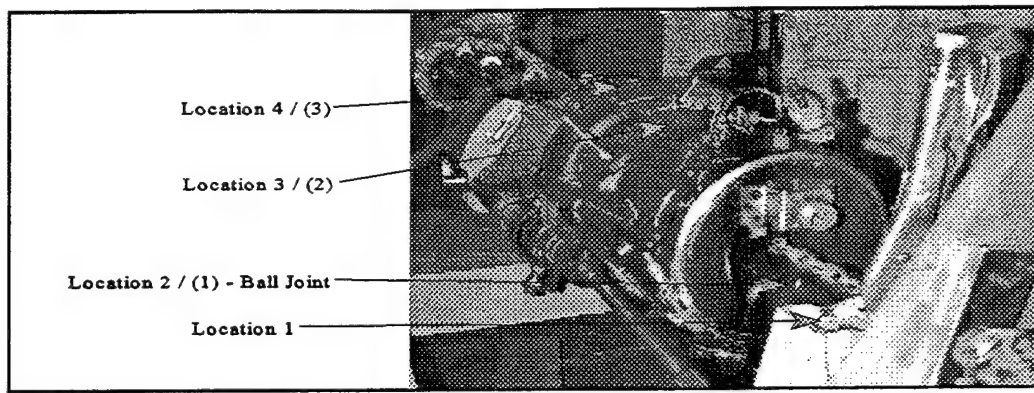


Figure 2-5. Accelerometer Locations for Configurations (1), 2, and 3, Back View.

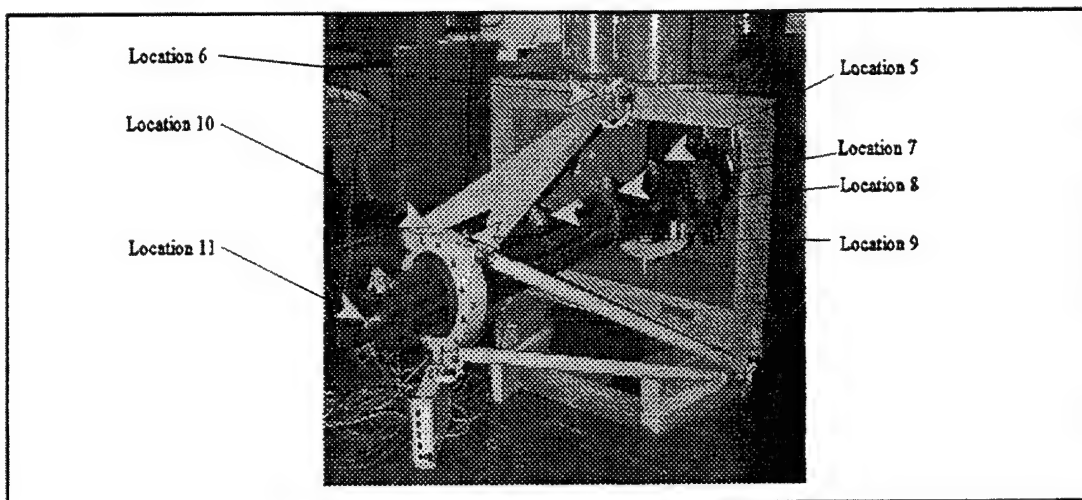


Figure 2-6. Accelerometer Locations for Configuration 3, Front View.

Configuration 3 utilized the most accelerometer locations, and so these are described first. For configuration 3 the first accelerometer location is at the base of the rear of the gun cradle, where the ball joint is attached to the back end of the cradle. The second location is on top of the ball joint housing. The third location is approximately mid-way along the gun body. The fourth location is on the front part of the gun body. The fifth location is at the base of the topmost barrel, as close as possible to where the barrel inserts into the stub rotor. The sixth location is on top of the muzzle restraint, where it attaches to the gun cradle. The seventh location is on top of the

topmost barrel, as close as possible to the mid-barrel clamp. The eighth location is at the center of the topmost barrel, between the mid-barrel and the muzzle restraint clamps. The ninth location is on top of the topmost barrel, just behind the muzzle restraint clamp. The tenth location is on top of the muzzle restraint clamp. The eleventh location is on top of the aluminum plate attached to the impedance head (see Figure 2-4).

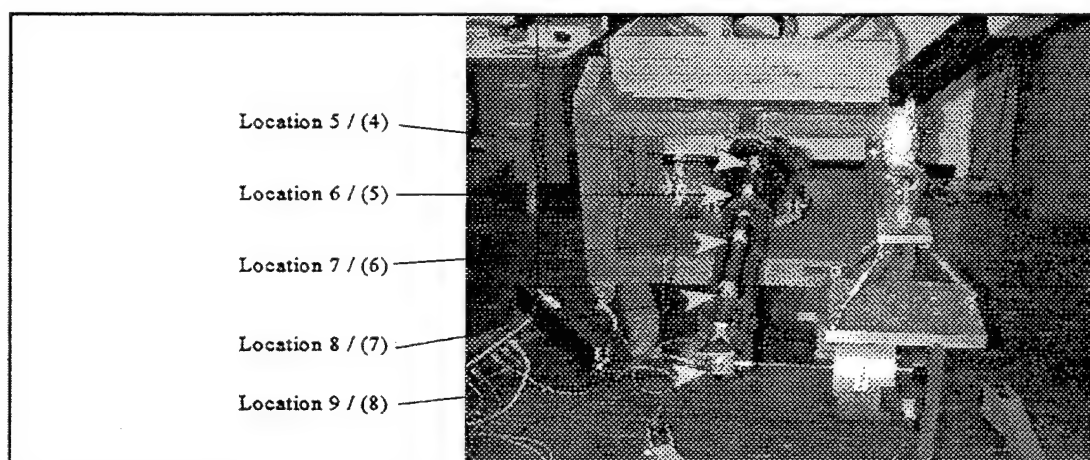


Figure 2-7. Accelerometer Locations for Configurations (1) and 2, Front View.

For configuration 2, the accelerometer locations are essentially the same as for configuration 3, with the exception of the two blocks attached to the muzzle restraint (locations 6 and 10 in Figure 2-6), which were not used in configuration 2. Configuration 1 accelerometer locations are identical to configuration 2, but the location at the rear of the cradle (location 1 in Figure 2-5) was not used, thus there were only eight locations.

E. FREQUENCY RESPONSE MEASUREMENTS

The force voltage signal from the impedance head's force gauge and the voltage signal from the accelerometer were respectively the inputs to channels 1 and 2 of the Hewlett-Packard

35665A dual-channel signal analyzer. The analyzer combined the two inputs in the frequency domain to obtain the frequency response, described below.

An efficient descriptor of a linear system is a frequency domain model called the frequency response function (FRF), and is defined as:

$$H(\omega) = \frac{X(\omega)}{F(\omega)} \quad (2-1)$$

It is the complex ratio of the output displacement, $X(\omega)$, to the input force, $F(\omega)$, as a function of frequency ω . The function $H(\omega)$ has a magnitude $|H(\omega)|$ and a phase angle $\angle H(\omega) = \phi(\omega)$.

[Ref 4] In a so-called linear system $H(\omega)$ may depend on the frequency ω , but it is independent of either $F(\omega)$ or $X(\omega)$.

In order to obtain the FRF of the gun system as a function of ω , the acceleration measured with the accelerometer must be transformed into displacement. To achieve this in the frequency domain requires the use of the equations of motion and some Fourier transformations. The displacement, $x(t)$, and the acceleration, $a(t)$, are related to their Fourier transforms, $X(\omega)$ and $A(\omega)$, respectively by:

$$x(t) = \int X(\omega) e^{j\omega t} d\omega \quad (2-2)$$

and,

$$a(t) = \int A(\omega) e^{j\omega t} d\omega. \quad (2-3)$$

But,

$$a(t) = \frac{d^2}{dt^2} x(t) = \int X(\omega) (j\omega)^2 e^{j\omega t} d\omega, \quad (2-4)$$

so, by equating the integrands we get,

(2-5)

$$X(\omega) = A(\omega) \frac{1}{(j\omega)^2}$$

The Hewlett-Packard dual-channel analyzer can be set to divide the measured acceleration frequency response by $(j\omega)^2$, thereby producing the displacement FRF, $H(\omega)$. Figure 2-8 presents an example of a displacement FRF measured by the H-P analyzer at the tip of the muzzle. The dB magnitudes plotted in all FRF graphs presented in this thesis have not been corrected using the transducer calibration and amplifier gains. For the FRF in dB re 1m/N, add 28.7 dB to the plotted values. Displacement FRF's were recorded for the three configurations at all accelerometer locations and can be found in Appendices C through G.

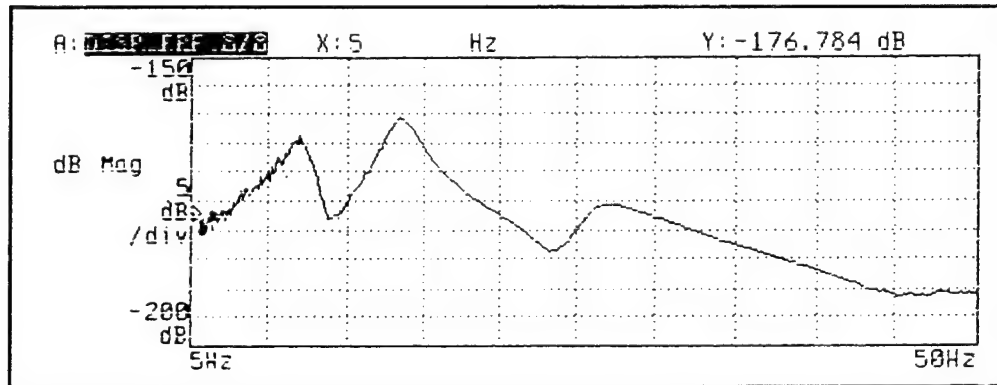


Figure 2-8. Displacement FRF for Configuration 1, Accelerometer Location 8.

III. FINITE ELEMENT MODEL OVERVIEW

A. FINITE ELEMENT CONSTRUCTION

Earlier NPS efforts in modeling the M61A1 gun employed the I-DEAS (Integrated Design Engineering Analysis) finite-element code [Ref. 11]. Michael Hatch, a private consultant who assisted in constructing the initial finite element model (FEM), created another model using the commercially available code ANSYS [Ref. 11]. ANSYS is currently the dominant finite element software utilized throughout many industries world-wide. In addition, a muzzle restraint FEM was designed and implemented to observe and predict the behavior of the restrained PHALANX gun. The ANSYS code was employed for all finite-element model analyses carried out in the present investigation.

1. Model Creation and Overview

Finite-element Model creation in ANSYS is a multi-step process. First, the blue-prints of the actual gun are used to create a drawing in an AUTOCAD file [Ref. 13]. Top and side views of the various assemblies are drawn. As much detail as practical is usually included to faithfully represent the physical object. Secondly, a local cartesian coordinate system is defined for each gun sub-assembly. Next, finite-element "nodes" are chosen on the sub-assemblies to represent the boundaries of the finite elements used later to build the full model in ANSYS. Following this, the Cartesian location of each node in the AUTOCAD model is written to an ASCII text file and edited as necessary using a text editor known as "BRIEF" [Ref. 14]. This file will become the ANSYS batch command script file for performing finite-element analyses. ANSYS commands are added to the script file to translate the node coordinates into various local and global coordinate systems and to generate additional nodes as required.

At this point, the gun model exists as a collection of points or "nodes" only. Material types and parameters, elements, etc. have yet to be defined. Standard ANSYS commands are added to the script file to define element types, material types, and real constants such as Young's modulus, density and element dimensions. Elements are defined by specifying the bounding nodes, element type, and real constants. Constraints are defined for various points on the model in order to specify boundary conditions. These may include translational (X,Y,Z) or rotational (about a local or global coordinate system) to simulate realistic motion constraints (or freedom) of attachment points, barrels etc. The model gun is assumed to be attached to an "isogrid", a rigid and stationary structure. Finally, other standard ANSYS commands are used to optimize the model to conserve execution time.

Synthesis of the model gun involves entering ANSYS and importing the BRIEF file. A graphic representation of the model as it appears on the computer screen is shown in Figure 3-1.

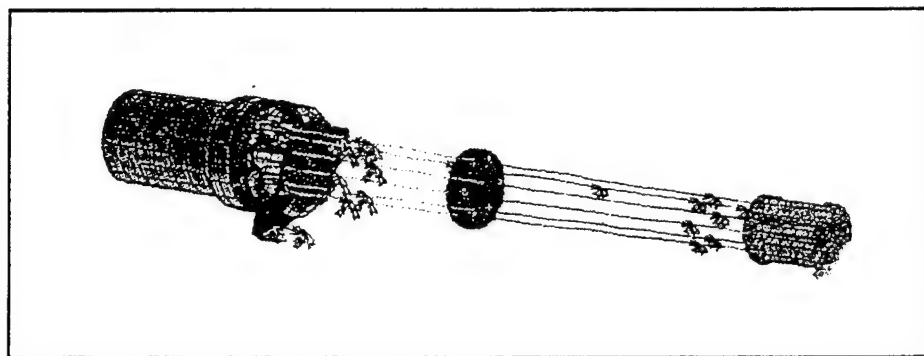


Figure 3-1. Composite Model Gun.

2. Element Types and Construction Materials

a. Element Types

Six element types are used in the ANSYS FEM of the M61A1 gun versus the five used in the I-DEAS version. Figure 3-2 illustrates these six elements along with the number of required, defining nodes and the structural/cartesian degrees of freedom. Table 3-1 and Appendix J list the applications of these element types to the sub-assemblies of the M61A1 gun.

b. Construction Materials

Three types of "materials" were used to construct the model. Low-carbon steel, a fictitious near-zero density, finite stiffness material for rigid connections, and aluminum. Appendix J lists the material parameters such as Young's modulus, density and real values such as the stiffness of the spring elements described in Table 3-1. Low-carbon steel is utilized for all of the gun components. Connections between barrels (beam elements) and their mating assemblies such as the muzzle clamp, mid-barrel clamp and stub rotor are modeled using rigid connections. The muzzle-restraint version is modeled using aluminum for all but the bearings and bearing races, which are modeled with the low-carbon steel. For historic reasons, English units are used throughout the finite-element model for real constants such as stiffness and Young's modulus.

B. COMPLETED MODEL

1. Unrestrained Gun

Figures 3-3 through 3-10 show a "step-by-step" appearance of the gun as it is constructed in ANSYS from the BRIEF script file. Figure 3-3 shows the solid elements of the rotor assembly. Figure 3-4 is the completed stub rotor, which is the primary attachment point of the barrel assembly. In Figure 3-5, the rotor and stub rotor are joined. In addition, the outer race of the 18-

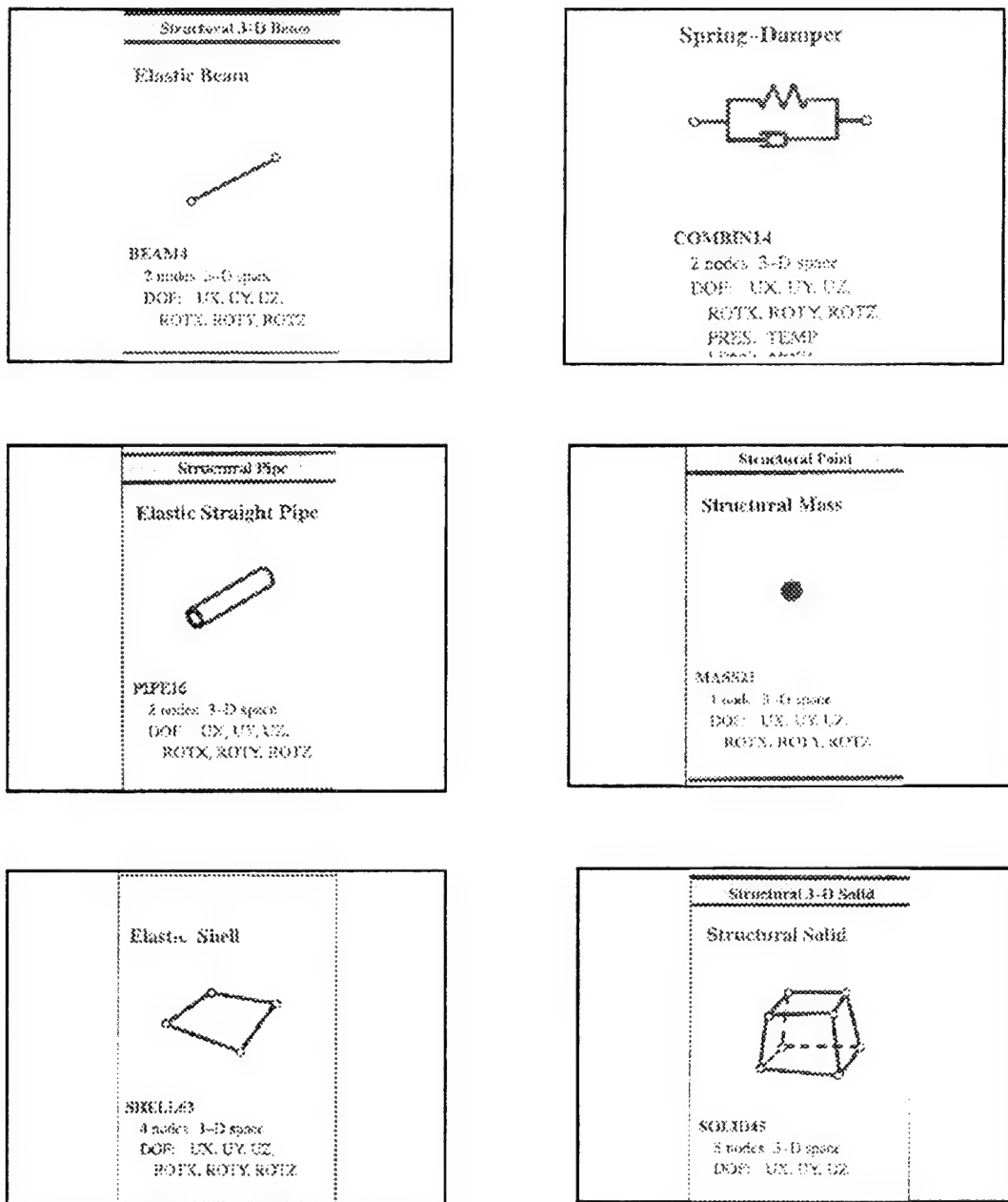


Figure 3-2. Element Types Used for M61A1 Finite Element Modeling.

ball bearing assembly is shown. Its single row of 18 balls are modeled by linear springs, as seen earlier in Table 3-1. This bearing assembly is the first point of support for the rotor inside of the gun body/ housing (See Figure 3-1). Figure 3-6 shows a rear-view of the rotor/stub rotor Assembly with its three "needle" bearings spaced 120 degrees apart. These are modeled as linear springs, and form the second critical point of support for the rotor by the gun body. The composite of the rotor, stub rotor, gun body and recoil ears is seen in Figure 3-7. The recoil ears and the ball joint, shown in a rear-view of the gun body, form the three support/attachment points of the entire gun model to the isogrid. The ball joint is modeled as an octagon of solid elements to which are attached four springs joined at the center (isogrid attachment). Two of these springs are in the vertical (global Z) direction, while the remaining two are oriented horizontally (global Y).

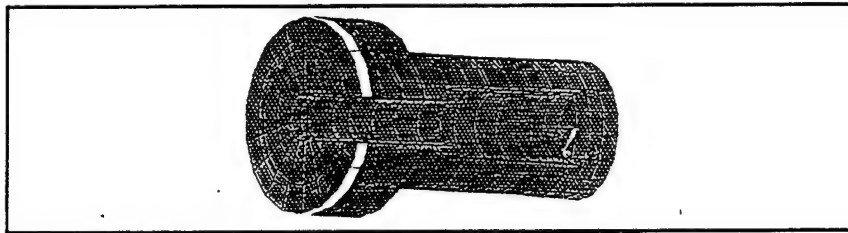


Figure 3-3. Rotor Solid Elements.

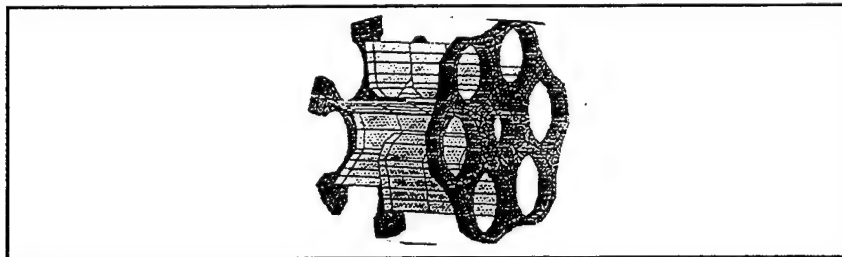


Figure 3-4. Stub Rotor Assembly.

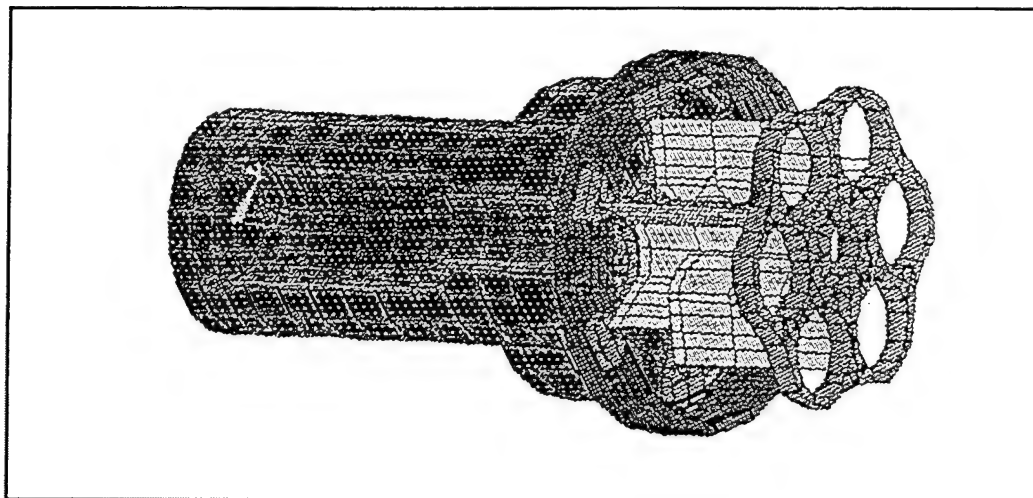


Figure 3-5. Rotor/Stub Rotor Assembly.

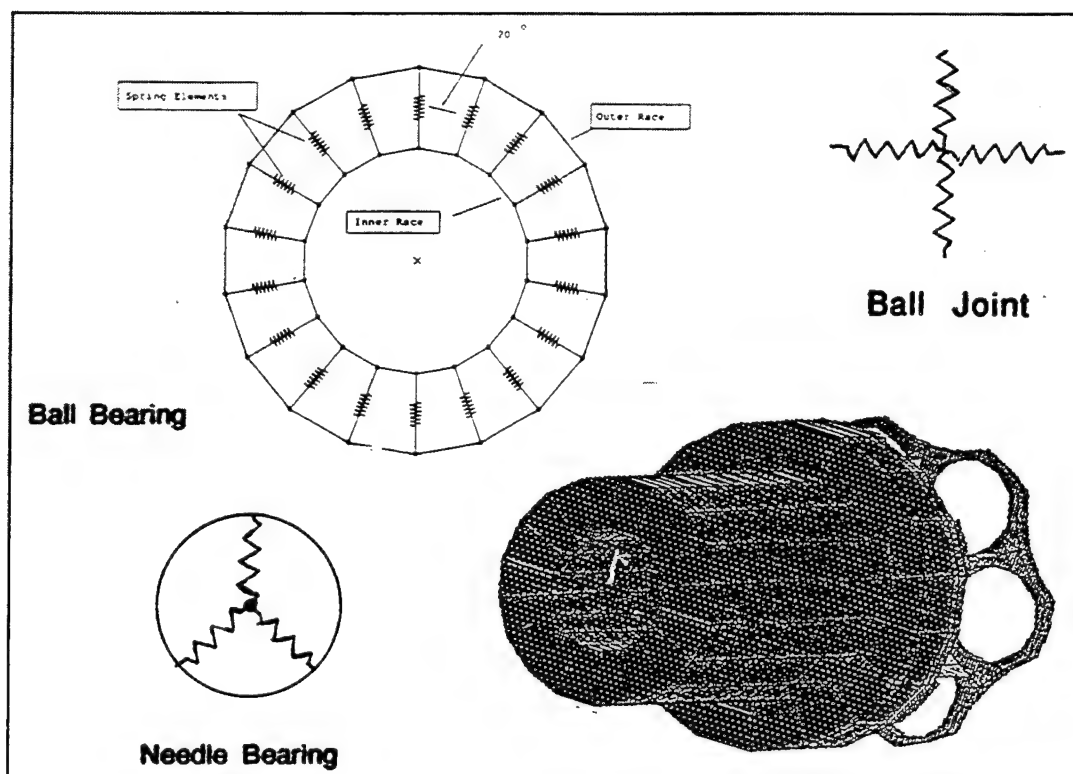


Figure 3-6. Rear View of Rotor/Stub Rotor Assembly.

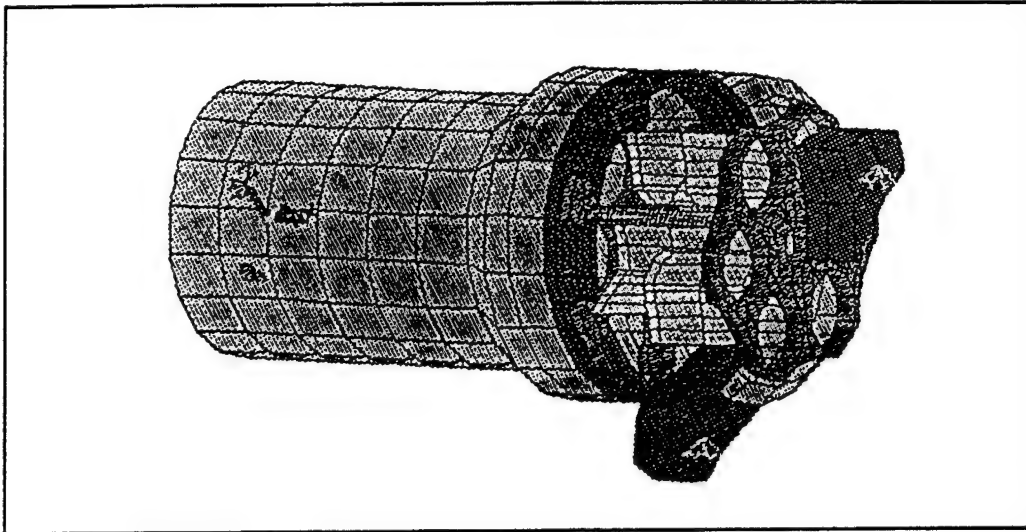


Figure 3-7. Complete Gun Body and Rotor Assembly.

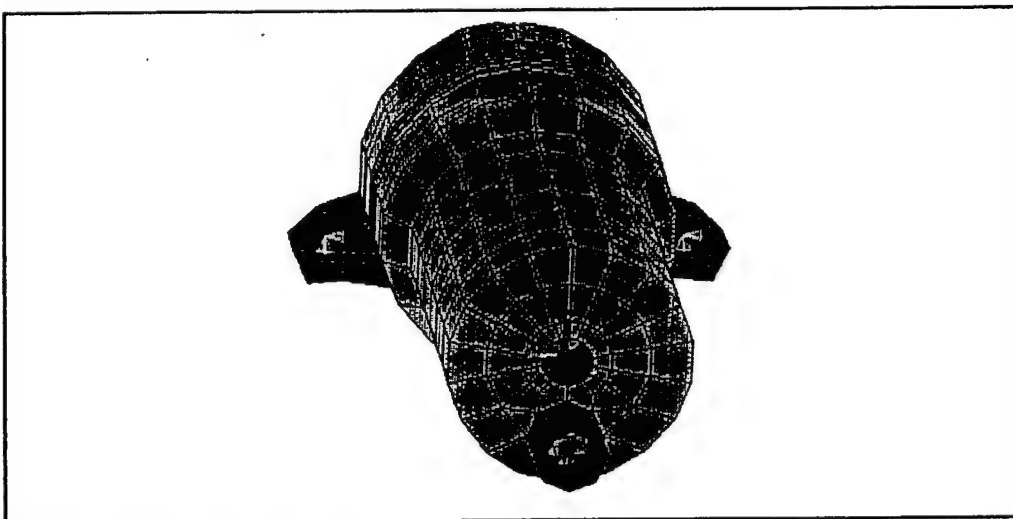


Figure 3-8. Rear of Gun Body Showing Ball Joint.

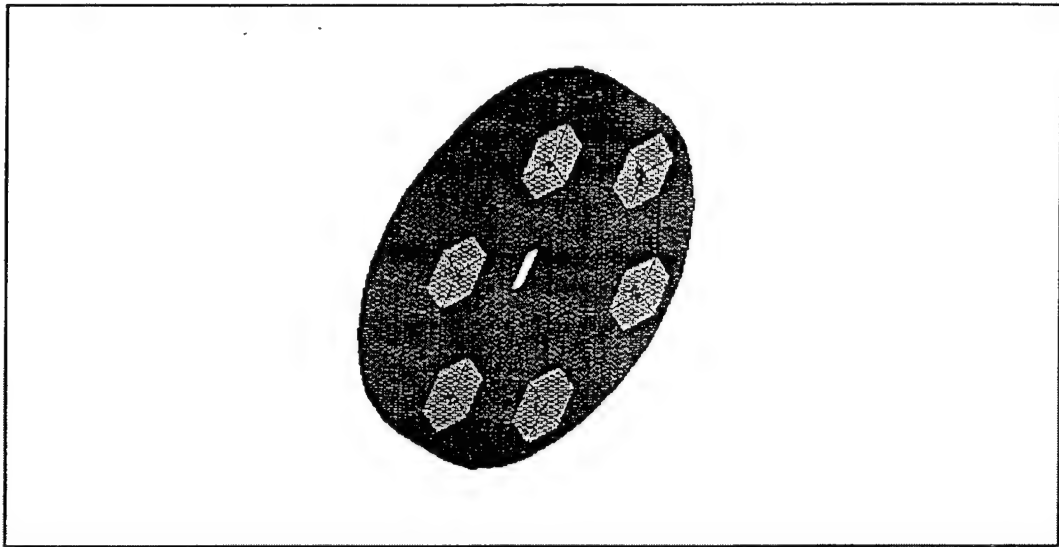


Figure 3-9. Mid-Barrel Clamp.

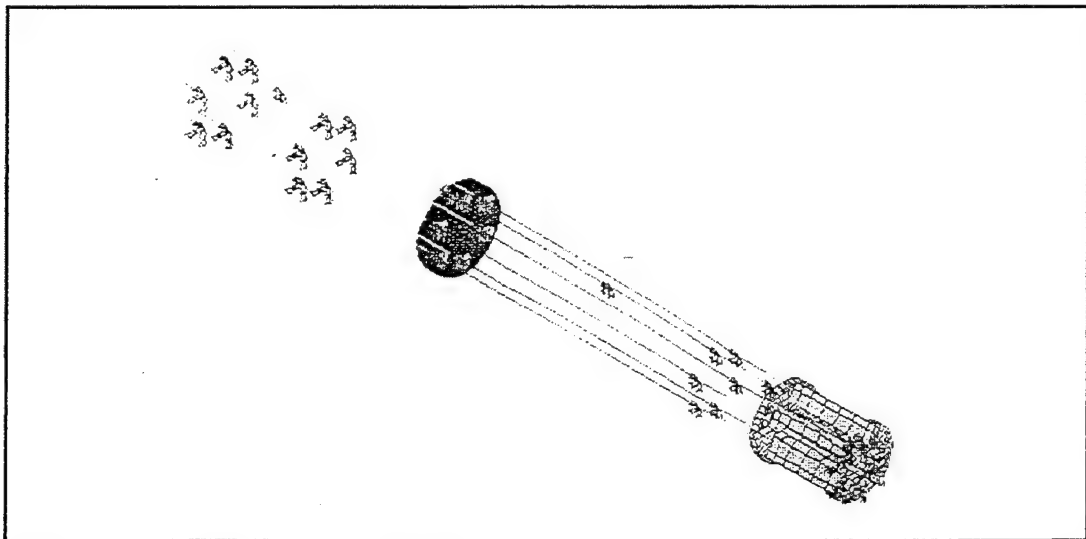


Figure 3-10. Barrels with Mid-Barrel and Muzzle Clamps.

The remaining portion of the ANSYS model consists of the six barrel assemblies and their corresponding clamps, which act to tie each of the six barrels into a unit. Figure 3-9 is a view of the mid-barrel clamp. A complete view of the six barrels and the mid-barrel and muzzle clamp are shown in Figure 3-10.

2. Gun With Muzzle Restraint

The model of the unrestrained gun discussed above was modified by adding finite-element components of the production muzzle restraint used currently in the fleet [Ref. 15]. The upper support arm is created using solid elements for the support grid or web (dark area in Figure 3-11) and shell elements for the smooth outer surfaces. The muzzle support ring uses solid elements for the bulk of the structure and a single-row ball-bearing set-up similar to the one used in the Rotor/Gun Body assembly. However, different stiffnesses for the springs are provided for the vertical and horizontal directions versus the isotropically stiff ball bearing assembly used in the gun rotor/body . The lower four struts are modeled using pipe elements with inside and outside diameters equal to the actual component. The apex of the upper support and the four struts are attached to the presumed infinitely stiff isogrid. Figure 3-12 is a complete view of the restrained M61A1 gun.

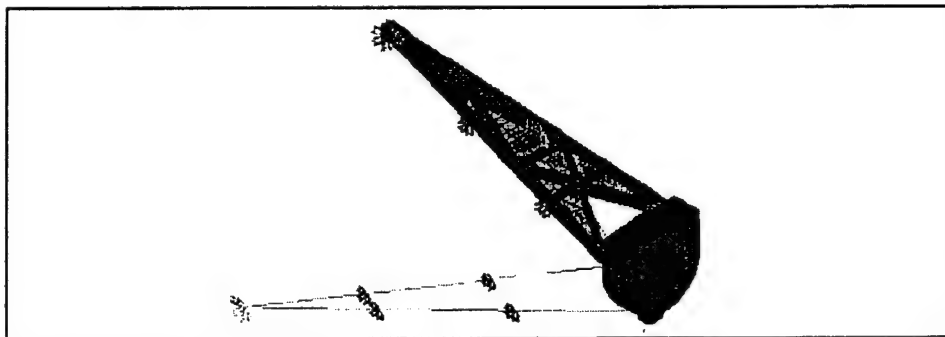


Figure 3.11. Muzzle Restraint Assembly.

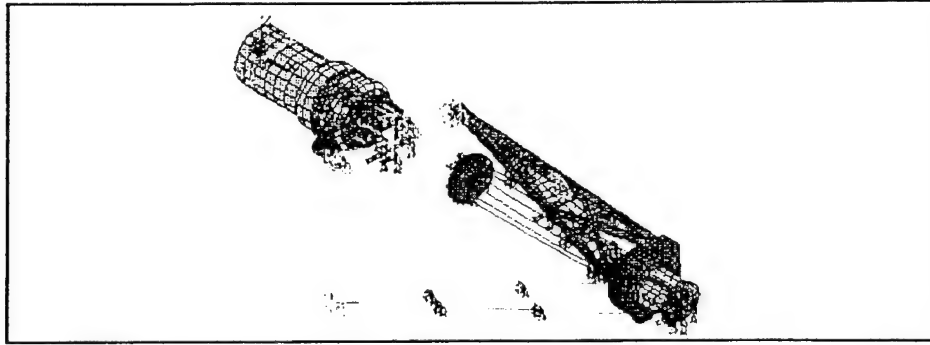


Figure 3-12. Restrained M61A1 PHALANX Gun.

C. ANSYS POST-RUN ANALYSIS

Once a finite-element model is created within ANSYS, several types of analysis may be conducted. These include modal analysis, harmonic analysis, transient analysis, and animation of the mode shapes. Since the vibrational behavior of the gun is of primary interest, only modal analysis, harmonic analysis and modal animation were used in this investigation.

1. Modal Analysis and Animation

Calculation of the natural mode frequencies and the corresponding mode shapes is the first step in computing the vibrational behavior of the entire M61A1 PHALANX gun. As detailed in Reference [11], this corresponds to the calculation of the eigenvalues (natural frequencies) and eigenvectors (eigenfunctions) which yield the mode shapes (displacements) of the vibration. Determination of the mode shapes is also known as "mode expansion" in ANSYS terminology. The number of desired modes and mode shapes are selectable within the ANSYS software. For this investigation, only the first twenty to fifty modes were explored, since program execution time is proportional to the number of modes "expanded."

Vibrational mode types observed using this model include vertical and horizontal displacement-type, axial (recoil-like effect of the gun), and torsional (or twisting) of the barrel

assemblies about the X (axial) axis. Only the vertical and horizontal displacements are of interest, since their contributions dominate the bullet dispersion effect.

Once the mode shapes are found, they may be displayed as static views , or they may be "animated" by computing a series of "stills" for a number of phases of each mode. These are stored in a graphics file. Display of these frames in rapid succession produces a "cartoon-like" animation of each mode shape. The animation views chosen in this investigation are isometric.

2. Harmonic Analysis

Once the modes of vibration are determined, it is useful to explore the harmonic response of the model gun to applied forces in the Y-and Z-(horizontal and horizontal) directions. This allows determination and confirmation of which modes are present in each cartesian direction. Since the goal of this investigation is to validate the model against experimentally-determined modes for a laboratory gun, the point of excitation (point of force application) and the response points should closely match those chosen in the experimental laboratory gun.

In order to match the experimental set-up discussed in Chapter II, a numerical "force" of one pound was applied to the FEM Node 5443, which is close to the center of the forward portion of the muzzle clamp assembly. This "force" was applied first horizontally and then vertically to simulate the laboratory excitation of the actual gun. ANSYS calculated the harmonic response for five points along the length of the top-most barrel (at top dead center). These points were nearly identical to those chosen for the true gun discussed in Chapter II.

Element Designation	Description	Usage in Model
BEAM4	3-D Elastic Beam	Gun Barrels
COMBIN14	Spring/Damper	Bearings and Joints
MASS21	Structural Mass	Muzzle End of Barrels
PIPE16	Elastic Straight Pipe	Barrels at Stub Rotor End, Muzzle Restraint Support Arms
SHELL63	Elastic Shell	Stub Rotor, Muzzle Restraint Upper Support Cladding, Muzzle Clamp, Ball Bearing Races
SOLID45	Structural Solid	Stub Rotor, Mid-Barrel Clamp, Muzzle Clamp, Rotor and Gun Body, Muzzle Restraint Upper Support Arm Grid

Table 3-1. Element Types and Usages in ANSYS Finite-Element Model.

IV. EXPERIMENTAL RESULTS

A. INTRODUCTION

When conducting a modal analysis of a system, one generally assumes that the structure being tested behaves linearly, so that the response is proportional to the excitation [Ref 3]. This implies that the measured frequency response functions (FRF's) are not dependent on the excitation. Before conducting a modal analysis of the PHALANX gun system, two tests were conducted to validate the linearity assumption. First, frequency response functions (FRF's) were recorded and compared with and without the axial load set-back previously discussed in Chapter II. Second, frequency response functions were recorded for a range of voltages applied to the shaker [Ref 6]. The results of linearity testing are discussed in the next section.

After testing the gun for non-linearities, frequency response functions (FRF's) were taken for all five configurations by the H-P analyzer. The results are summarized in section C. The complete record of FRF's for all five configurations can be found in Appendices C through G. Each appendix has the FRF analyzer traces recorded for each configuration. The importance of these traces is that they were the data sources used to identify the resonance peaks, from which curve fit bands (to determine modal parameters) were selected (see Appendix A).

Following the recording of FRF's, these were analyzed using STARModal [Ref 16] and modal frequencies and mode shapes were obtained. These are presented in sections D and E. These modal parameters and the display of the modes in animation were compared with the mode frequencies and shapes obtained using the finite-element model (FEM) discussed in Chapter V. Appendices C through G show the modal shapes derived by STARModal and tables of amplitudes and phase angles for each mode for all five configurations.

B. LINEARITY RESPONSE TESTING

In the first set of linearity tests, frequency response function (FRF) measurements taken without and with an axial load applied to the gun were compared. The same excitation force level was applied to the shaker for both gun arrangements and the FRF was measured for the accelerometer located at the drive point (see Figure 2-4). Figure 4-1 shows the FRF's for both gun arrangements, with and without the axial load. The similarity between the two traces shows that the dependence of the modal response on the gun axial load is small. All discrepancies were small compared to the levels of prominent peaks for the measured frequency range. These results are consistent with prior NPS experiments conducted on the PHALANX gun [Ref 5].

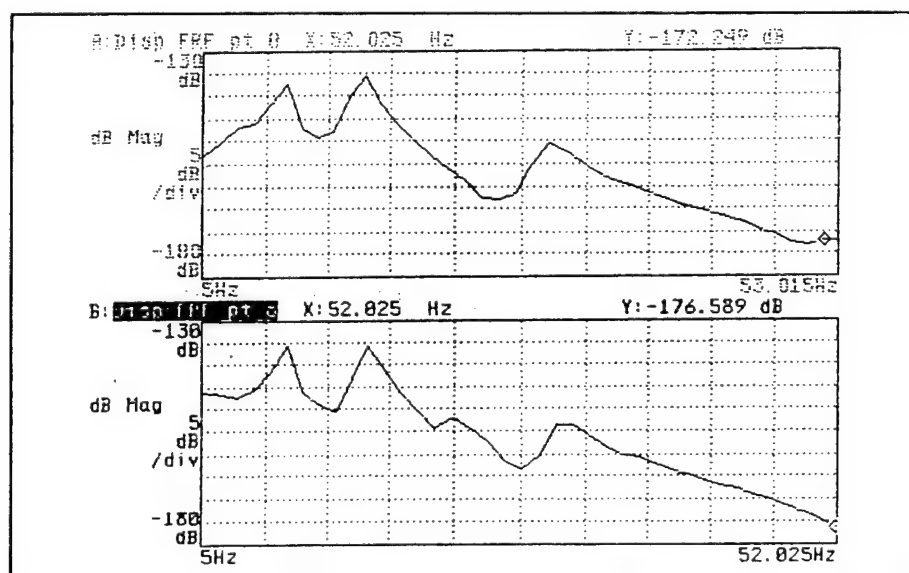


Figure 4-1. FRF's Recorded With (Top) and Without (Bottom) Gun Axial Load.

In the second set of linearity tests, various force levels were applied to the barrel-tip and the resulting FRF's were recorded. The observed frequencies for each mode were tabulated for each force level. Table 4-1 lists the frequency observed for each mode for the force level given.

The lowest force level was 0.5 N and the highest was 7.0 N. The lower force level limit was chosen because it was the lowest level at which noise in the system is negligible; the upper limit was the force level at which the ENDEVCO signal conditioner started to overload.

Mode	0.5 N	1.0 N	2.0 N	3.0 N	4.0 N	5.0 N	6.0 N	7.0 N
1	11.04	11.08	10.97	11.01	10.93	10.94	11.02	10.91
2	17.05	16.59	16.56	16.48	16.47	16.45	16.48	16.41
3	31.62	30.80	29.02	28.96	28.61	27.98	27.34	26.84

Table 4-1. Frequencies for Each Mode in Hz for Varying Force Levels.

Figure 4-2 is a graphic representation of table 4-1 and shows the modal frequency progression for each force level. Mode 3 shows the only significant variation in modal frequency with force. It is concluded that the PHALANX gun system behaves practically as a linear system for the forces in excess of about 2 N. For this reason the force level chosen to conduct the remaining experiments was 4 N.

The results of these two tests confirmed the assumption that the PHALANX gun system behaves practically linearly under test conditions.

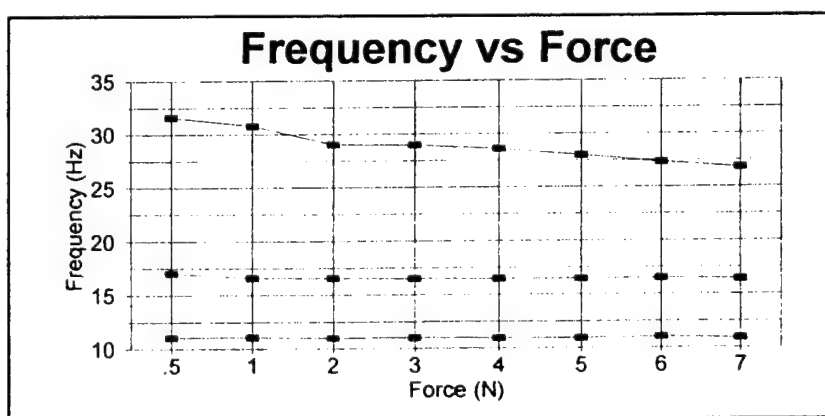


Figure 4-2. Frequency vs Force Level.

C. FREQUENCY RESPONSE FUNCTION RECORDING

1. Configuration 1

A measurement set of eight FRF's representing data taken from each accelerometer location was recorded for configuration 1. Configuration 1 was only tested in the horizontal direction (Y-axis). The reason for this was that during testing it was discovered that there was excessive vibration of the gun cradle (isogrid). Significant vibration of the cradle in the lab is undesirable because it is not representative of the vibration of an actual gun cradle structure, which is bolted to the deck of a ship. To simulate the rigidity provided by a gun cradle bolted to the ship, six lead storage canisters weighing a total of approximately twelve hundred pounds were placed on top of the gun cradle. This additional weight provided sufficient rigidity to the gun cradle structure in the lab and its vibration was drastically reduced.

Appendix C shows the FRF's and modal parameters found for configuration 1 using STARModal. These results were not used to validate the finite-element model. To monitor the vibration of the gun cradle, an additional accelerometer mount was added to the back end of the gun cradle for test configurations 2 and 3.

2. Configurations 2 and 3

A measurement set of nine FRF's representing data taken from each accelerometer location was recorded for configuration 2 in both directions, horizontal (Y-axis) and vertical (Z-axis). A measurement set of eleven FRF's representing data taken from each accelerometer location was recorded for configuration 3 in both directions. Appendices D through G show all the FRF's for configurations 2 and 3 for both directions.

Since there are over forty FRF's for both configurations, one was chosen as an example. Figures 4-3 through 4-5 show the FRF's obtained for configuration 2, vertical direction (Zaxis) (Again, add 28.7 dB to these to obtain the FRF in dB re 1m/N). Three frequency response resonance peaks were identified using the H-P analyzer for accelerometer location 9, which is at the drive point. The first peak occurs at about 20 Hz, the second at about 70 Hz, and the third at about 110 Hz. These three peaks are present at approximately the same frequency in the FRF's for all other accelerometer locations. Note that the shape of each resonance peak remains well defined for all accelerometer locations.

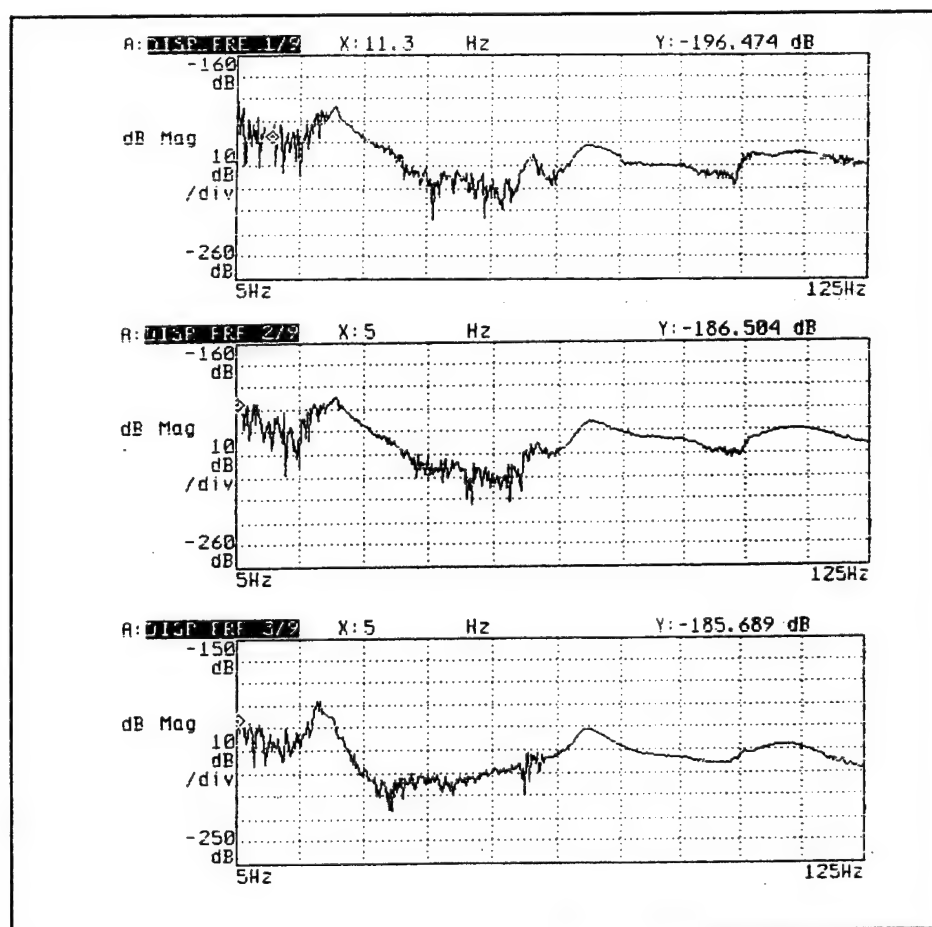


Figure 4-3. FRF's Recorded for Configuration 2, Z-Direction, Accelerometer Locations 1-3.

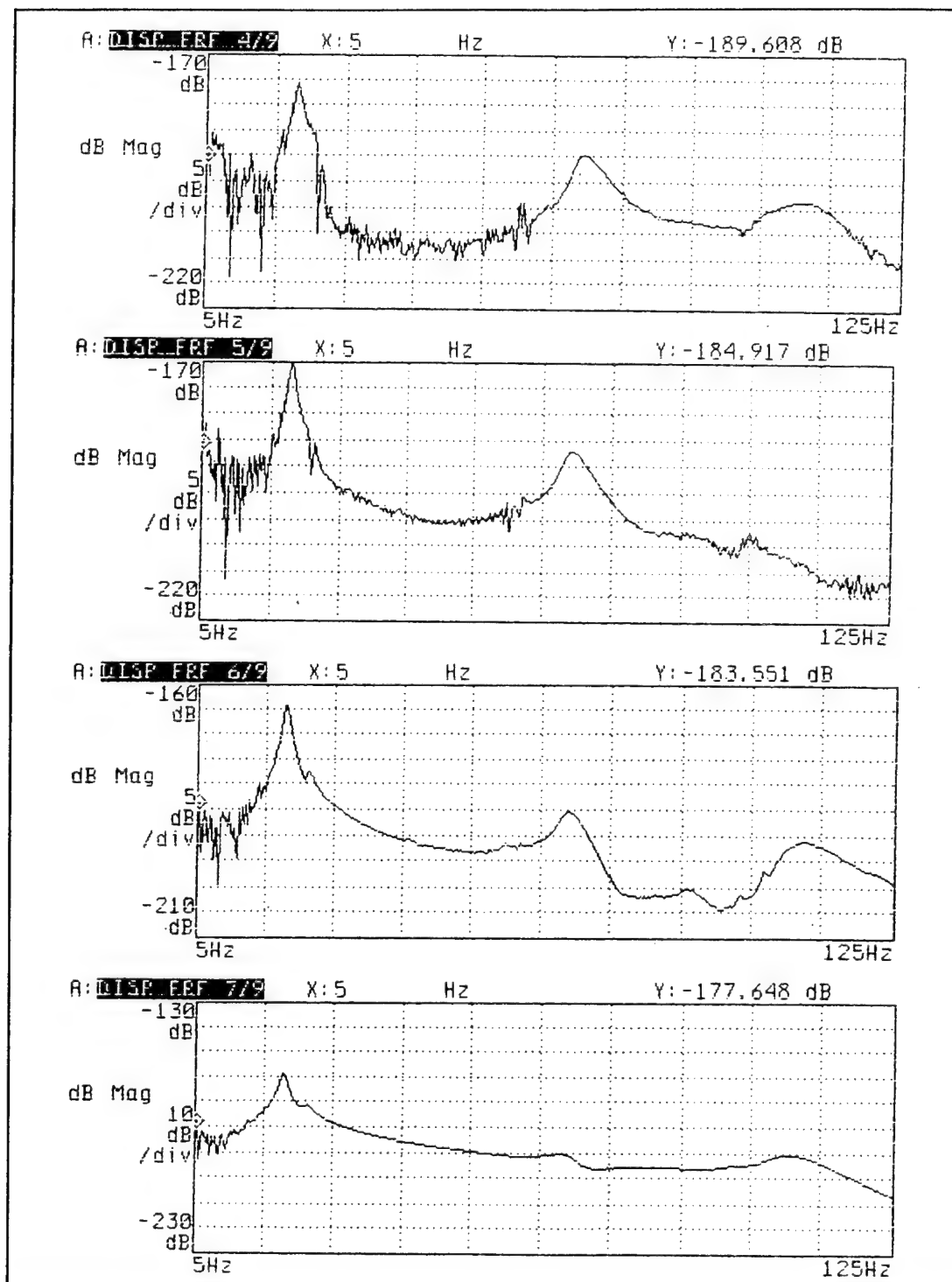


Figure 4-4. FRF's Recorded for Configuration 2, Z-Direction, Accelerometer Locations 4-7.

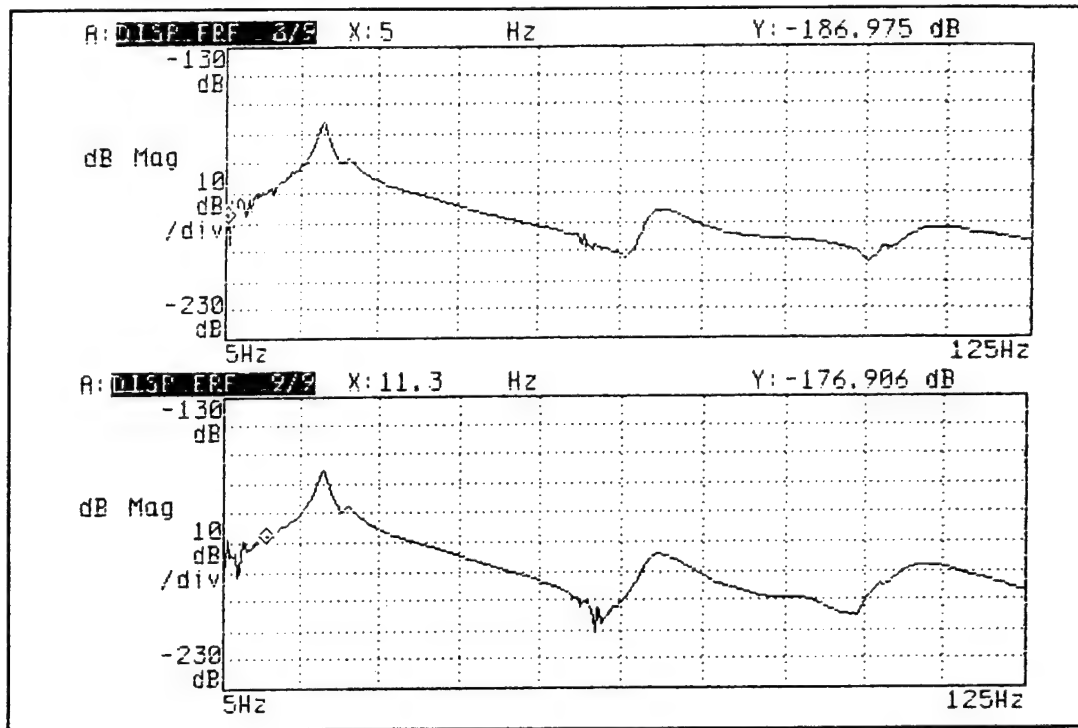


Figure 4-5. FRF's Recorded for Configuration 2, Z-Direction, Accelerometer Locations 8-9.

D. MODAL PARAMETERS EXTRACTED BY STARMODAL

Table 4-2 summarizes the modal frequencies and percent of critical damping that STARModal extracted from the data taken for the three configurations for all accelerometer locations. The corresponding mode shapes can be found in Appendices C through G. Three

MODE	CONFIG 1 Y-DIR	CONFIG 2 Y-DIR	CONFIG 2 Z-DIR	CONFIG 3 Y-DIR	CONFIG 3 Z-DIR
	Freq %Dmp	Freq %Dmp	Freq %Dmp	Freq %Dmp	Freq %Dmp
1	11.09 0.80	14.73 5.14	20.25 3.08	16.44 6.00	28.84 7.47
2	16.69 2.19	48.61 11.72	69.68 4.13	41.74 5.42	44.69 5.64
3	28.69 2.71	97.37 6.52	109.64 5.18	71.43 10.17	76.87 5.29
4				103.31 2.66	101.36 3.08

Table 4-2 . Modal Frequencies and Percent of Critical Damping for Each Configuration.

modal frequencies were identified for configuration 2 in the frequency range of 5 Hz to 125 Hz. Four modal frequencies were identified for configuration 3. Note that the fundamental frequency for the horizontal direction (Y-axis) is lower than for the vertical direction (Z-axis). This is the case also for configuration 3. It is worth noting that the same was found for the modal frequencies calculated using the finite-element model (Chapter VI) For the Z-axis, the modal frequencies obtained are consistent with previous experiments conducted on the same gun assembly [Ref 5].

E. MODAL SHAPES OBTAINED BY STARMODAL

Modal shapes derived by STARModal and a table of amplitudes and phase angles are included in Appendices C through G. They are arranged in numerical order. Again, configuration 2, vertical direction (Z-axis) is chosen as an example. Figures 4-6 through 4-8 show the mode shapes and frequencies for configuration 2 (Z-axis) (the amplitude scale is arbitrary). Three modes were identified in the measured frequency range.

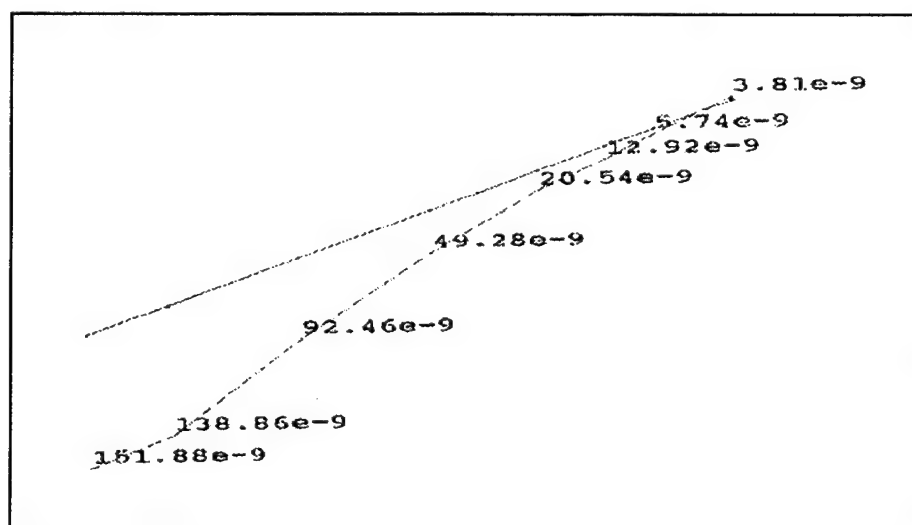


Figure 4-6. Configuration 2, First Z-Mode: 20.25 Hz.

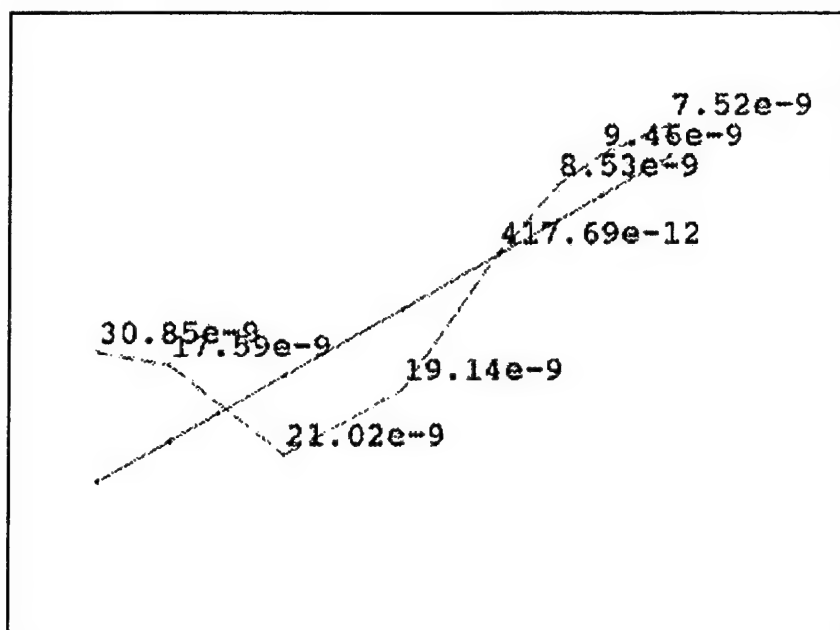


Figure 4-7. Configuration 2, Second Z-Mode: 69.68 Hz.

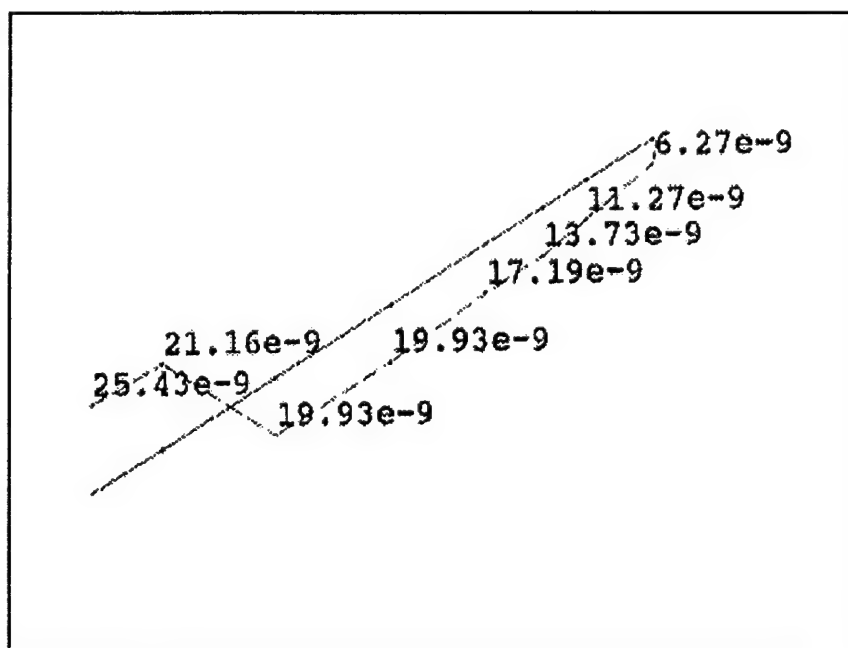


Figure 4-8. Configuration 2, Third Z-Mode: 109.64 Hz.

The mode shapes derived by STARModal can be animated so that they can be compared with those obtained using the finite-element analysis (FEM) method. This comparison is one of the main tools in validating the results obtained by computer simulation. Chapter V discusses the results of several attempts to correlate the experimentally measured and finite-element model calculated modal parameters.

V. FINITE ELEMENT MODEL CORRELATION

A. INTRODUCTION

The experimental results reported in the previous chapter show the frequency of the first Y-Axis bending mode of the laboratory gun occurs at about 14 Hz. However, the original (unvalidated) ANSYS model calculated a first Y-axis bending mode frequency at about 29 Hz, nearly twice the observed value. Computed frequencies of higher-order modes were also at least twice as high as those observed in the laboratory experiments discussed in Chapter IV. Therefore, the final objective in this investigation is to modify the original unvalidated ANSYS finite-element model to obtain results which closely match the experimentally observed modal parameters obtained in the laboratory. This chapter describes efforts to determine values for the most important parameters in the finite element model, namely the ball joint, needle bearing and ball bearing stiffnesses, in order to obtain the best agreement with experiments.

B. PRELIMINARY MODIFICATIONS

Before investigating critical stiffnesses, several unrelated ANSYS command script file modifications were made which were not related to these stiffnesses. Changes were required to update the ANSYS command syntax and to correct the boundary conditions of the original model to emulate the laboratory gun.

The finite element model created in 1993 by Mike Hatch used the 4.4a version of ANSYS [Ref. 17]. The Physics Department Phalanx Gun Lab received the subsequent ANSYS 5.0 version [Ref. 12] in the Summer of 1995. Several weeks of preliminary work involved changing much of the command syntax within the two-thousand line ANSYS batch command script (BRIEF text file) to reflect the changes in the new version of the ANSYS software.

Additional modifications were made in order to make the model more closely agree with the laboratory arrangement. For example, a portion of the script which "couples" several nodes in the rotor/gun body assembly to simulate the pneumatic motor-to-gear drive engagement which rotates each of the six barrels into firing position on an operational PHALANX system, was deleted. This was done because the laboratory gun does not have a drive motor or driving gear assembly and is free to rotate about the x-axis. The removal of this rotational constraint results in a rigid-body "pure rotational" mode of zero frequency, which will be seen later in the chapter. In addition, rotational constraints about the y-axis were deleted for the original model of the recoil adapter-to-isogrid nodes to better simulate the pin-and-clevis attachment points found in the laboratory and operational gun.

C. INVESTIGATIONS OF CRITICAL STIFFNESSES: UNRESTRAINED GUN

1. Stiffness Modifications by Trial and Error Using Y Bending Mode Frequencies

The only parameters of the finite-element model which were considered not well known were the stiffness values of the three bearing assemblies: the ball bearing, needle bearing, and ball joint. The values initially chosen were based on the simulation of bearing properties given bearing size, number of balls, bearing loads, etc. Five cases were considered in investigating the stiffnesses of the bearings. Case 1 has the unmodified (original) model stiffnesses. In cases 2,3 and 4, one and only one of the three bearing stiffnesses was reduced by a factor of a 100. In case 5, all three bearing stiffnesses were simultaneously reduced by a factor of 100. These cases are summarized in Table 5-1 and their effects on the modal frequencies are discussed below.

Case	Ball Joint	Needle Bearing	Ball Bearing
1	442.50	1220.0	856.61
2	4.4250	1220.0	856.61
3	442.50	12.20	856.61
4	442.50	1220.0	8.5700
5	4.42	12.2	8.57

Table 5-1. Reduced Bearing Stiffness Cases (klb/in).

Table 5-2 shows a synopsis of the ANSYS results for the modal frequencies for the first three Y bending modes for the five cases. Note that only reducing the needle bearing stiffness (case 3) has a drastic effect on the frequency of the first Y bending mode. Reducing only the ball bearing stiffness (case 4) tends to have a greater effect on the frequency of the second Y bending mode, but not on the first. Reducing only the ball joint stiffness (case 2) greatly affects all three bending mode frequencies. Reducing all three stiffnesses by a factor of 100 (case 5) produces the best agreement with the experiment, especially for the second and third Y bending mode frequencies.

Mode No.	Y-Modal Frequencies					
	Exp Freq	Case 1	Case 2	Case 3	Case 4	Case 5
1	14.7	28.6	16.2	16.9	19	10.3
2	51.77	103.1	86.6	95.6	77.2	50.3
3	91.57	150.4	108.9	124.2	122	91.3

Table 5-2. Modal Frequencies for Stiffness Cases.

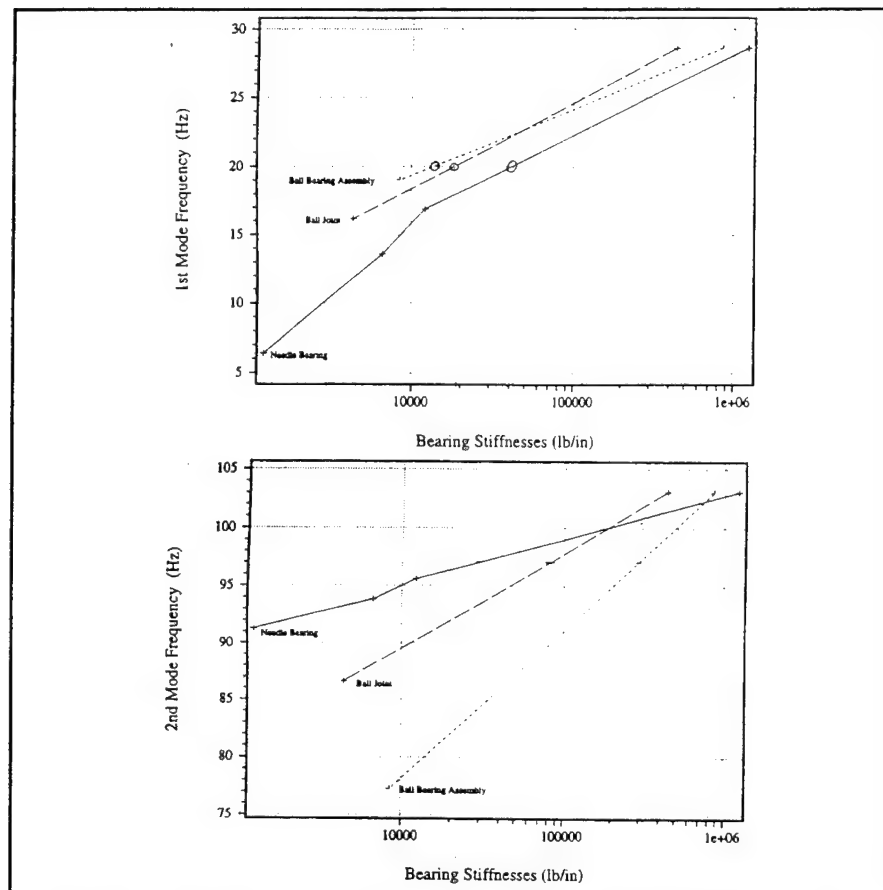


Figure 5-1. Stiffness Effects on 1st (top) and 2nd (bottom) Ymode.

Bearing	Stiffness (lb/in)
Ball Bearing	8566.07
Needle Bearing	12200.0
Ball Joint: Lower Vertical and Horizontal Springs	4425.0
Ball Joint Upper Spring	221250.0

Table 5-3. Final Bearing Stiffnesses.

The determination of final stiffness values for the three bearings was accomplished more or less by "trial and error" in the observation of over fifty ANSYS FEM iterations using various combinations of bearing stiffness. Although stiffness values in the range of several thousand lb/in seemed extremely low for a structure such as the M61A1 gun, these greatly reduced values produced modal frequencies and mode shapes which were much more consistent with both previous and current experimental data.

2. Stiffness Modifications : Matrix Method Using Y Bending Mode Frequencies

Another method investigated for estimating the stiffness values for all three bearing assemblies involved using a "matrix method" to linearly extrapolate the required changes to the original model stiffnesses for each bearing. One at a time, the stiffnesses for each bearing assembly were reduced by a factor of ten from the original values, in three steps. Figure 5-1 shows a plot of these results. A total of nine modal analyses were conducted using the ANSYS FEM and the corresponding modal frequencies were recorded. The ratios of the changes (from original) in the 1st, 2nd and 3rd Y modal frequencies to the changes in each stiffness were used to create a 3X3 derivative matrix. This matrix is shown in equation 5-1, where the numerator subscripts 1,2, and 3 denote the mode number. The units are Hz/(lb/in). In the denominator, these subscripts denote the frequencies and stiffnesses for the needle bearing, ball joint and ball bearing respectively.

$$\begin{bmatrix} \frac{\Delta f1}{\Delta s1} & \frac{\Delta f1}{\Delta s2} & \frac{\Delta f1}{\Delta s3} \\ \frac{\Delta f2}{\Delta s1} & \frac{\Delta f2}{\Delta s2} & \frac{\Delta f2}{\Delta s3} \\ \frac{\Delta f3}{\Delta s1} & \frac{\Delta f3}{\Delta s2} & \frac{\Delta f3}{\Delta s3} \end{bmatrix} = \begin{bmatrix} 9.6e-6 & 28.4e-6 & 11.2e-6 \\ 6.2e-6 & 38.8e-6 & 30.42e-6 \\ 22.0e-6 & 94.7e-6 & 33.4e-6 \end{bmatrix} \text{ (Hz/(lb/inch))}, \quad (5-1)$$

Assuming a linear relation between changes in stiffness and changes in modal frequencies, the inverse of this matrix may be used to estimate the changes in bearing stiffnesses required to change the modal frequencies by a certain amount, as shown in Equation 5-2.

$$\begin{bmatrix} \Delta s1 \\ \Delta s2 \\ \Delta s3 \end{bmatrix} = \begin{bmatrix} \frac{\Delta f1}{\Delta s1} & \frac{\Delta f1}{\Delta s2} & \frac{\Delta f1}{\Delta s3} \\ \frac{\Delta f2}{\Delta s1} & \frac{\Delta f2}{\Delta s2} & \frac{\Delta f2}{\Delta s3} \\ \frac{\Delta f3}{\Delta s1} & \frac{\Delta f3}{\Delta s2} & \frac{\Delta f3}{\Delta s3} \end{bmatrix}^{-1} \cdot \begin{bmatrix} \Delta f1 \\ \Delta f2 \\ \Delta f3 \end{bmatrix}, \quad (5-2)$$

$$\begin{bmatrix} \Delta s1 \\ \Delta s2 \\ \Delta s3 \end{bmatrix} = \begin{bmatrix} 3.12e5 & -.221e5 & -.846e5 \\ -.91e5 & -.146e5 & .438e5 \\ .525e5 & .56e5 & -.387e5 \end{bmatrix}^{-1} \cdot \begin{bmatrix} \Delta f1 \\ \Delta f2 \\ \Delta f3 \end{bmatrix} \quad ((inch/lb)/Hz), \quad (5-3)$$

Taking $\Delta f1 = -13.9$ Hz, $\Delta f2 = -51.3$ Hz, $\Delta f3 = -58.8$ Hz, (Experimental values minus Case 1), the changes for needle bearing, ball joint and ball bearing stiffness computed using this procedure are, respectively :

$\Delta s1 = 1.77e6$ (lb/in), $\Delta s2 = -.56e6$ (lb/in), $\Delta s3 = -1.33e6$ (lb/in). The resulting values for the stiffnesses are $s1 = 2.99e6$ (lb/in), $s2 = -1.21e5$ (lb/in), $s3 = -4.77e5$ (lb/in).

Table 5-3 shows a comparison of the original and calculated stiffness values. Clearly negative values for stiffness cannot be correct. We conclude that the gun system is not sufficiently linear to us this method with only one iteration. Additionally, given the amount of

error in the original stiffness values, it is questionable whether this method would ever work at all. A multi-iterative process is required. Each iteration requires a day of execution time, therefore this technique was abandoned for this portion of the investigation.

Original Stiffness Values (lb/in)	Matrix Stiffness Values (lb/in)
Ball Joint: 442500	-560000
Needle Bearing: 1220000	+1770000
Ball Bearing: 856607	-1330000

Table 5-4. Comparison of Extrapolated Stiffnesses With Original Values.

3. Anisotropy of Ball Joint Assembly; Further Stiffness Modifications by Trial and Error Using Z Bending Mode Frequencies

Because the bearing assemblies were modeled as isotropic elements within ANSYS, the modal frequencies and shapes for both the horizontal (Y) and vertical (Z) directions are nearly identical (within 2 Hz). Observed experimental values reported in Chapter IV and Appendix D show that such isotropic modal behavior does not occur in the actual gun. Corresponding horizontal and vertical modes may differ in frequency as greatly as 20 Hz. Once correlation in the horizontal direction was obtained, further investigation into the construction of the bearing assemblies was required to ascertain the cause of the anisotropic behavior. The most likely source to consider is the ball joint. It is modelled as an octagon of solid elements which serve as connection points for four orthogonal linear springs (see Chapter III). The ball joint of the actual gun contains a "notch" which is cast into the bottom of the joint. The effect of this is reduced stiffness in the vertical direction. Several ANSYS modal analyses were carried out in which the

two horizontal springs (Y-axis) and the lower spring oriented in the vertical direction (Z-axis) were reduced by a factor of fifty as compared to the upper spring. This effort brought the frequencies of the first three Z-bending modes within a reasonable range of the experimental values. These values are shown in Table 5-3.

4. Final Stiffness Values and Resulting Modal Frequencies

The resulting modal frequencies, mode types and mode shapes are detailed in Table 5-4 and Figure 5-2 through Figure 5-7 for the final stiffness values reported above for the unrestrained gun. Note that only bending modes are considered in Figures 5-2 through 5-7, since these are the only displacements measured by experiment in Chapter IV and are assumed to be responsible for some portion of projectile dispersion phenomenon.

Mode Number	Experimental Frequency (Hz)	Calculated Frequency (Hz)	Mode Type
1	-	0.0	Rotational (pure)
2	14.73	13.62	1st Y (Lateral)
3	-	15.33	1st Axial
4	20.25	18.713	1st Z (Elevation)
5	-	39.665	1st Torsion
6	51.77	51.767	2nd Y (Lateral)
7	69.83	77.540	2nd Z (Elevation)
8	91.57	91.568	3rd Y (Lateral)
9	109.7	114.53	3rd Z (Elevation)
10	-	123.24	2nd Axial

Table 5-5. Modal Frequencies for Final Bearing Stiffness.

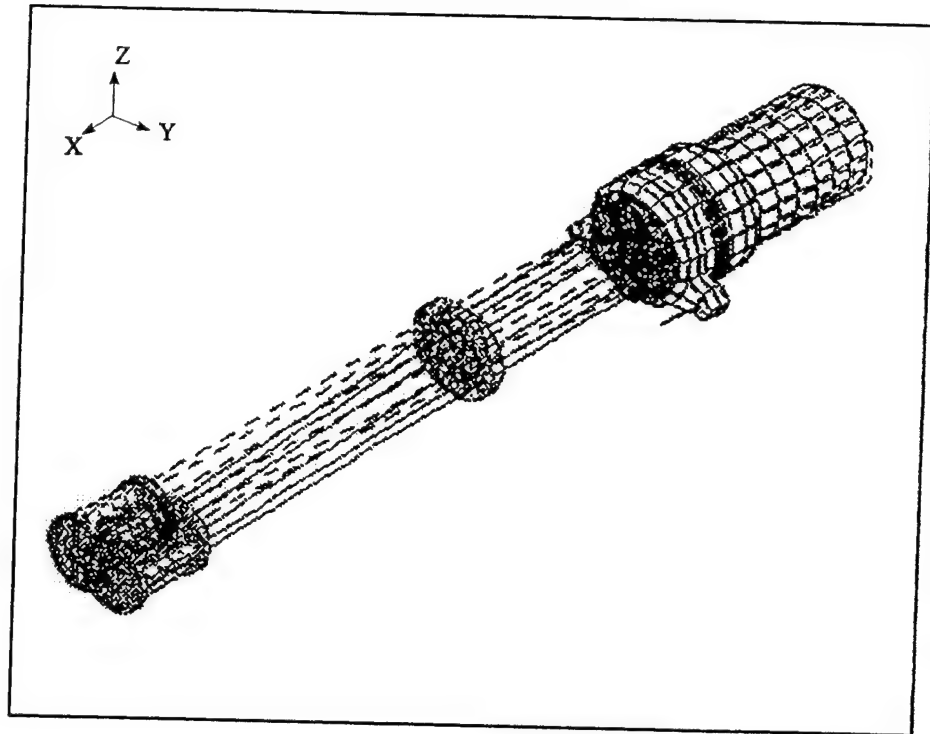


Figure 5-2. 1st Y Mode: 13.62 Hz.

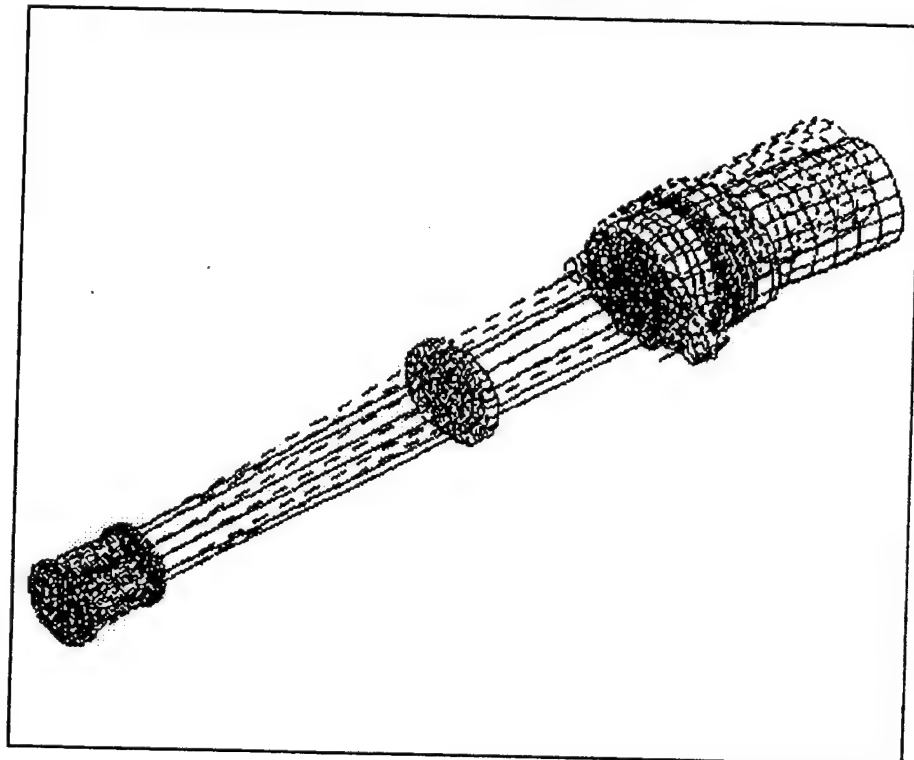


Figure 5-3. 2nd Y Mode: 51.77Hz.

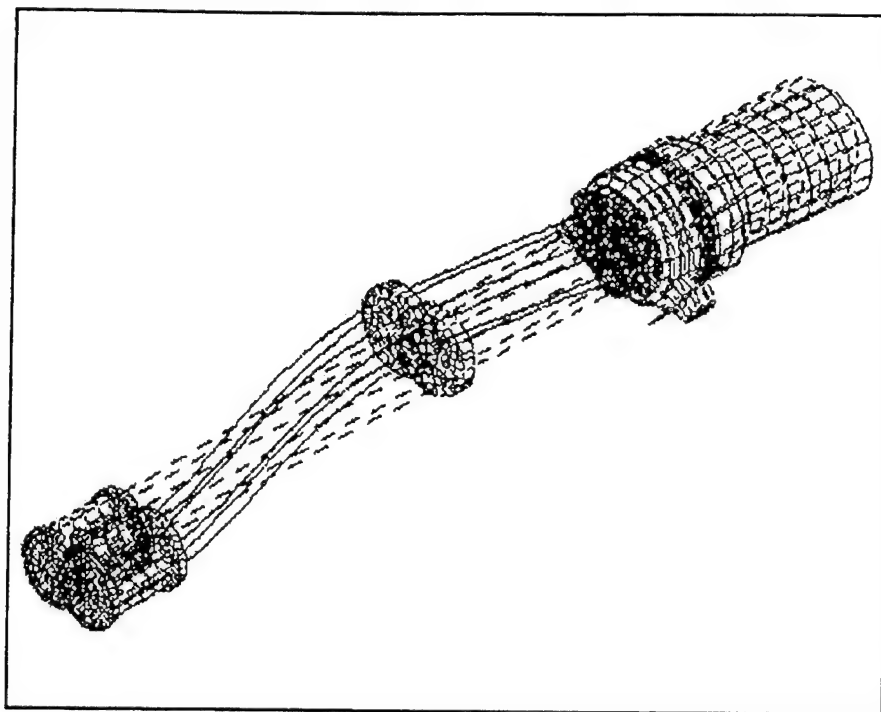


Figure 5-4. 3rd Y Mode: 91.57 Hz.

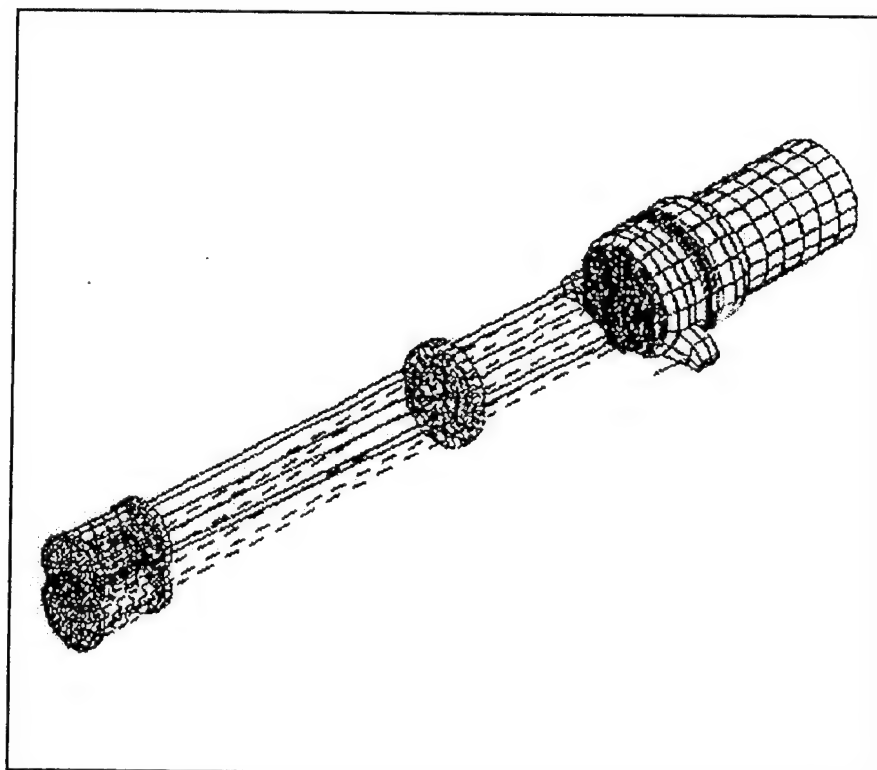


Figure 5-5. 1st Z Mode: 18.71 Hz.

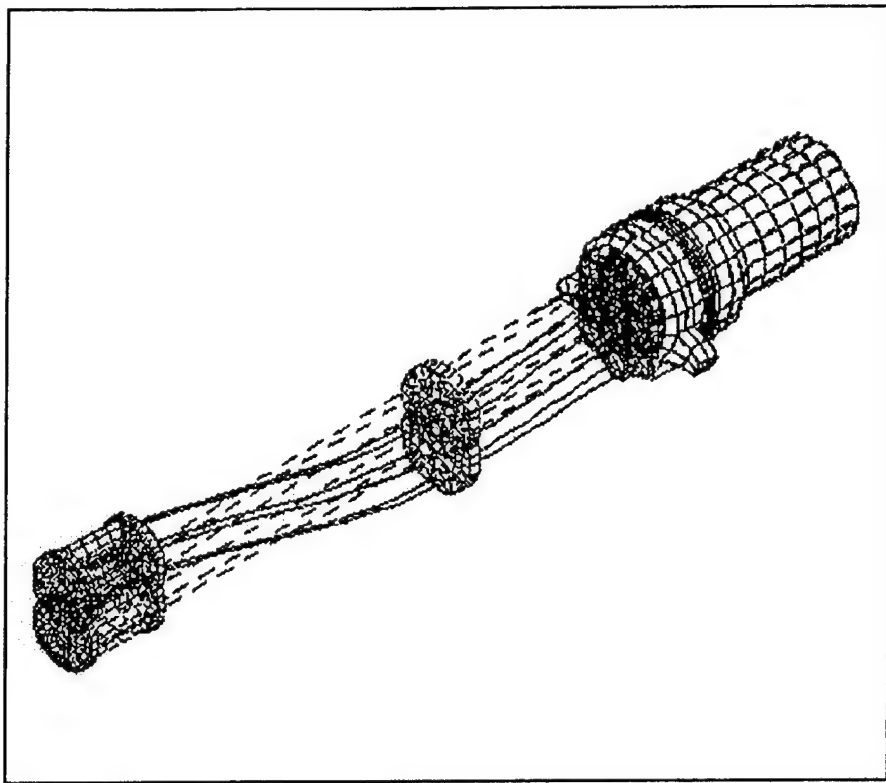


Figure 5-6. 2nd Z Mode: 77.54 Hz.

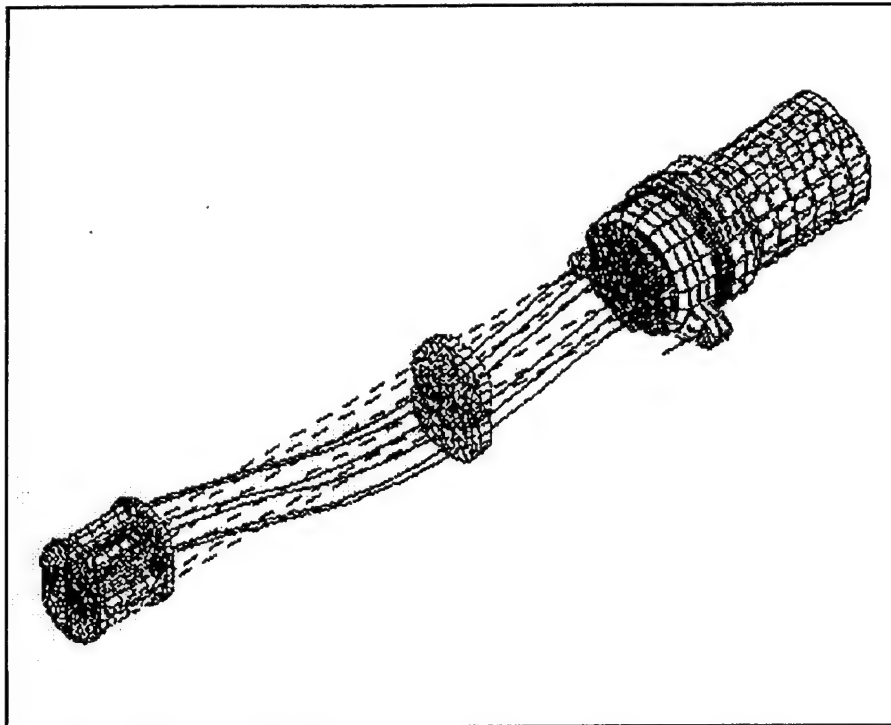


Figure 5-7. 3rd Z Mode: 114.53 Hz.

The extremely low bearing stiffnesses required to obtain such closely matching results is felt to be primarily due to the modeling of the gun body assembly. Figure 5-8 is the blue-print of the gun body assembly found in the actual M61A1 gun. Note the many cut-outs and reinforcements which are cast or machined into the real gun body for attachment of other assemblies, access, etc. Such provisions result in a structure which is much less rigid than a solid-cylinder such as represented in the finite-element model, (See Figures 3-7 and 3-8). Therefore, bearing assembly stiffness must be lowered drastically within the model to account for the absence of detail and realistic gun body rigidity.

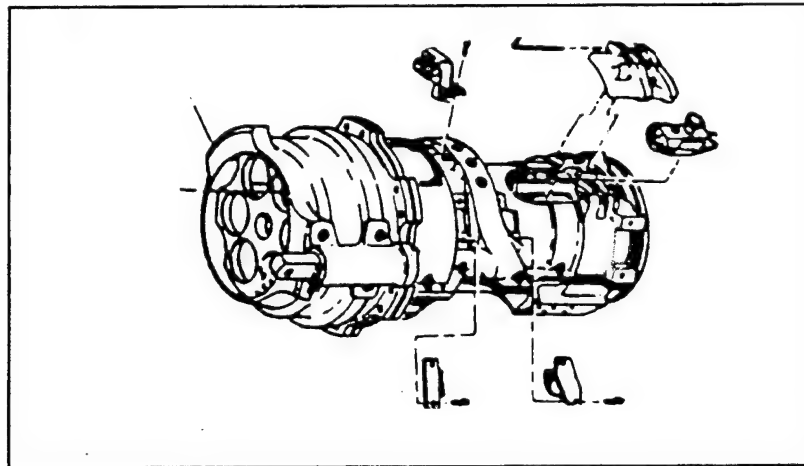


Figure 5-8. Actual M61A1 Gun Body Assembly.

D. HARMONIC RESPONSE: UNRESTRAINED GUN

The utility of harmonic analysis was discussed in Chapter III. Figures 5-9 and 5-10 show the harmonic response at the barrel-tip of the (final) model gun to an applied force of one pound at the node closest to the center of the muzzle clamp (node 5443). Five percent damping was used, as this is the average value of damping observed in the experimental data reported in Chapter IV. Appendix J shows the harmonic response for this and other points (nodes) of the

model gun selected to correspond as closely as possible to the measurement points. The modes that are excited correspond to those shown in Table 5-4 and Figures 5-2 through 5-7. The peak at 40 Hz in Figure 5-9, labeled with a "T" occurs due to the excitation of the first torsional mode. This mode is excited because the force (at node 5443), is not applied along the centerline of the gun (X-axis).

Figures 5-9 and 5-10 also show the experimental FRF (transfer function) and FEM harmonic response plots at the barrel-tip. The torsional mode at 40 Hz is not excited. The mode at about 50 Hz in the FRF is the second Y-mode. It is not visible in the computer response. The right hand side of each experimental FRF graph is marked with the displacement value for a 1 lb (4.5 N) applied force. Note that the first two modes ("1" and "2" the Figures 5-8 and 5-10) for

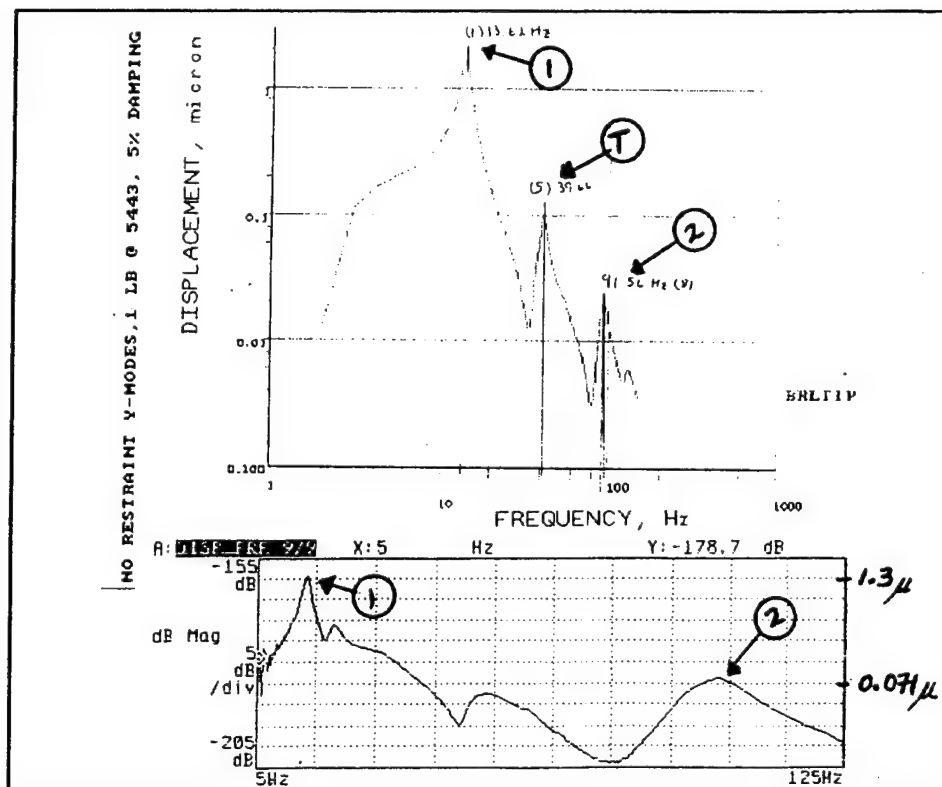


Figure 5-9. Horizontal (Y) FEM (top) and FRF Harmonic Response (bottom).

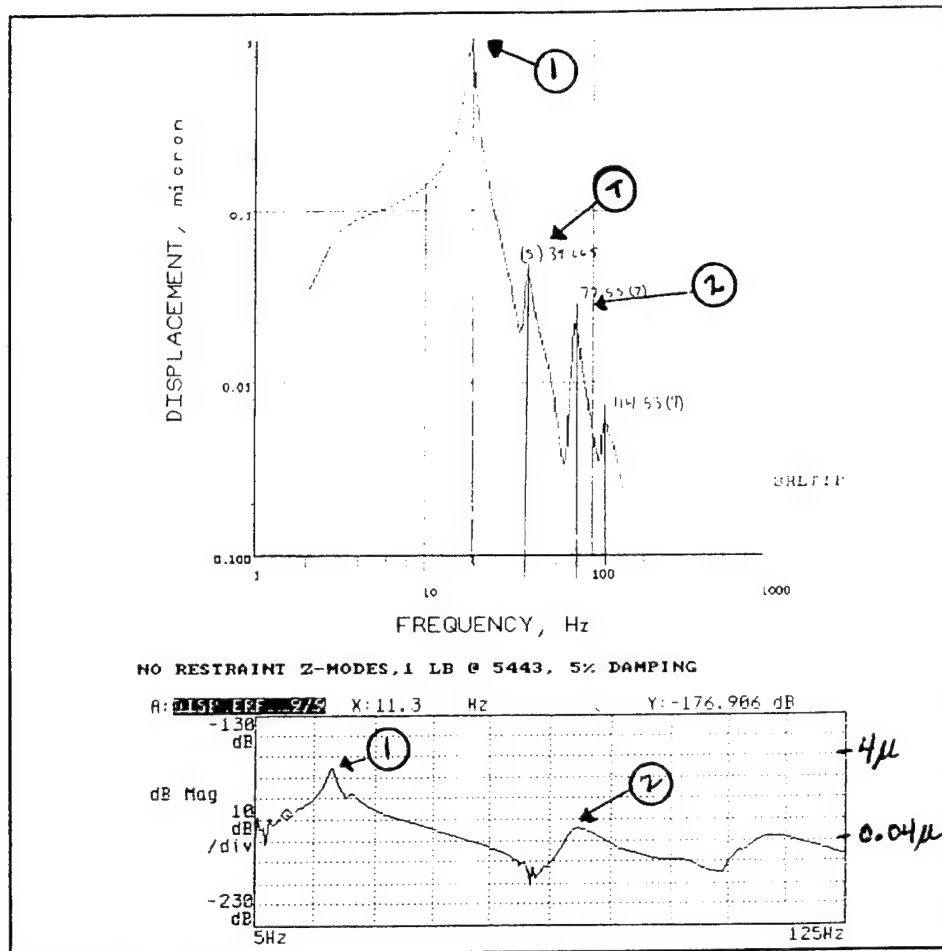


Figure 5-10. Vertical (Z) FEM (top) and FRF Harmonic Response (bottom).

both the horizontal and vertical directions show a good match in both frequency and magnitude (within a factor of 2).

E. MODAL BEHAVIOR-RESTRAINED GUN

A modal analysis of the gun with the addition of the muzzle restraint was conducted using the best values of bearing stiffness, as described in the previous section. Table 5-5 shows the frequencies of the first three vertical modes of vibration found by ANSYS as compared to the experimental values found in Chapter IV. There is great disagreement in the results. Potential reasons for this are several. First, it is suspected that a portion of these discrepancies are the

result of barrel-tip droop which occurs when the muzzle restraint is installed. As an example, the barrel tip was displaced by 0.2 millimeters downward when the restraint was added for the second set of experimental measurements. Such displacements effectively "pre-load" all of the bearings in the gun, which in turn could alter their stiffnesses and also their modal behavior. The ANSYS finite-element model does not account for this effect. To eliminate droop as a potential cause of disagreement between the experimental and finite-element results, the muzzle restraint must be installed and adjusted so that the barrel tips are not displaced from their unrestrained configuration. Second, the attachment points of the muzzle restraint on the laboratory gun use a pin-and-clevis arrangement. At least two of these points demonstrated "play" in excess of 1 millimeter. The FEM assumes that all attachment points are perfectly rigid.

Vertical (Z) Modes	FEM (HZ)	Experimental Values
1	60.7	27.2
2	88.7	44.6
3	94.7	76.7

Table 5-6. Comparison of FEM and Experimental Restrained Gun Vertical Modes.

VI. CONCLUSIONS

A. SUMMARY

Experimental and finite-element modal analysis of a PHALANX gun assembly were conducted in the laboratory at the Naval Postgraduate School. The main goals of these investigations were to provide an experimental set of modal parameters and to validate (and modify as appropriate) the finite-element model (FEM). The investigations were conducted with and without the production muzzle restraint used currently in the fleet.

The resulting correlation between the laboratory measurements and finite-element model calculations of gun modal parameters, i.e. frequencies and mode shapes, in the unrestrained condition is encouraging. A visual comparison of the modes was made by simultaneously examining both the computed FEM and STARModal animated mode shapes. Modal frequencies and shapes match very closely, although phase differences may be noted between the FEM and experimental mode-shape plots. Table 6-1 shows a comparison between the experimental and finite-element modal frequencies. Five of the six frequencies shown correlate well (within eight percent), but this was obtained only by using low stiffness values for the bearings as described in Chapter V. In addition, the resonance peaks in the FEM harmonic analysis plots closely match the experimental FRF plots in both frequency and magnitude. In the case of the gun with muzzle restraint, agreement between the experimental and finite-element results was poor. It is suspected that this is due to "play" in the actual muzzle restraint mounting system which is not modeled by the finite-element model.

Mode	Frequency (Hz), Experimental	Frequency (Hz), FEM	% Difference
First Horizontal (Y)	14.73	13.62	7.5
Second Horizontal (Y)	51.77	48.61	6.1
Third Horizontal (Y)	91.57	97.37	6.3
First Vertical (Z)	20.25	18.71	7.6
Second Vertical (Z)	69.83	77.56	11.1
Third Vertical (Z)	109.7	114.53	4.4

Table 6-1. Comparison of Experimental and Finite-Element Results (Unrestrained).

B. SUGGESTIONS FOR FOLLOW-ON INVESTIGATIONS

The finite-element model should be improved so that the gun body assembly closely matches the actual gun. This would entail detailed measurements and modeling of the various cut-outs and reinforcements described above. This would allow the inclusion of more reasonable figures for bearing stiffness, such as the original values found in Appendix J. A more disciplined method, of obtaining "exact" values might then be used with greater reliability.

The restrained gun presents an even more challenging problem. Measurements of the barrel-tip position should be taken in the unrestrained condition. Once the restraint is installed, it should be adjusted to return the barrel tips to their known, unrestrained displacement. FEM correlation could then be pursued using the unrestrained bearing stiffness values.

Finally, the effects of intentional misadjustment of the muzzle restraint could be explored on the experimental modal behavior of the gun. This would readily demonstrate the ramifications of improper installation/adjustment of the restraint by fleet personnel. Modal measurements could be taken in a variety of "distorted" configurations to identify the impact of such scenarios.

APPENDIX A. STARMODAL ANALYSIS SYSTEM

A. STARMODAL SOFTWARE

The frequency response spectra taken at all accelerometer locations for each configuration were translated into files that could be read by the Structural Measurement Systems (SMS) Structural Testing, Analysis, and Reporting (STAR) System [Ref 16] software using STAR's Disk Translator.

STARModal is one in a series of STAR System software products for testing and analyzing the dynamics of mechanical structures. It uses the FRF method to identify modal parameters and display the modes in animation. The FRF can either be imported directly via GPIB (IEEE488) interface bus or from disk storage.

The complete STARModal procedure from input of disk storage data to animation of structure modes can be found in Reference 16.

B. STARMODAL DATA PROCESSING

Using the FRF method, STARModal identifies the modal parameters of a structure. Frequency response functions made with the H-P signal analyzer are first stored on disk, then translated into STAR-compatible files by the disk translator for processing. During processing, an analytical model of the FRF is fit (in a least-squares sense) to the measured data and, as a result, the modal parameters are identified. This is the curve fitting process. [Ref 4] [Ref 5]

The procedure to identify modal parameters has several major steps. They are outlined in Table A-1. [Ref 5]

The first step in the modal parameter identification process is the determination of how many modes are present in the frequency range of the data. Each mode is represented by a peak in the data, called a resonance peak. There should be a peak at approximately the same frequency in the FRF for every measurement location. If a measurement point is at or near a node of a certain mode, where the mode shape is zero, the FRF will not show (much of) a peak for that mode. If a peak at a particular frequency is negligible or absent for a significant fraction of FRF's, modal parameters will not be identified by STARModal for that peak and there will not be a one-to-one correspondence between resonance peaks and modes. A local mode is one for which a modal peak does not appear in a large number of measurements, i.e. a mode with zero shape for many measurement locations. [Ref 5]

Table A-1. Major Steps of Parameter Identification in STAR.

- | |
|---|
| <ol style="list-style-type: none">1. Identify the number of modes in the measurements both visually and with STAR's Modal Peaks function.2. Set up curve fitting bands; this entails bracketing a frequency band for one or more modes, setting a mode number range, and selecting a curve fitting method.3. Use the Autofit feature in STAR to perform a simultaneous curve fit to data in the selected bands for all FRF's. |
|---|

Next is the bracketing of curve fitting bands, each band representing the width, or frequency range, of a resonance peak. The hand-selected data for all measurement locations will be simultaneously curve fit to analytic expressions for the FRF's using one of the methods offered by STARModal.

In the third step the user executes the STARModal autofit feature which performs the curve fitting. The data are fit to a polynomial function using the Rational Fraction Least Squares (RFLS) method. The modal frequencies, mode shapes, and the percent of critical damping (the modal parameters) for each mode are calculated. These values are stored in a table to be used in the animation display.

Examination of the results entails nothing more than clicking on the **Show Structure** command in the Gateway menu. The structure is automatically presented in the animation window, waving in its first mode.

A complete description of the use of STARModal to accomplish parameter identification can be found in Reference 16.

APPENDIX B. ANALYZER INPUT AND MEASUREMENT STATES

The input and measurement states of the HP 35665A analyzer used in this investigation are included to facilitate replication of the experiment. The measurement state includes the excitation characteristics as well as the analyzer display layout.

Inst Mode	[SINE]		2 Channel
	Capture	Off	
Meas Data	Data A	D2	Data B D2
Trac Coord	Coord A	dB Mag	Coord B dB Mag
Freq	Start	5 Hz	Stop 125 Hz
	Est Swp	1.1906 ks	
	Directn	Up	Spacing Linear
	Resoltn	AUTO	Min Res 401 Pnt/Swp
	Max Chg	2.5 %	
Avg	Settle T	15 Cycle	Int T 25 Cycle
	Fast Avg	Off	
Source	Level	95.394 mVrms	Ramp Rt 1 Vrms/S
	Auto Lvl	On	Ref Lvl 4 Vrms
	Ref Chn	Channel 1	Ref Tol 0.1 dB
	Max Src	120.01 mVrms	Max Inpt 100 mVrms

Figure B-1. Measurement State for H-P Analyzer During Data Collection.

Input	--- CHANNEL 1 ---	--- CHANNEL 2 ---
	Status On	Status On
	Range 3.5481 Vrms	Range 2.8184 mVrms
	EngrUnit Off	EngrUnit Off
	EU Label EU	EU Label EU
	EU Mult 1 V/EU	EU Mult 1 V/EU
	Auto Rng On	Auto Rng On
	Coupling AC	Coupling AC
	InputLow Ground	InputLow Ground
	ICP Off	ICP Off
	AliasFlt Off	AliasFlt Off
	A WtFltr Off	A WtFltr Off
	--- TACHOMETER ---	
	Puls/Rev 1	
	Level 0 V	
	Range +/- 4 V	
	Slope Positive	
	Holdoff 0 s	

Figure B-2. Input State for H-P Analyzer During Data Collection.

APPENDIX C. FREQUENCY RESPONSE FUNCTIONS AND MODAL SHAPES FOR CONFIGURATION 1, Y-DIRECTION

Gun configuration 1, Y-direction, had the topmost barrel at top dead center, a static load pulling back on the stub rotor to simulate the load during firing, no lead weights on top of the gun cradle, and no muzzle restraint.

Figures C-1 and C-2 show the frequency response functions (FRF) (horizontal displacement/horizontal force) measured for accelerometer locations 1 through 8 for this configuration. The dB magnitudes plotted in the FRF graphs have not been corrected using the transducer calibration and amplifier gains. For the FRF's in dB re 1m/N, add 28.7 dB to the plotted values.

STARModal identified three modes (Figures C-3 to C-6) in the 0-50 Hz excitation range for this configuration. The numbers on the shape plots are displacement in arbitrary units..

Table C-1 lists the amplitudes and phase angles computed by STARModal for configuration 1.

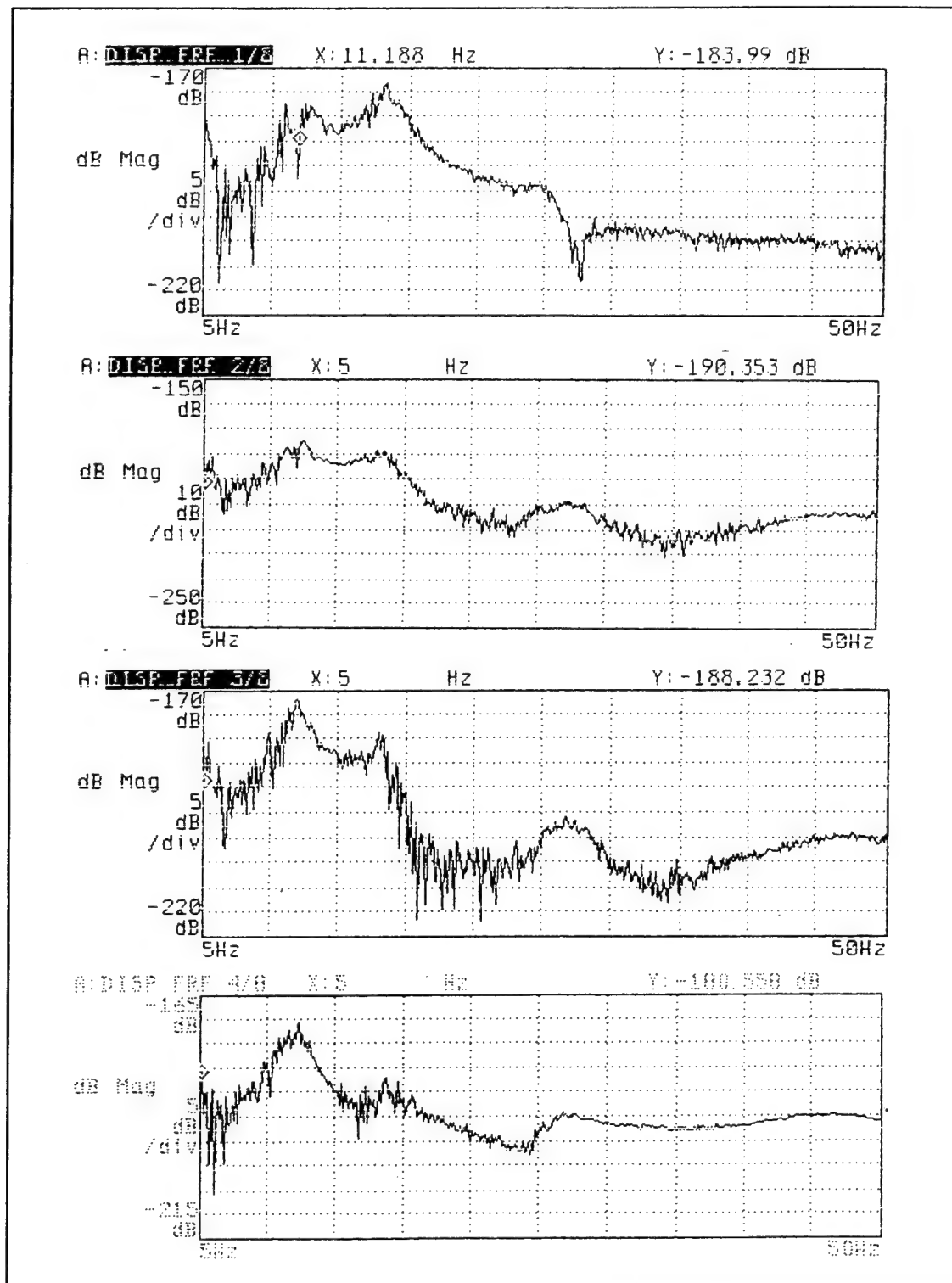


Figure C-1. FRF's Recorded for Configuration 1, Y-Direction, Accelerometer Locations 1-4.

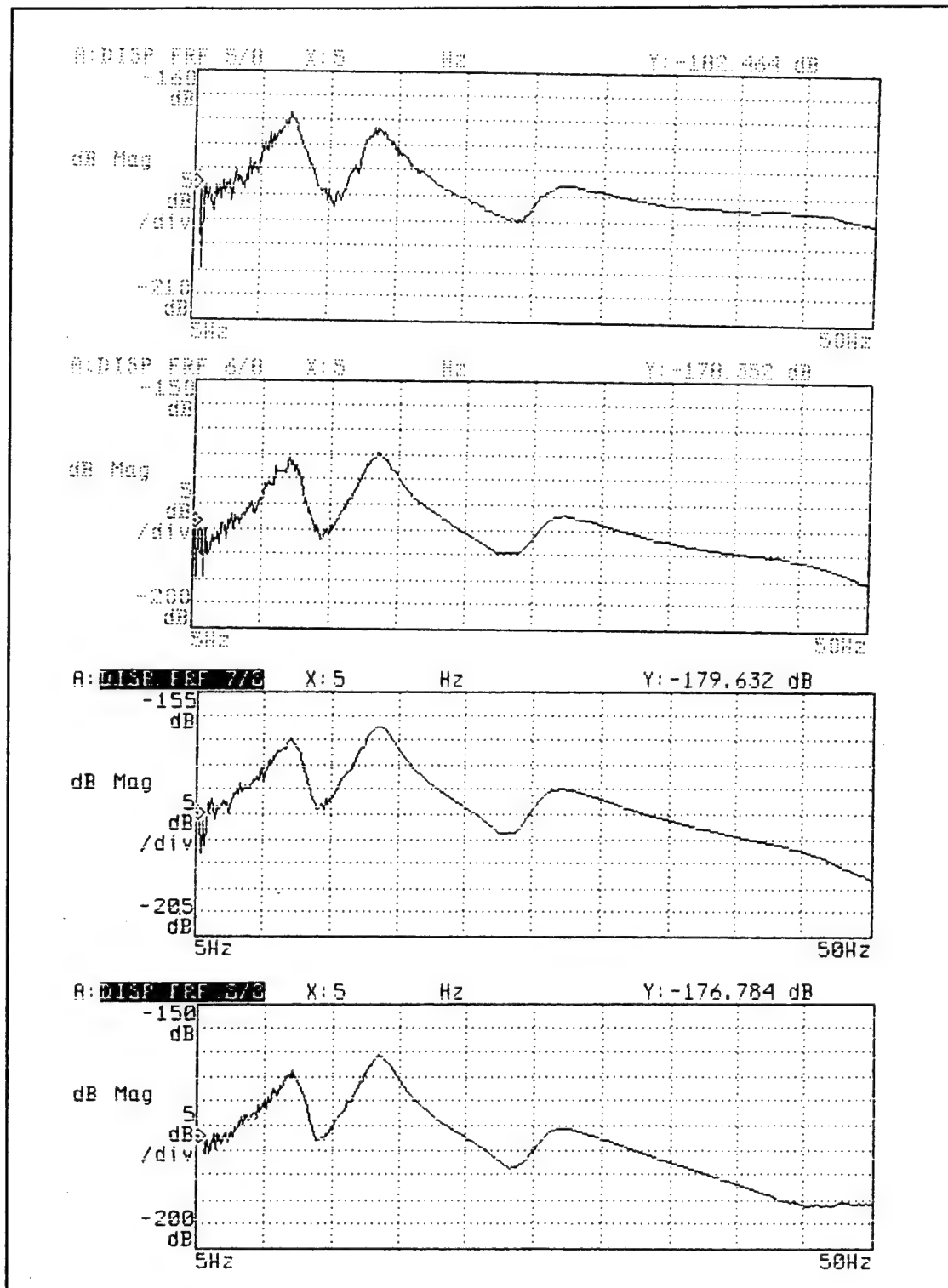


Figure C-2. FRF's Recorded for Configuration 1, Y-Direction, Accelerometer Locations 5-8.

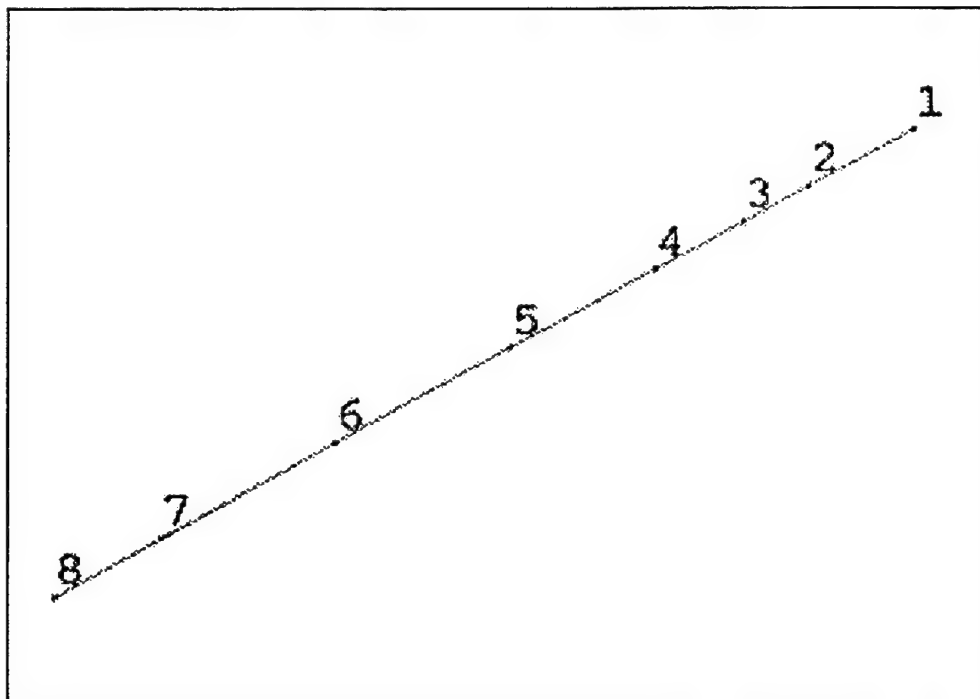


Figure C-3. Configuration 1, Geometry.

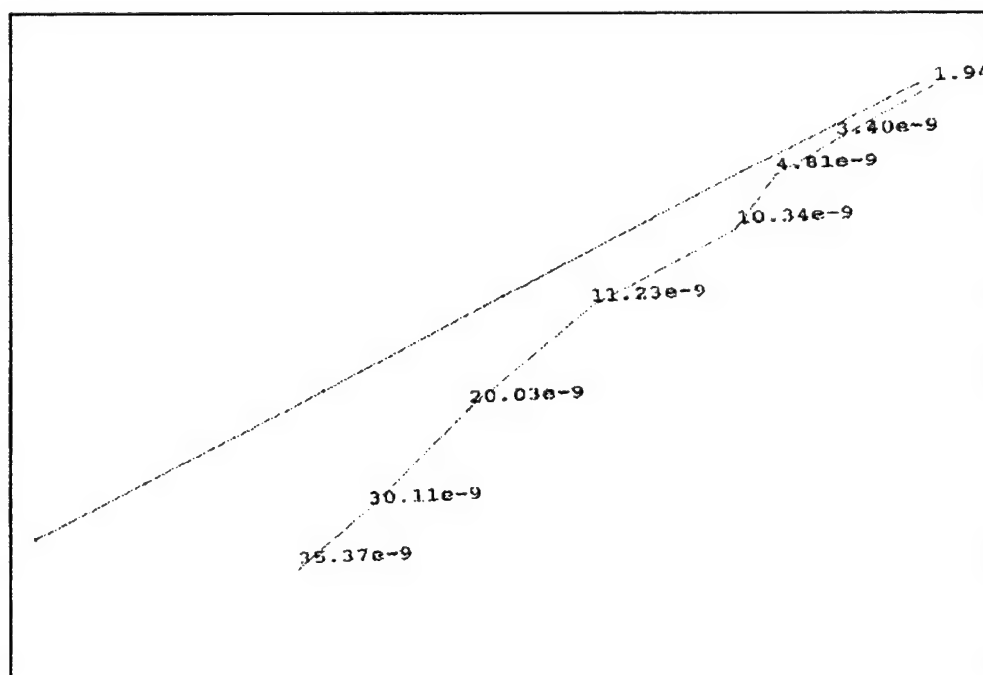


Figure C-4. Configuration 1, First Y-Mode: 11.09 Hz.

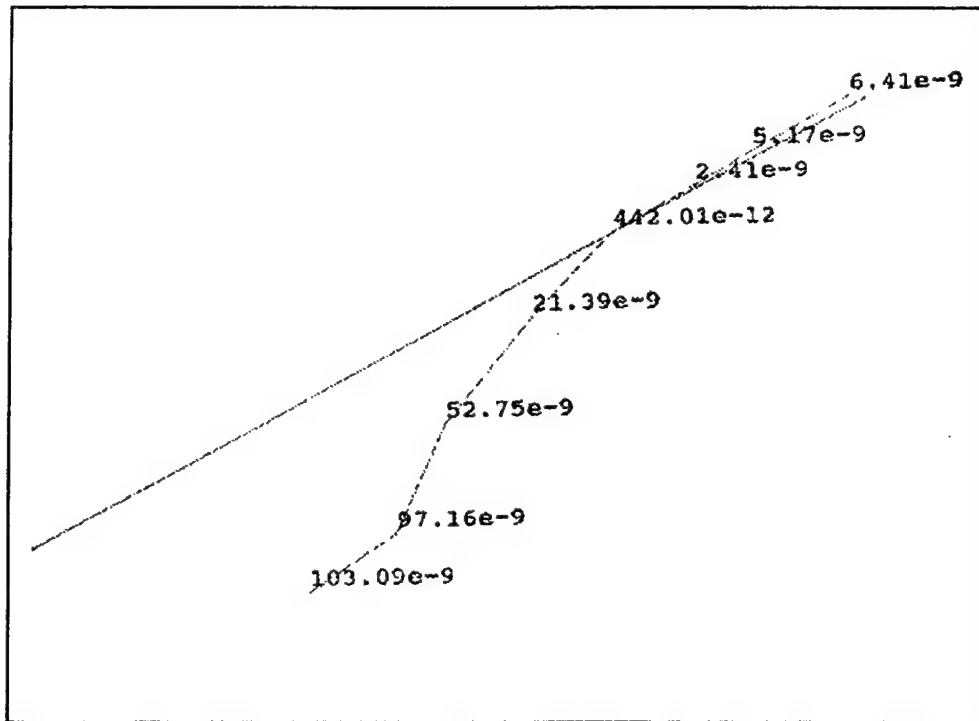


Figure C-5. Configuration 1, Second Y-Mode: 16.69 Hz.

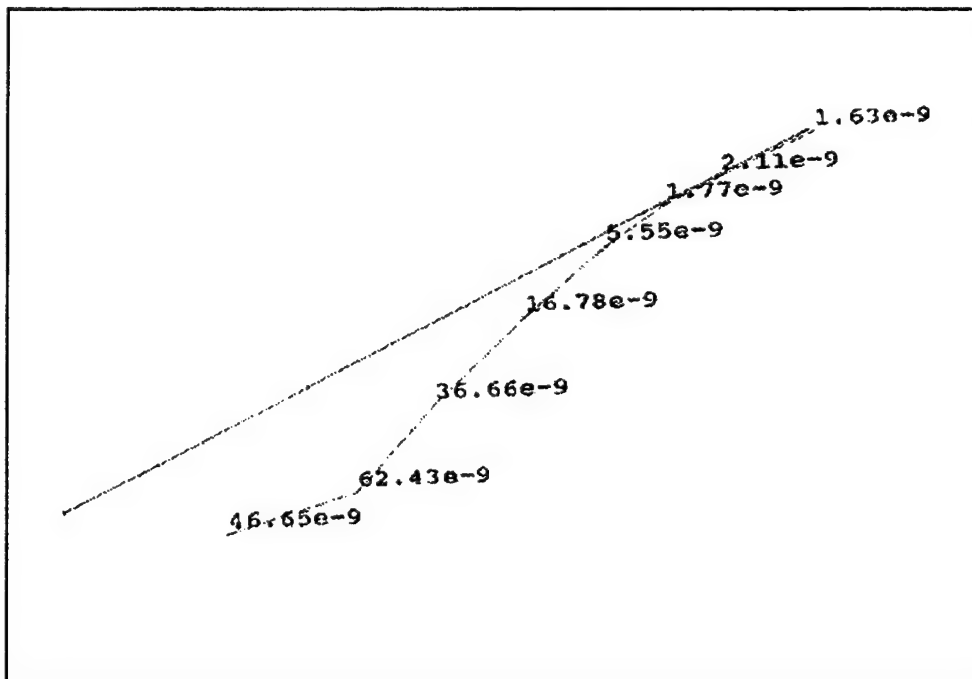


Figure C-6. Configuration 1, Third Y-Mode: 28.69Hz.

Mode	Accelerometer Location	Relative Amplitude	Relative Phase Angle
1	1	1.94e-9	111.47
	2	3.40e-9	116.68
	3	4.81e-9	124.64
	4	10.34e-9	98.76
	5	11.23e-9	106.21
	6	20.03e-9	116.81
	7	30.11e-9	116.15
	8	35.37e-9	115.52
2	1	6.41e-9	-91.92
	2	5.17e-9	-80.30
	3	2.41e-9	-77.30
	4	0.442e-9	-78.25
	5	21.39e-9	54.19
	6	52.75e-9	59.22
	7	97.16e-9	55.57
	8	103.09e-9	59.48
3	1	1.63e-9	-14.84
	2	2.11e-9	-74.21
	3	1.77e-9	-52.01
	4	5.55e-9	14.74
	5	16.78e-9	9.05
	6	36.66e-9	28.26
	7	62.43	34.32
	8	46.65e-9	27.32

Table C-1. Amplitudes and phases computed by STARModal for configuration 1, Y-direction.

APPENDIX D. FREQUENCY RESPONSE FUNCTIONS AND MODAL SHAPES FOR CONFIGURATION 2, Y-DIRECTION

Gun configuration 2, Y-direction, had the topmost barrel at top dead center, a static load pulling back on the stub rotor to simulate the load during firing, lead weights on top of the gun cradle, and no muzzle restraint.

Figures D-1 and D-3 show the frequency response functions (FRF) (horizontal displacement/horizontal force) measured for accelerometer locations 1 through 9 for this configuration. The dB magnitudes plotted in the FRF graphs have not been corrected using the transducer calibration and amplifier gains. For the FRF's in dB re 1m/N, add 28.7 dB to the plotted values.

STARModal identified three modes (Figures D-4 to D-7) in the 0-125 Hz excitation range for this configuration. The numbers on the shape plots are displacement in arbitrary units..

Table D-1 lists the amplitudes and phase angles computed by STARModal for configuration 2, Y-direction.

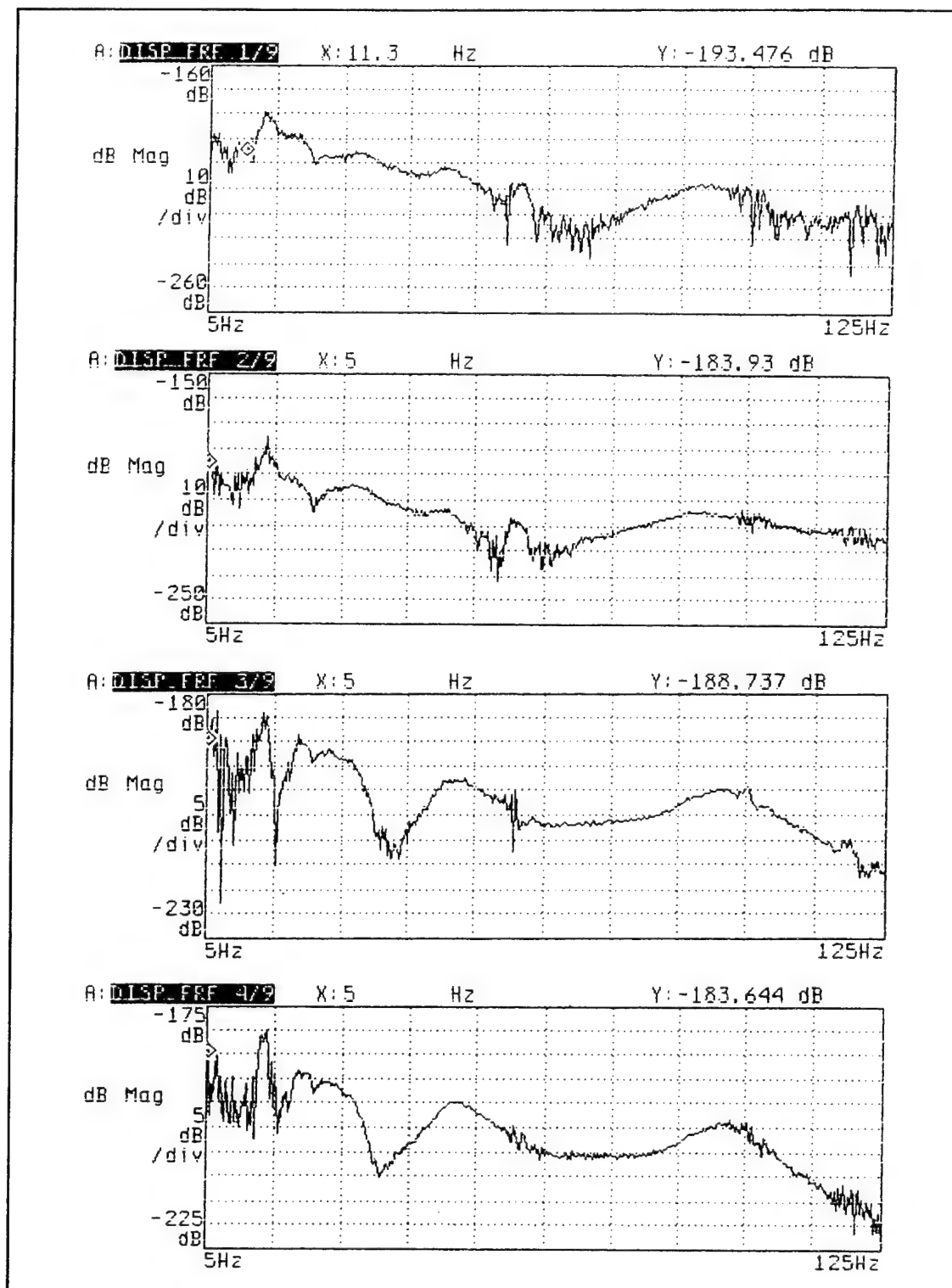


Figure D-1. FRF's Recorded for Configuration 2, Y-Direction, Accelerometer Locations 1-4.

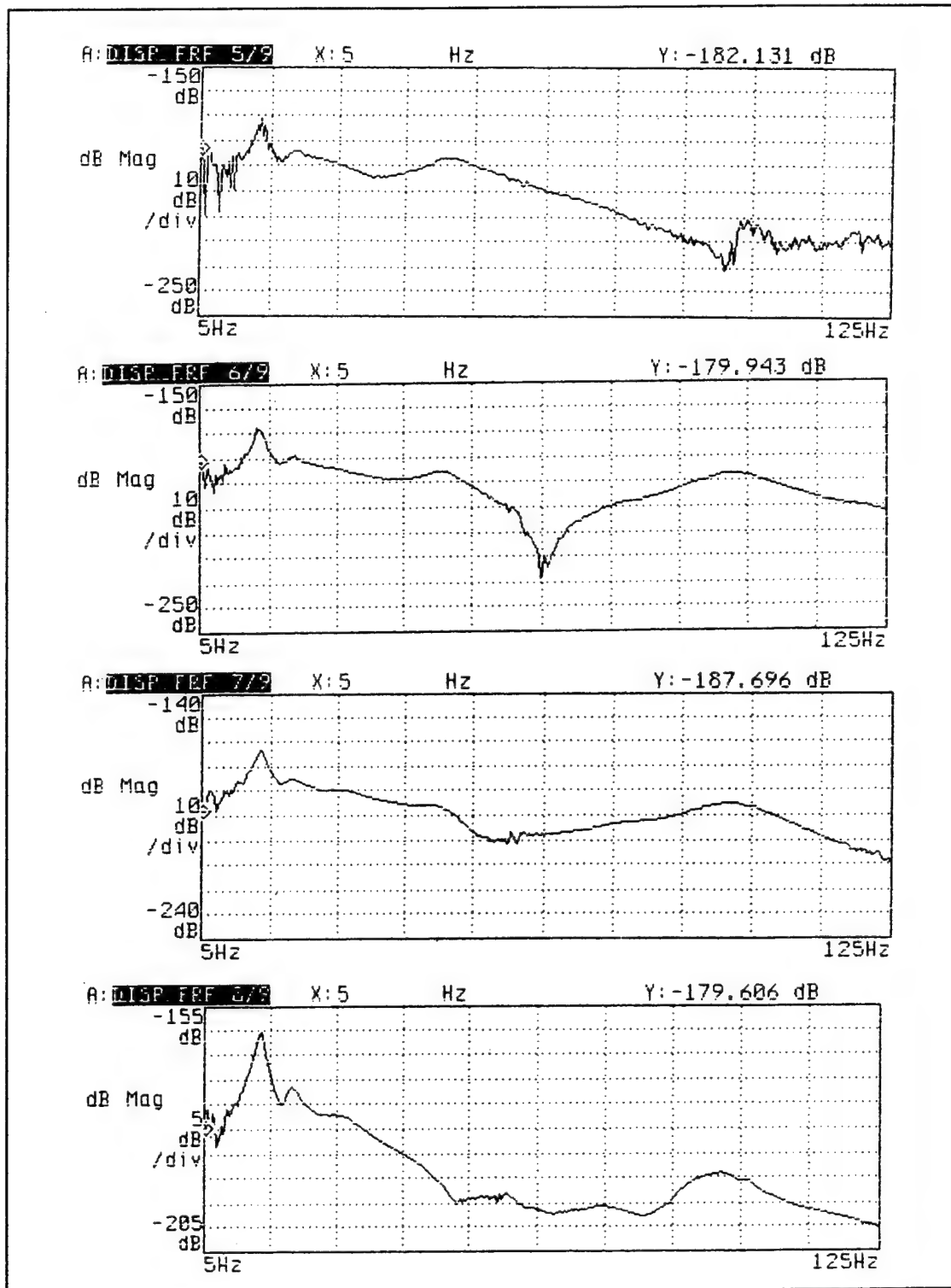


Figure D-2. FRF's Recorded for Configuration 2, Y-Direction, Accelerometer Locations 5-8.

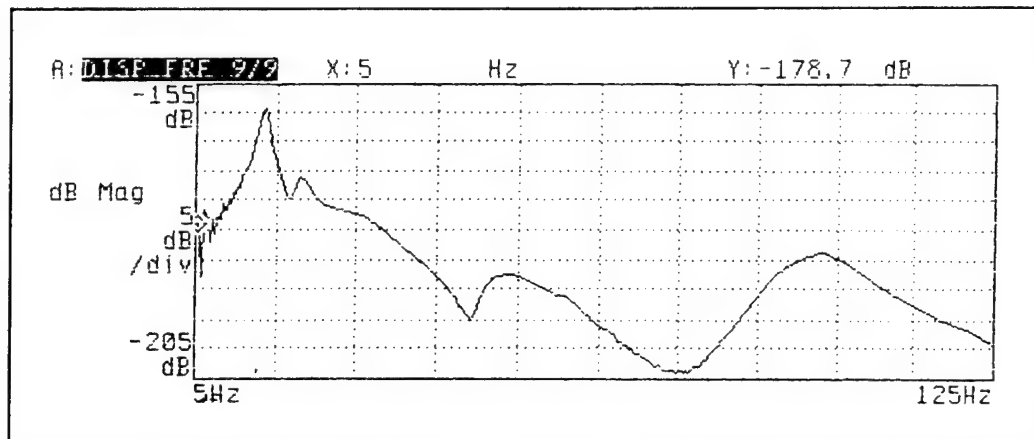


Figure D-3. FRF Recorded for Configuration 2, Y-Direction, Accelerometer Location 9.

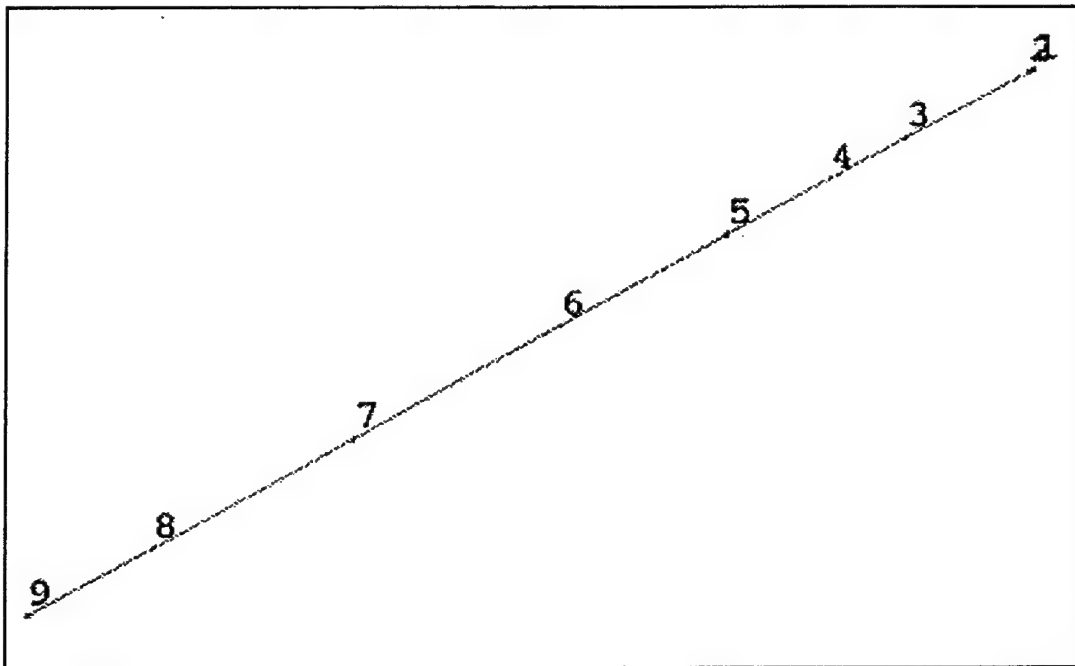


Figure D-4. Configuration 2, Geometry.

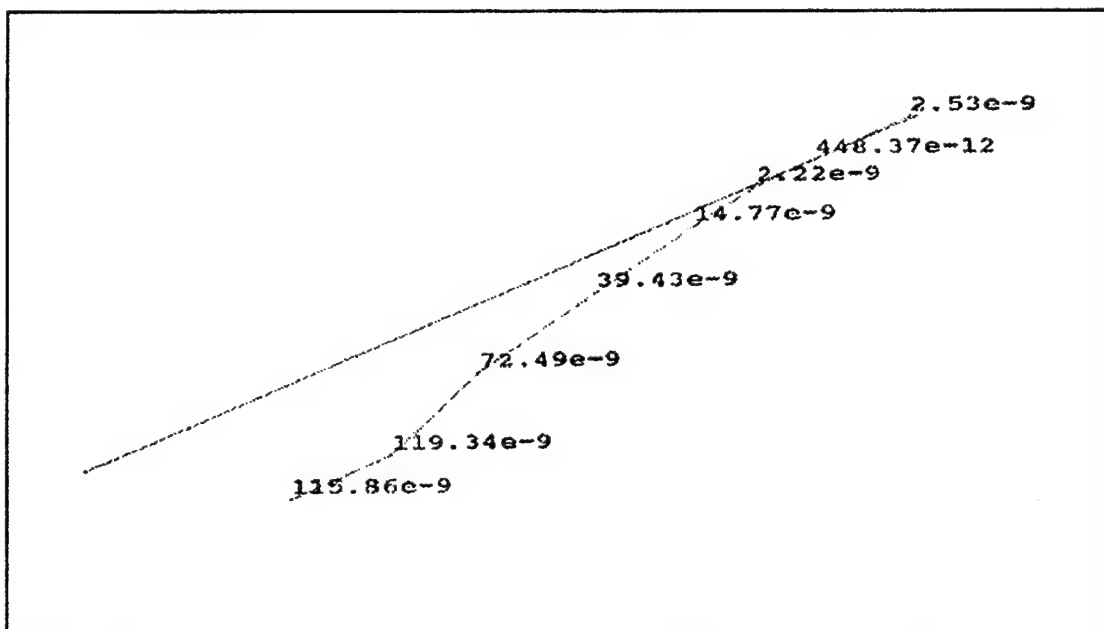


Figure D-5. Configuration 2, First Y-Mode: 14.73 Hz.

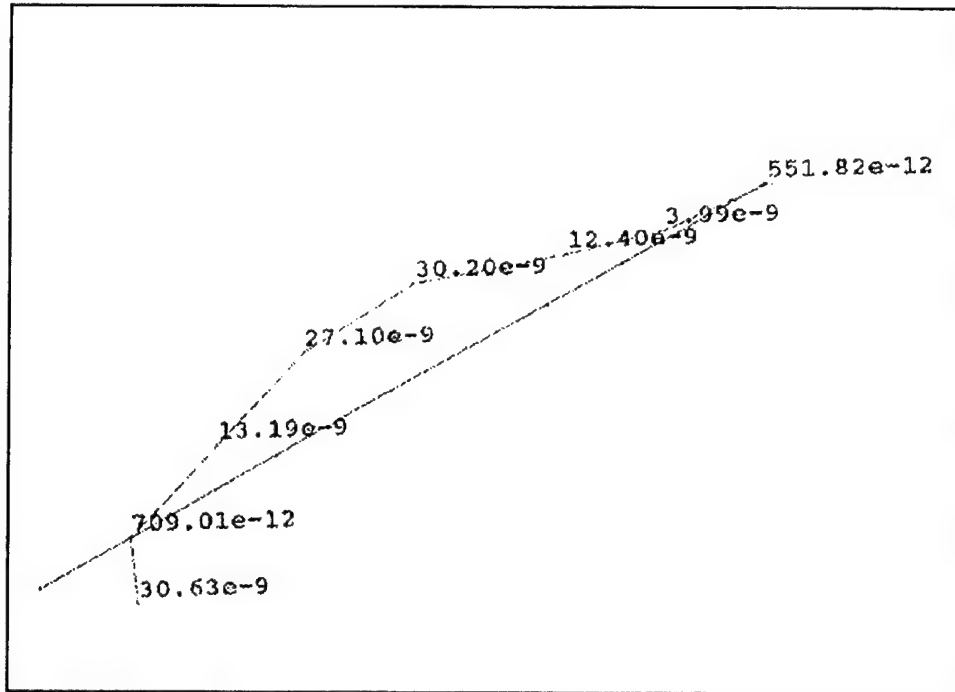


Figure D-6. Configuration 2, Second Y-Mode: 48.61 Hz.

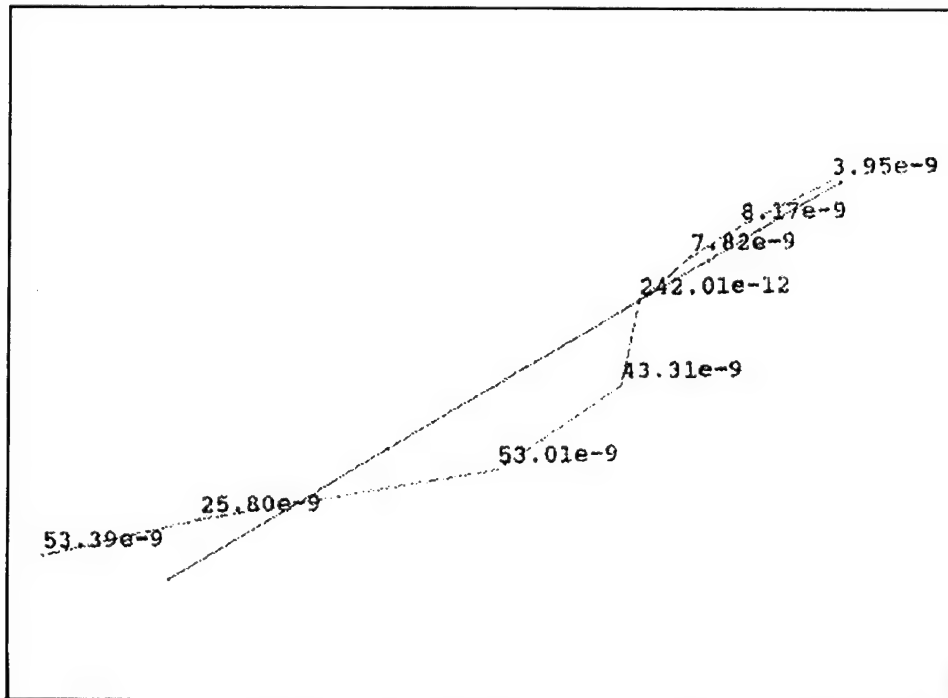


Figure D-7. Configuration 2, Third Y-Mode: 97.37 Hz.

Mode	Accelerometer Location	Relative Amplitude	Relative Phase Angle
1	1	6.36e-9	-50.15
	2	2.53e-9	-102.99
	3	0.448e-9	169.53
	4	2.29e-9	110.96
	5	14.77e-9	75.18
	6	39.43e-9	102.27
	7	72.49e-9	66.41
	8	119.34e-9	60.88
	9	115.86e-9	68.24
2	1	1.98e-9	85.61
	2	0.552e-9	79.18
	3	3.99e-9	-142.54
	4	12.40e-9	-109.40
	5	30.20e-9	-112.83
	6	27.10e-9	-105.75
	7	13.19e-9	-92.89
	8	0.709e-9	164.20
	9	30.63e-9	35.81
3	1	2.47e-9	-73.16
	2	3.95e-9	-7.53
	3	8.17e-9	19.07
	4	7.82e-9	22.09
	5	0.242e-9	-112.73
	6	43.31e-9	-155.70

Table D-1. Amplitudes and phases computed by STARModal for configuration 2, Y-direction.

Mode	Accelerometer Location	Relative Amplitude	Relative Phase Angle
	7	53.01e-9	-143.78
	8	25.80e-9	-24.31
	9	53.39e-9	7.64

Table D-1 (cont.).

APPENDIX E. FREQUENCY RESPONSE FUNCTIONS AND MODAL SHAPES FOR CONFIGURATION 2, Z-DIRECTION

Gun configuration 2, Z-direction, had the topmost barrel at top dead center, a static load pulling back on the stub rotor to simulate the load during firing, lead weights on top of the gun cradle, and no muzzle restraint.

Figures E-1 and E-3 show the frequency response functions (FRF) (vertical displacement/vertical force) measured for accelerometer locations 1 through 9 for this configuration. The dB magnitudes plotted in the FRF graphs have not been corrected using the transducer calibration and amplifier gains. For the FRF's in dB re 1m/N, add 28.7 dB to the plotted values.

STARModal identified three modes (Figures E-4 to E-6) in the 0-125 Hz excitation range for this configuration. The numbers on the shape plots are displacement in arbitrary units.

Table E-1 lists the amplitudes and phase angles computed by STARModal for configuration 2, Z-direction.

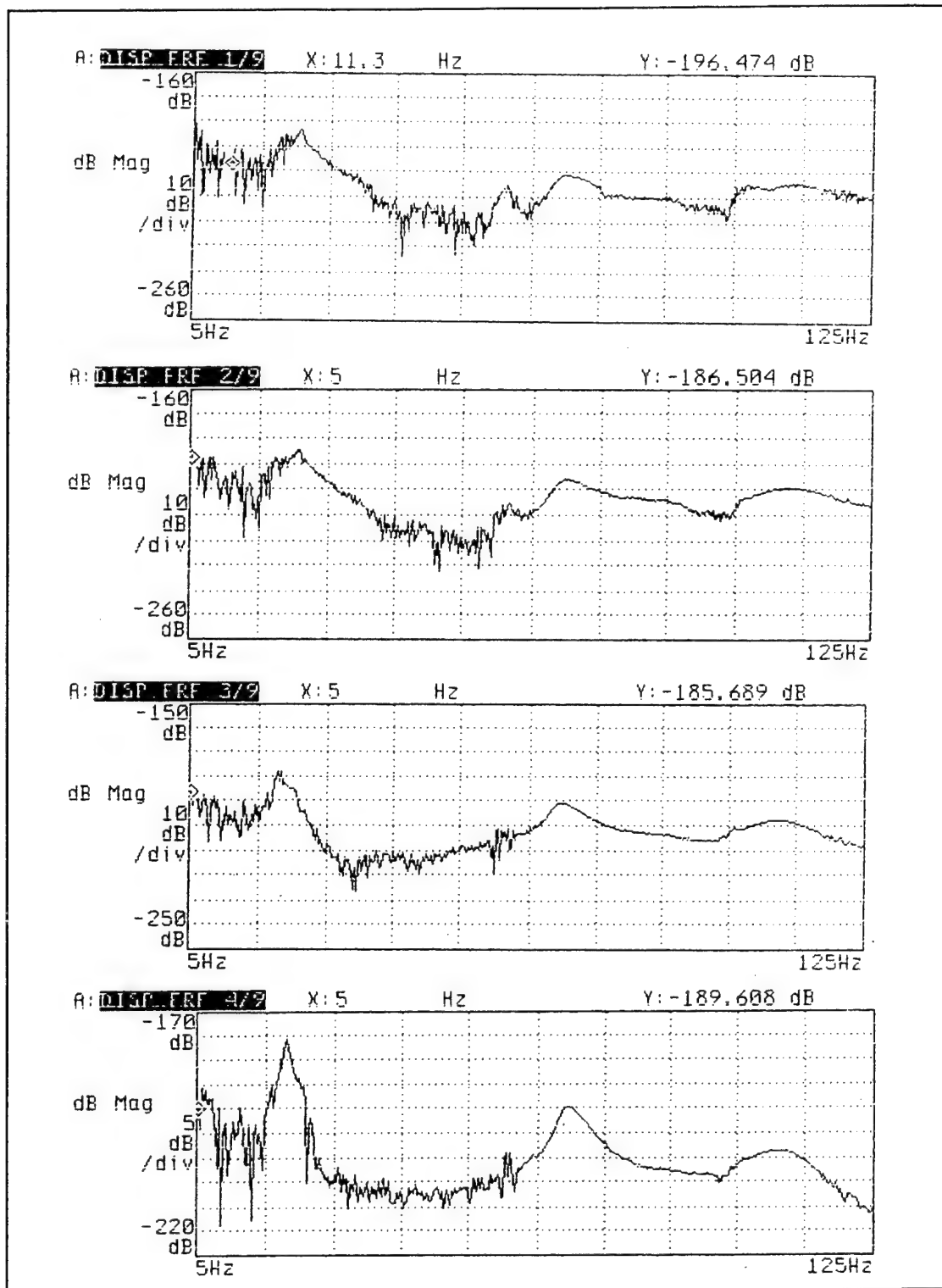


Figure E-1. FRF's Recorded for Configuration 2, Z-Direction, Accelerometer Locations 1-4.

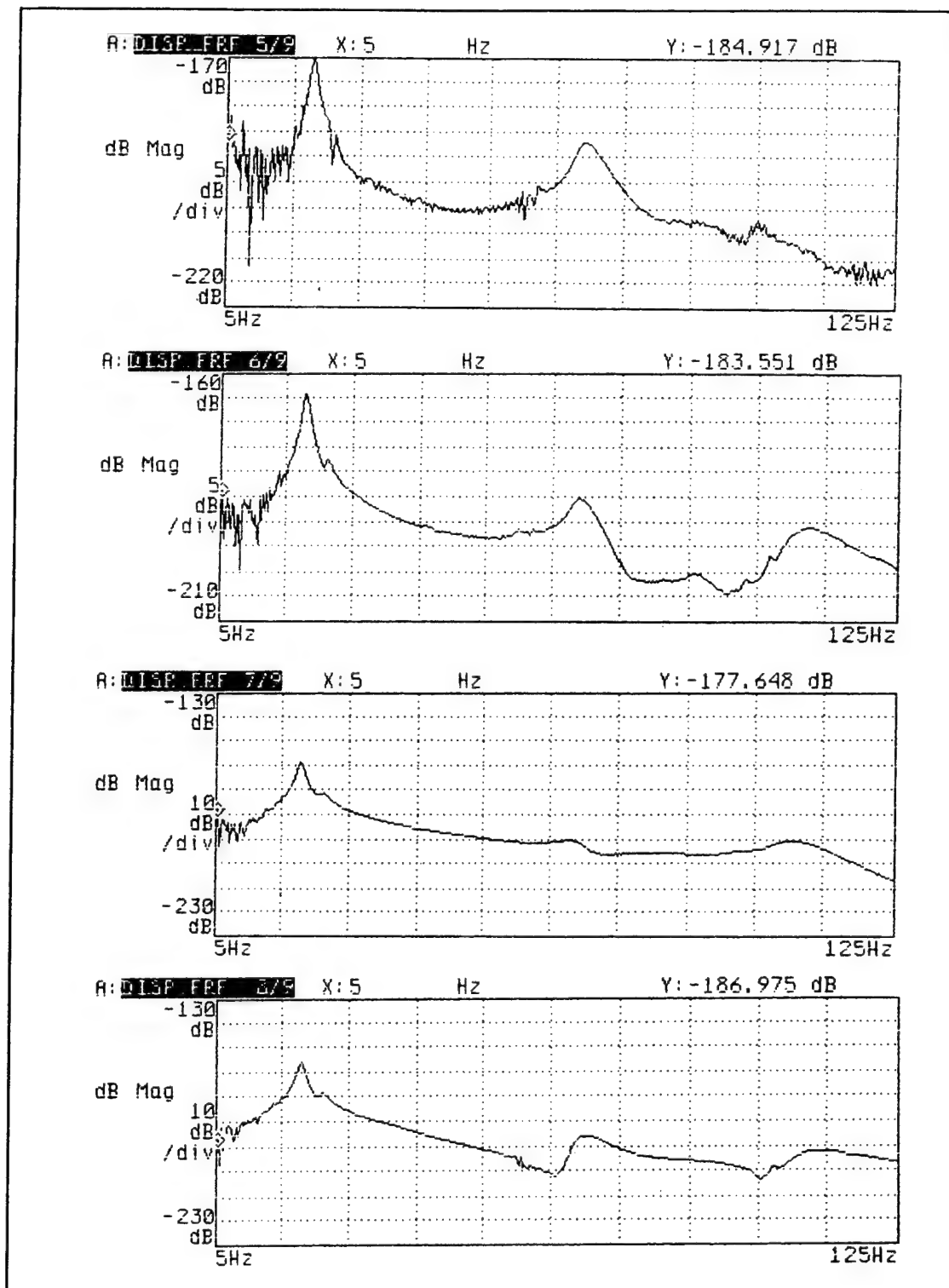


Figure E-2. FRF's Recorded for Configuration 2, Z-Direction, Accelerometer Locations 5-8.

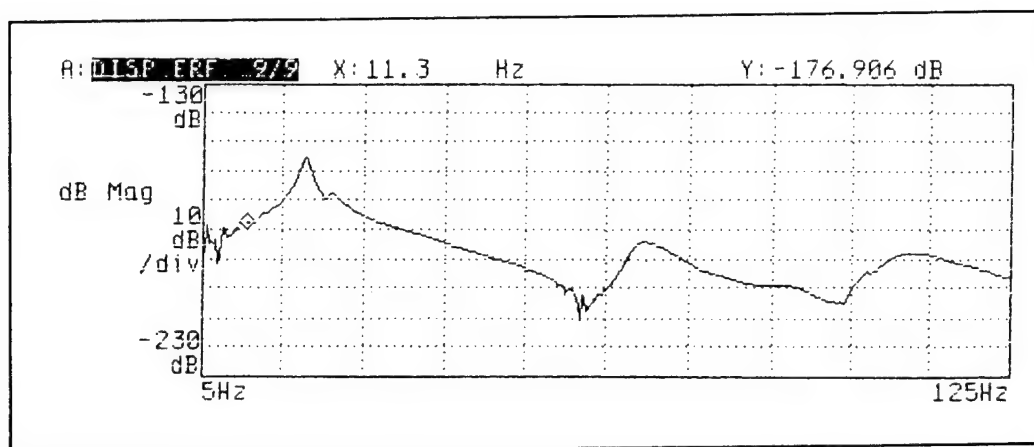


Figure E-3. FRF Recorded for Configuration 2, Z-Direction, Accelerometer Location 9.

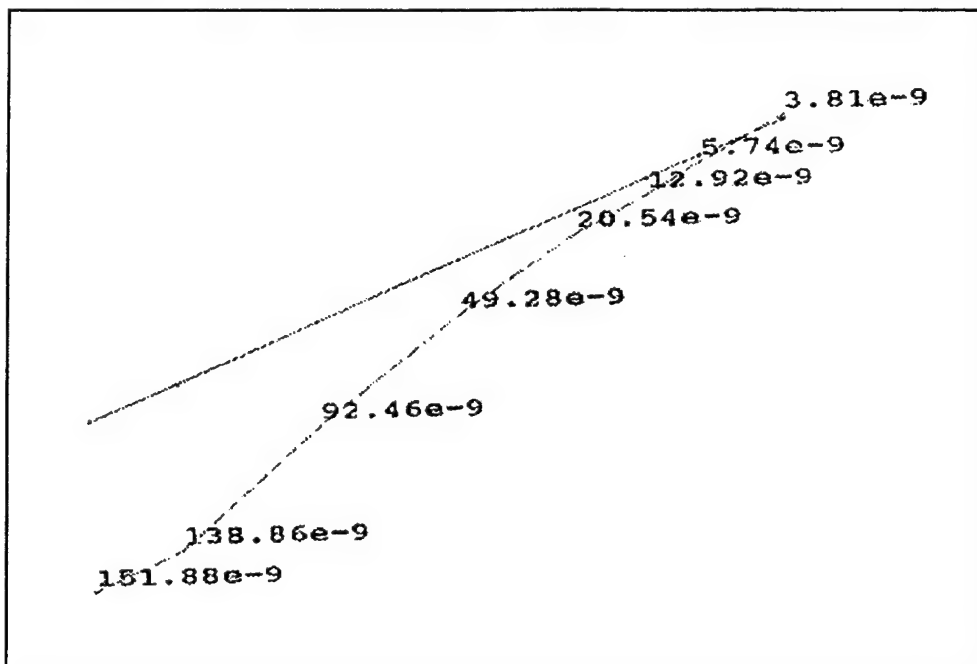


Figure E-4. Configuration 2, First Z-Mode: 20.25 Hz.

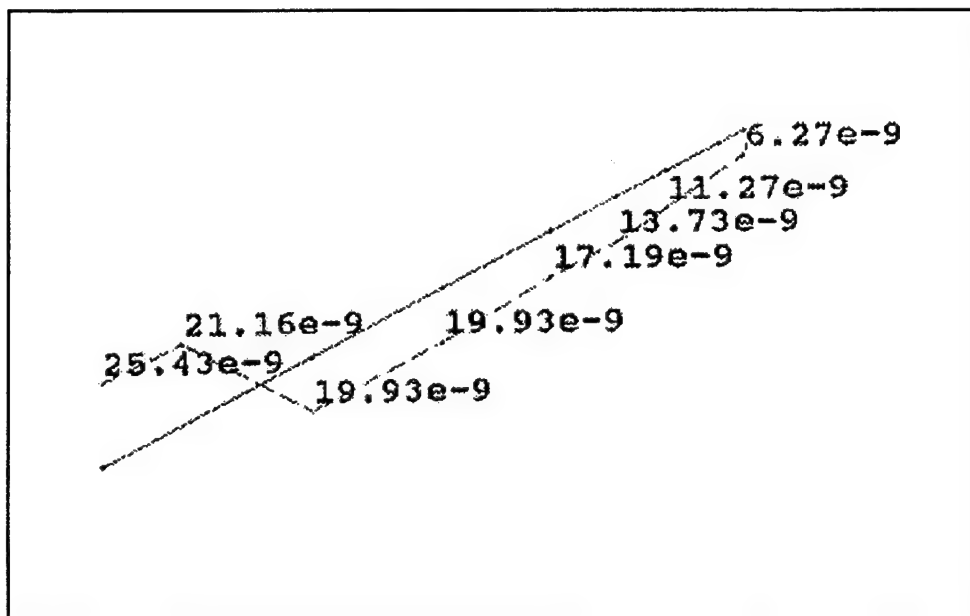


Figure E-5. Configuration 2, Second Z-Mode: 69.68 Hz.

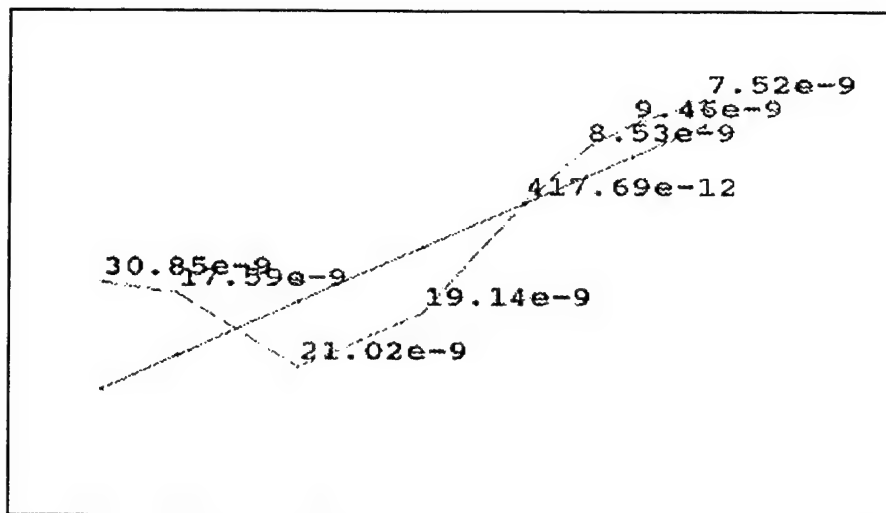


Figure E-6. Configuration 2, Third Z-Mode: 109.64 Hz.

Mode	Accelerometer Location	Relative Amplitude	Relative Phase Angle
1	1	1.39e-9	47.05
	2	3.81e-9	-139.05
	3	5.74e-9	65.75
	4	12.92e-9	48.63
	5	20.54e-9	52.70
	6	46.28e-9	60.33
	7	92.46e-9	60.17
	8	138.86e-9	58.30
	9	151.88e-9	60.12
2	1	3.65e-9	-142.69
	2	6.27e-9	-143.50
	3	11.27e-9	-140.58
	4	13.73e-9	-136.49
	5	17.19e-9	-134.19
	6	19.93e-9	-133.23
	7	19.93e-9	-133.23
	8	21.16e-9	37.46
	9	25.43e-9	42.50
3	1	3.78e-9	-32.46
	2	7.52e-9	-4.73
	3	9.46e-9	13.66
	4	8.53e-9	17.30
	5	0.417e-9	-5.02
	6	19.14e-9	-159.05

Table E-1. Amplitudes and phases computed by STARModal for configuration 2, Z-direction.

Mode	Accelerometer Location	Relative Amplitude	Relative Phase Angle
	7	21.02e-9	-147.42
	8	17.59e-9	11.83
	9	30.85e-9	16.79

Table E-1 (cont.).

APPENDIX F. FREQUENCY RESPONSE FUNCTIONS AND MODAL SHAPES FOR CONFIGURATION 3, Y-DIRECTION

Gun configuration 3, Y-direction, had the topmost barrel at top dead center, a static load pulling back on the stub rotor to simulate the load during firing, lead weights on top of the gun cradle, and no muzzle restraint.

Figures F-1 and F-3 show the frequency response functions (FRF) (horizontal displacement/horizontal force) measured for accelerometer locations 1 through 11 for this configuration. The dB magnitudes plotted in the FRF graphs have not been corrected using the transducer calibration and amplifier gains. For the FRF's in dB re 1m/N, add 28.7 dB to the plotted values.

STARModal identified three modes (Figures F-4 to F-8) in the 0-125 Hz excitation range for this configuration. The numbers on the shape plots are displacement in arbitrary units.

Table F-1 lists the amplitudes and phase angles computed by STARModal for configuration 3, Y-direction.

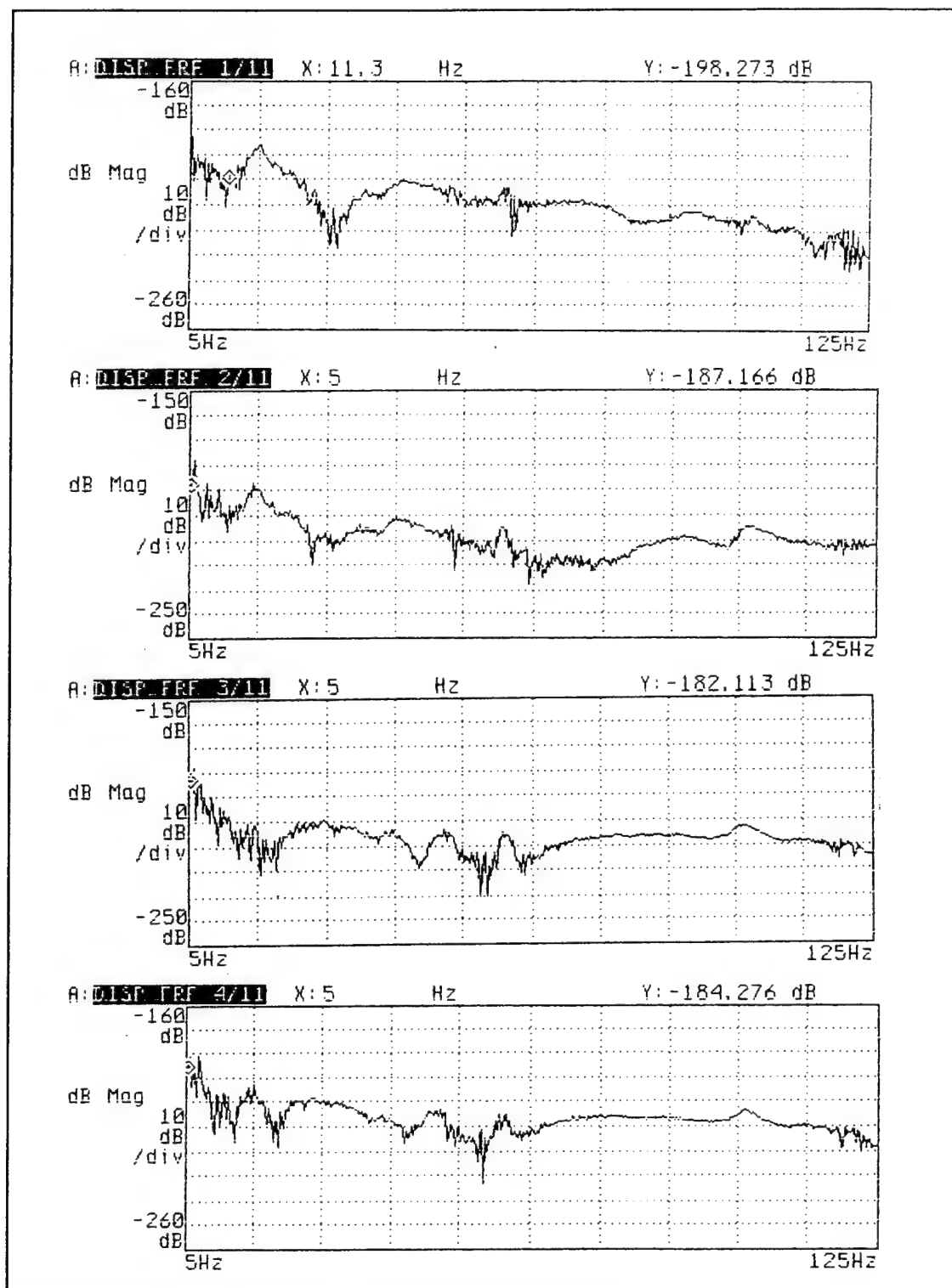


Figure F-1. FRF's Recorded for Configuration 3, Y-Direction, Accelerometer Locations 1-4.

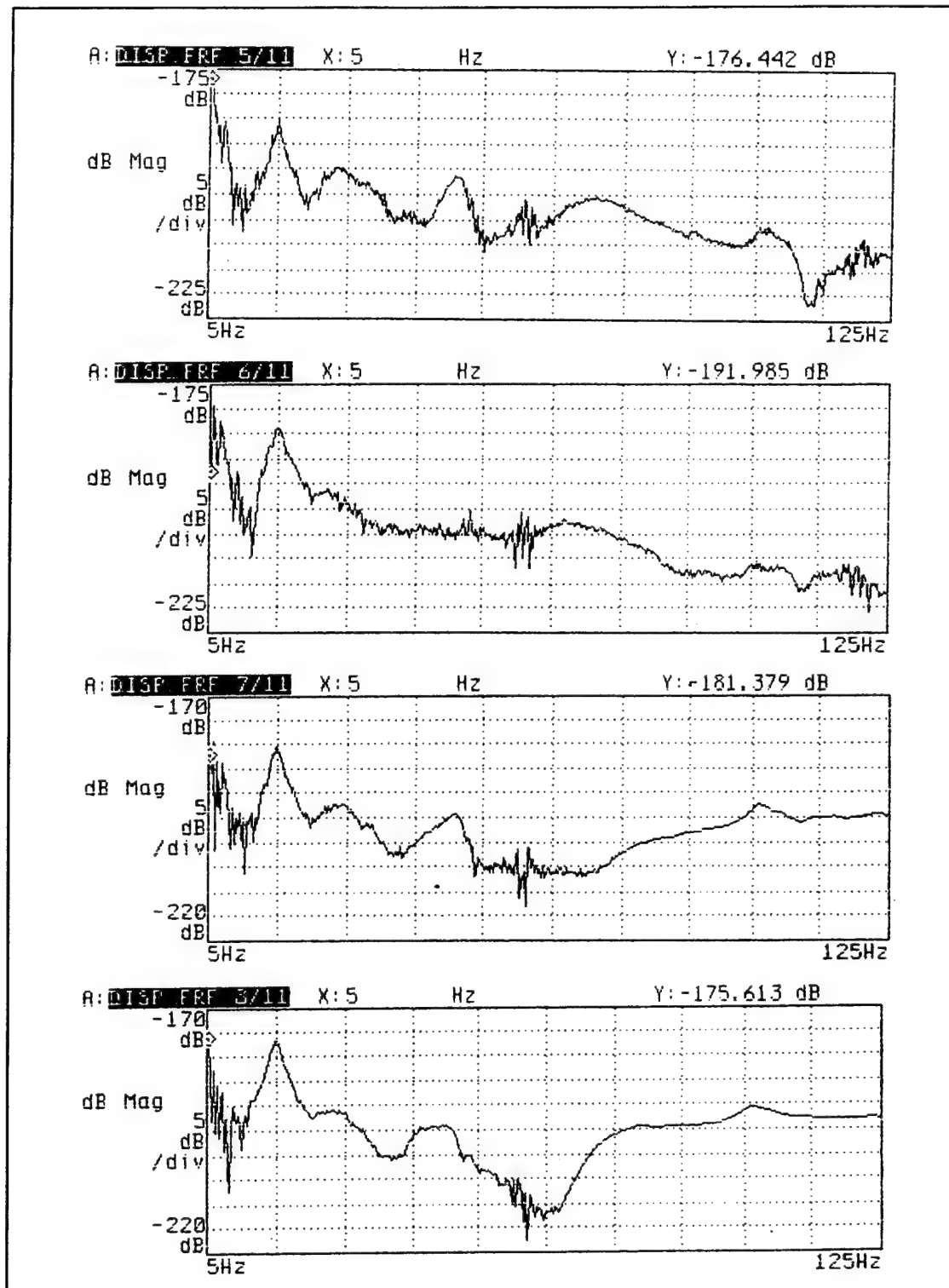


Figure F-2. FRF's Recorded for Configuration 3, Y-Direction, Accelerometer Locations 5-8.

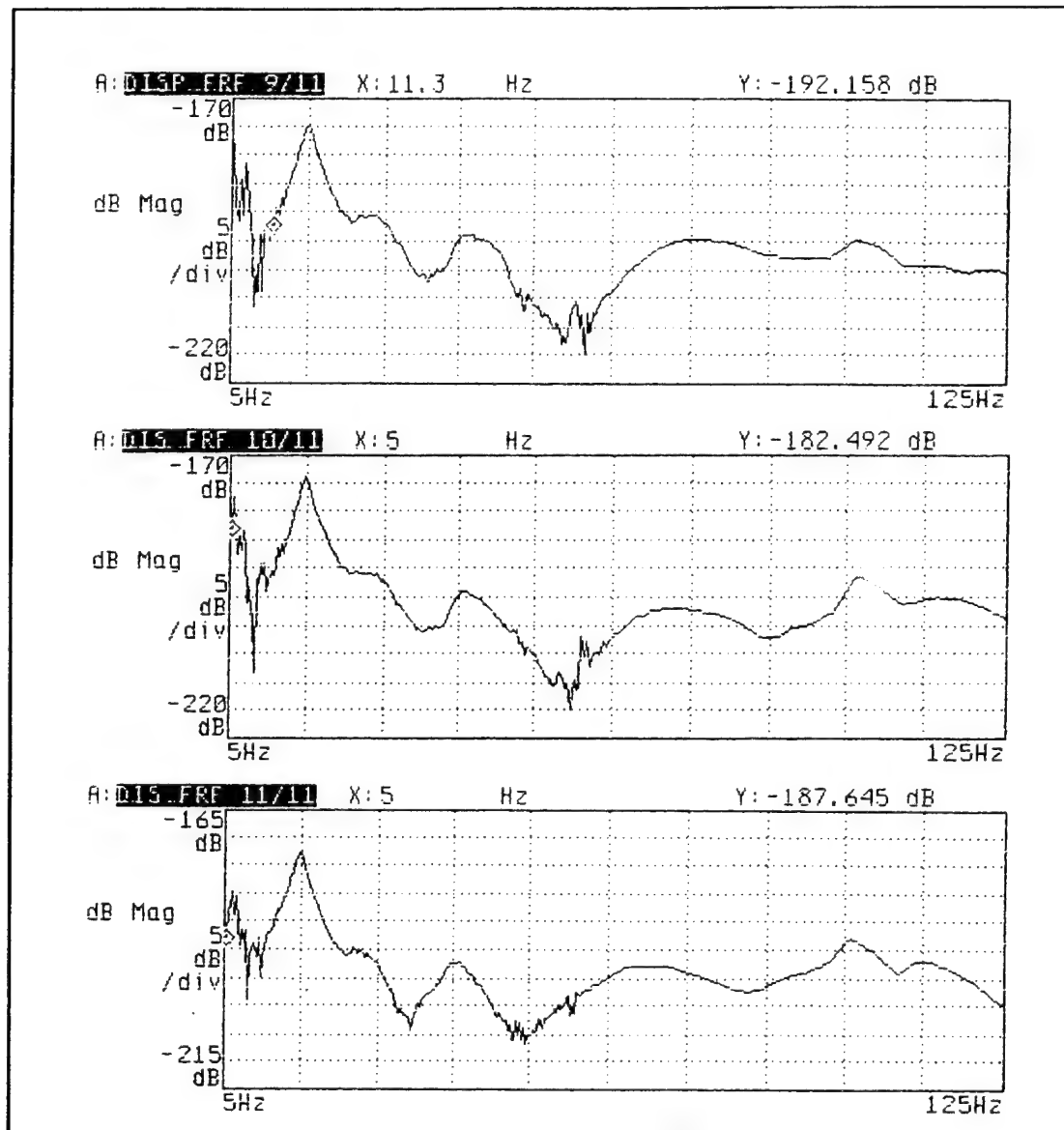


Figure F-3. FRF's Recorded for Configuration 3, Y-Direction, Accelerometer Locations 9-11.

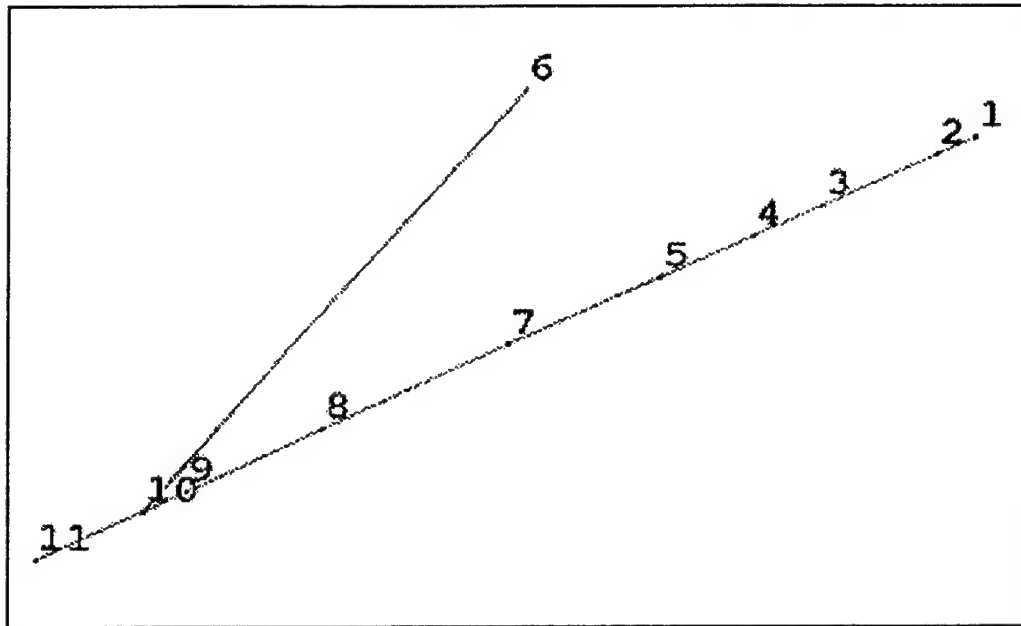


Figure F-4. Configuration 3, Geometry.

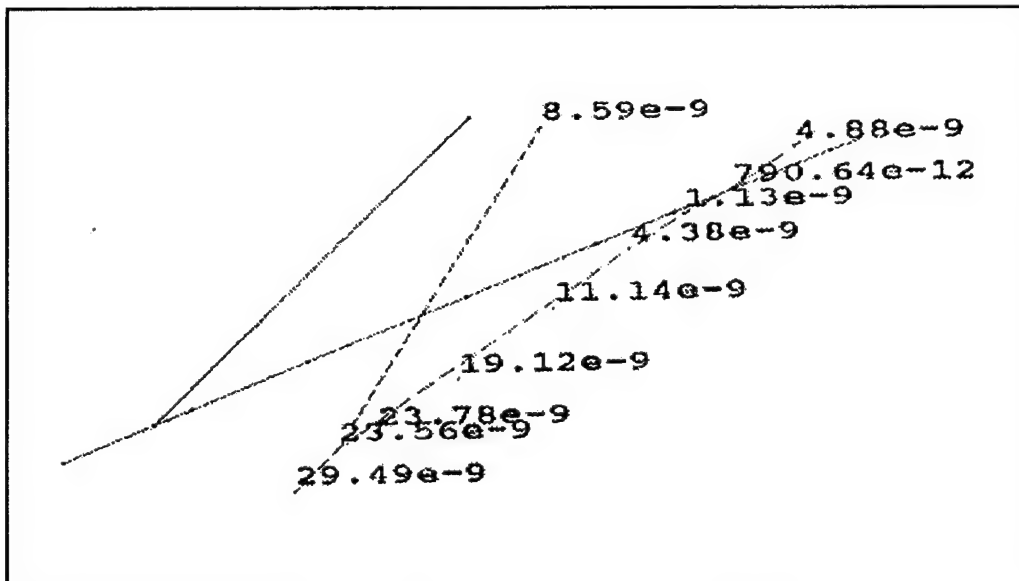


Figure F-5. Configuration 3, First Y-Mode: 16.44 Hz.

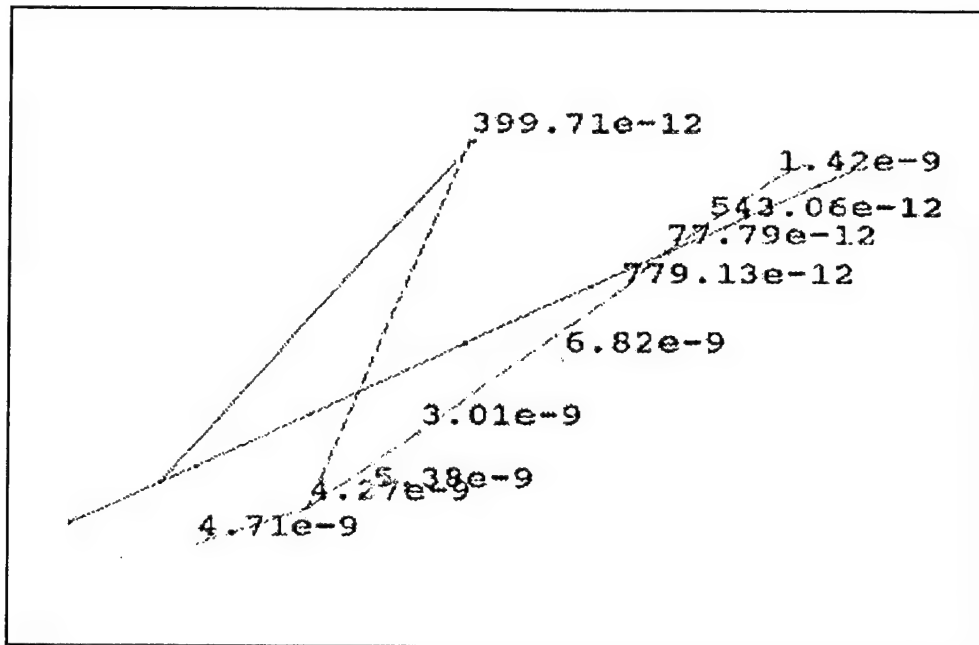


Figure F-6. Configuration 3, Second Y-Mode: 41.74 Hz.

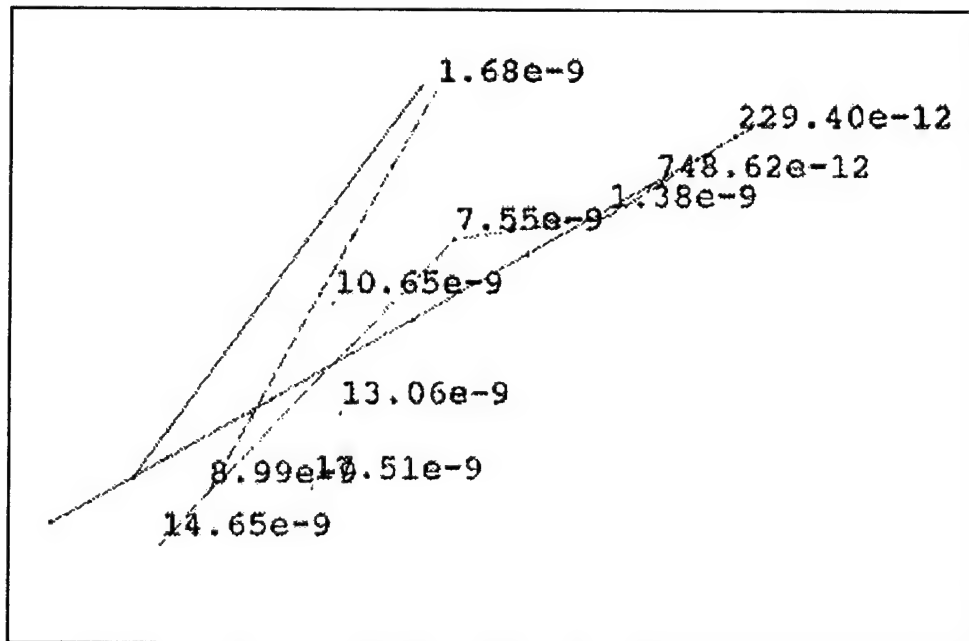


Figure F-7. Configuration 3, Third Y-Mode: 71.43 Hz.

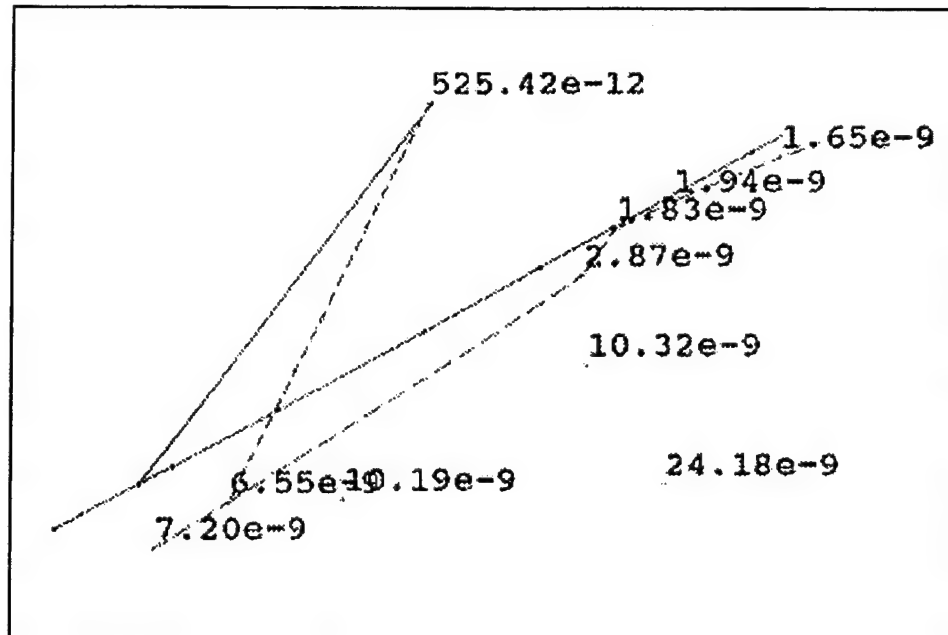


Figure F-8. Configuration 3, Fourth Y-Mode: 103.31 Hz.

Mode	Accelerometer Location	Relative Amplitude	Relative Phase Angle
1	1	6.92e-9	-99.11
	2	4.88e-9	-101.15
	3	0.790e-9	-56.94
	4	1.13e-9	66.44
	5	4.38e-9	70.31
	6	8.59e-9	66.41
	7	11.14e-9	68.29
	8	19.12e-9	68.00
	9	23.78e-9	67.97
	10	23.56e-9	71.00
	11	29.49e-9	69.44
2	1	1.38e-9	-174.48
	2	1.42e-9	-168.50
	3	0.543e-9	-178.52
	4	0.077e-9	-151.75
	5	0.779e-9	-18.98
	6	0.399e-9	-133.64
	7	6.82e-9	-93.34
	8	3.01e-9	-12.28
	9	5.38e-9	0.104
	10	4.27e-9	-2.58
	11	4.71e-9	22.32
3	1	0.132e-9	-38.29
	2	0.229e-9	92.48

Table F-1. Amplitudes and phases computed by STARModal for configuration 3, Y-direction.

Mode	Accelerometer Location	Relative Amplitude	Relative Phase Angle
	3	0.748e-9	-41.57
	4	1.38e-9	-39.53
	5	7.55e-9	161.44
	6	1.68e-9	-27.61
	7	10.65e-9	137.84
	8	13.06e-9	65.74
	9	17.51e-9	42.67
	10	8.99e-9	39.34
	11	14.65e-9	50.97
4	1	2.16e-9	-23.75
	2	1.65e-9	-14.99
	3	1.94e-9	46.07
	4	1.83e-9	59.68
	5	2.87e-9	-57.94
	6	0.525e-9	75.27
	7	10.32e-9	-2.68
	8	24.18e-9	-5.74
	9	10.19e-9	-37.57
	10	6.55e-9	12.70
	11	7.20e-9	14.54

Table F-1 (cont.).

APPENDIX G. FREQUENCY RESPONSE FUNCTIONS AND MODAL SHAPES FOR CONFIGURATION 3, Z-DIRECTION

Gun configuration 3, Z-direction, had the topmost barrel at top dead center, a static load pulling back on the stub rotor to simulate the load during firing, lead weights on top of the gun cradle, and no muzzle restraint.

Figures G-1 and G-3 show the frequency response functions (FRF) (vertical displacement/vertical force) measured for accelerometer locations 1 through 11 for this configuration. The dB magnitudes plotted in the FRF graphs have not been corrected using the transducer calibration and amplifier gains. For the FRF's in dB re 1m/N, add 28.7 dB to the plotted values.

STARModal identified three modes (Figures G-4 to G-7) in the 0-125 Hz excitation range for this configuration. The numbers on the shape plots are displacement in arbitrary units.

Table G-1 lists the amplitudes and phase angles computed by STARModal for configuration 3, Z-direction.

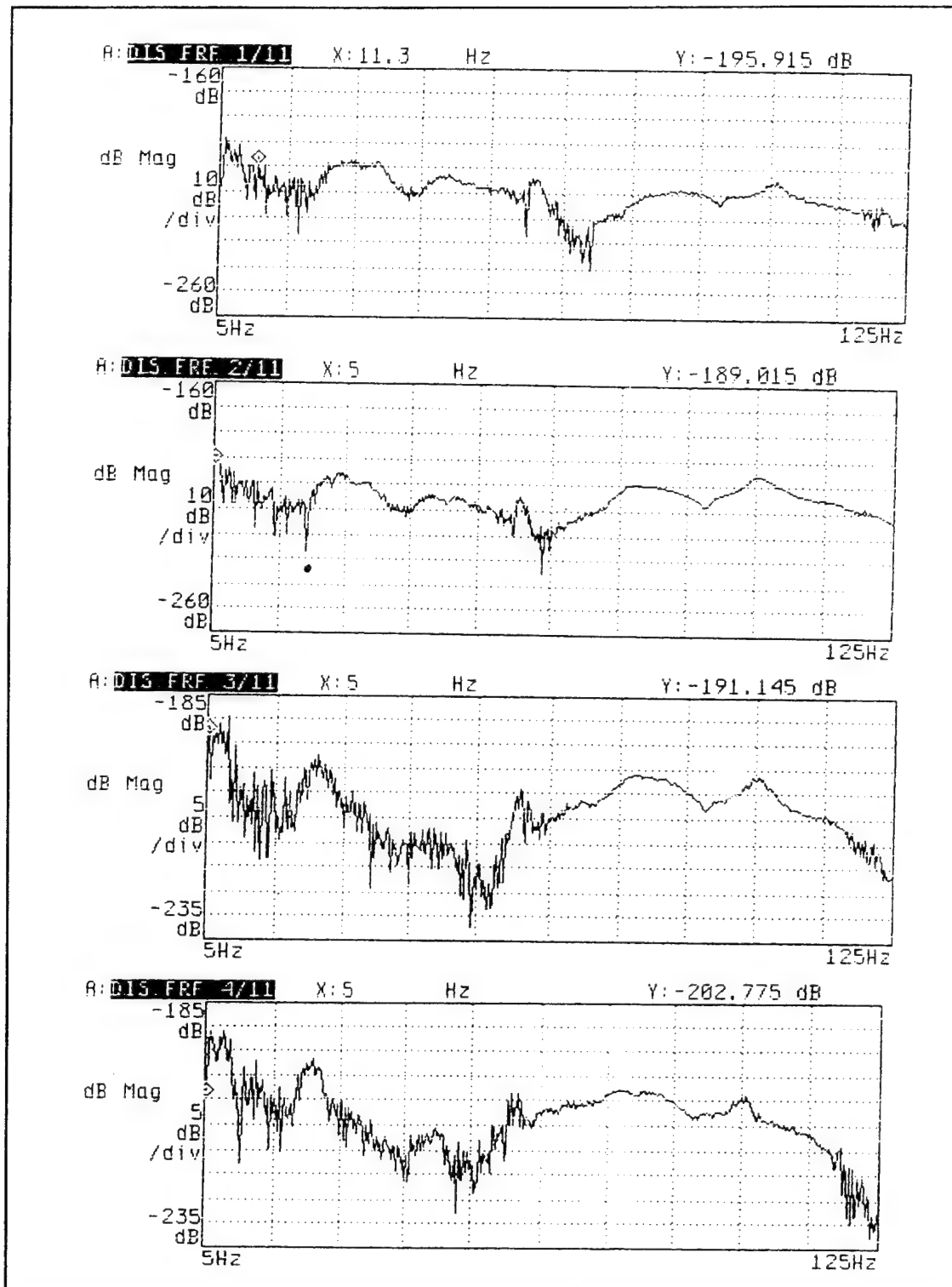


Figure G-1. FRF's Recorded for Configuration 3, Z-Direction, Accelerometer Locations 1-4.

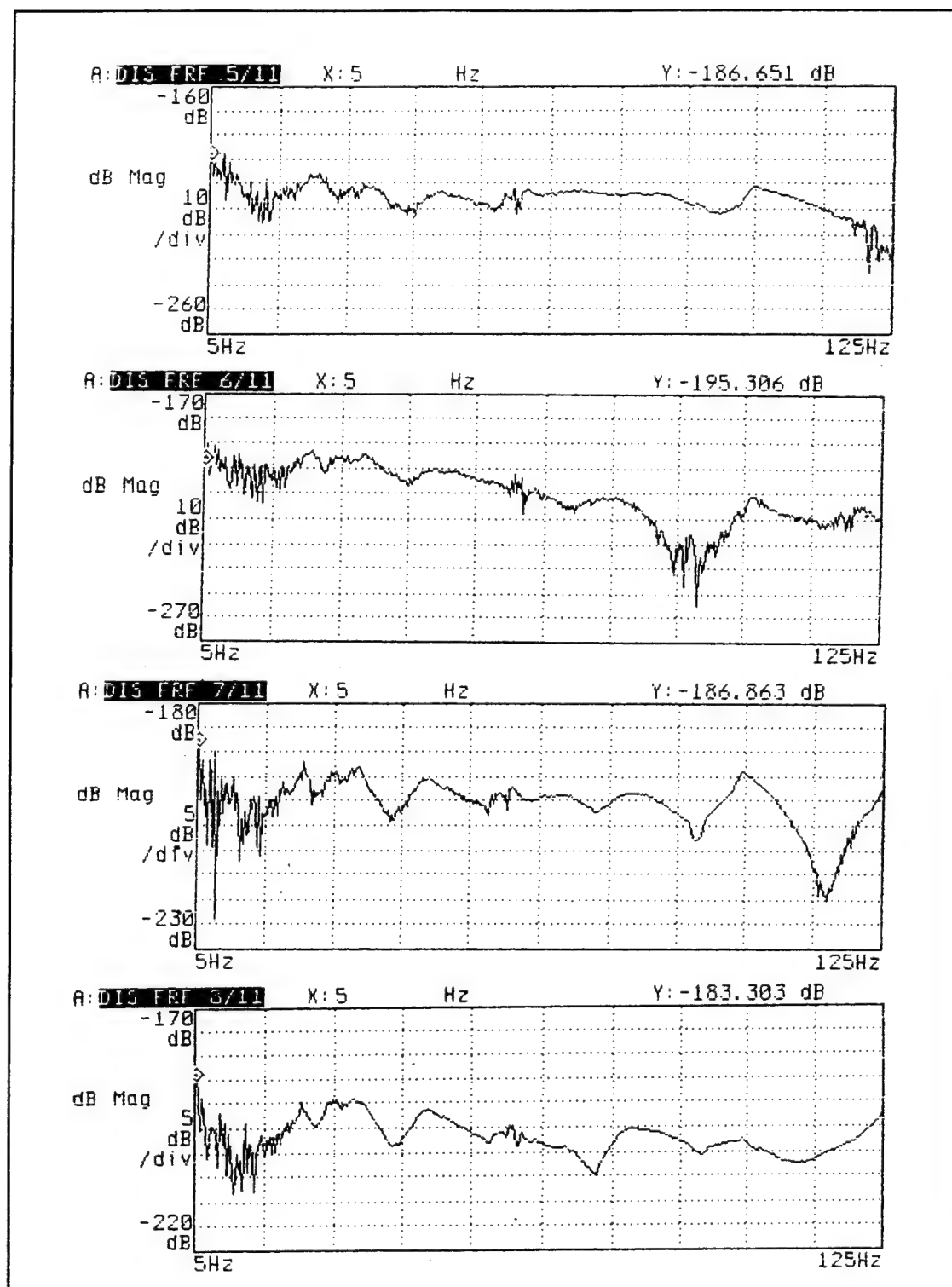


Figure G-2. FRF's Recorded for Configuration 3, Z-Direction, Accelerometer Locations 5-8.

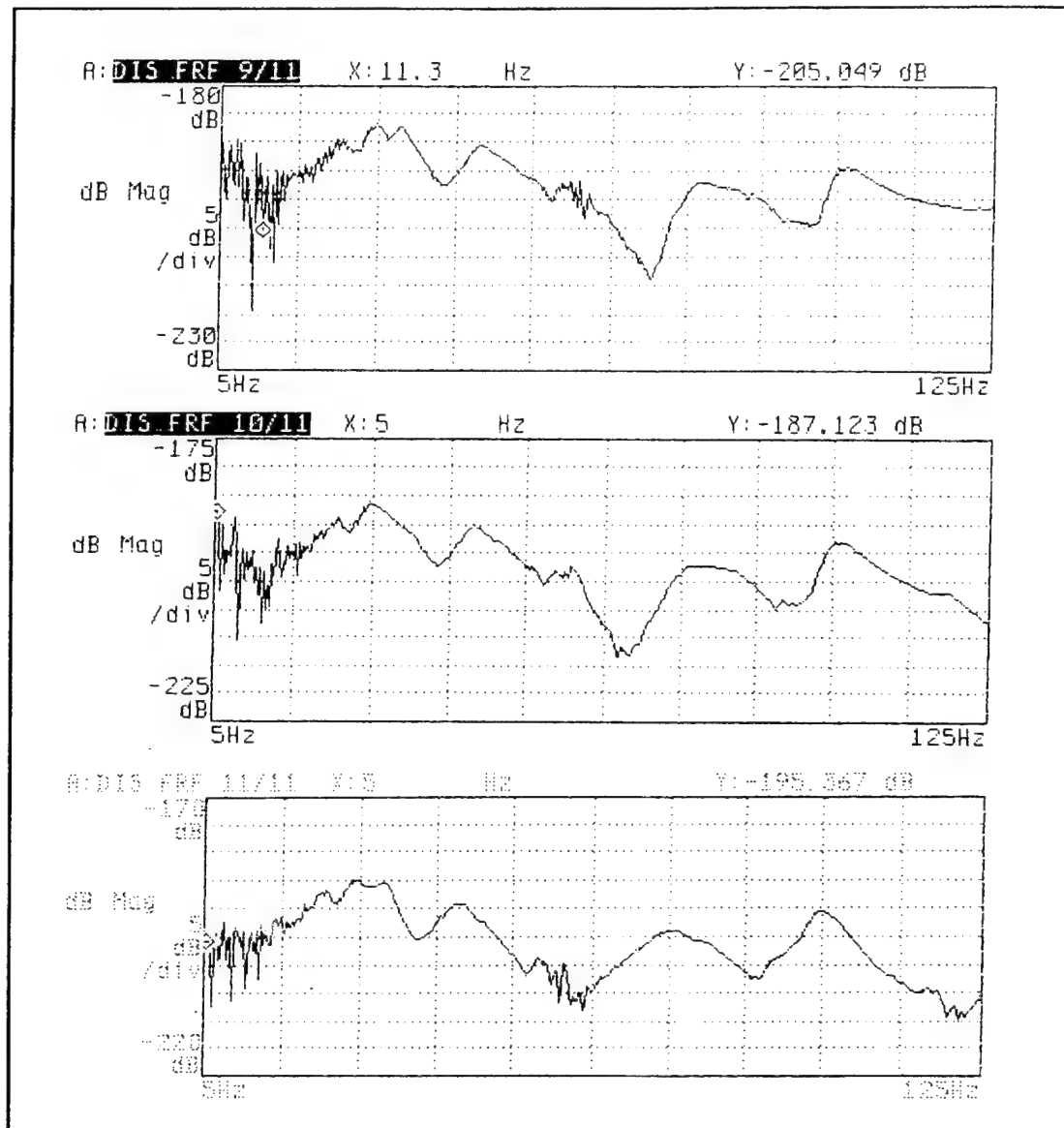


Figure G-3. FRF's Recorded for Configuration 3, Z-Direction, Accelerometer Locations 9-11.

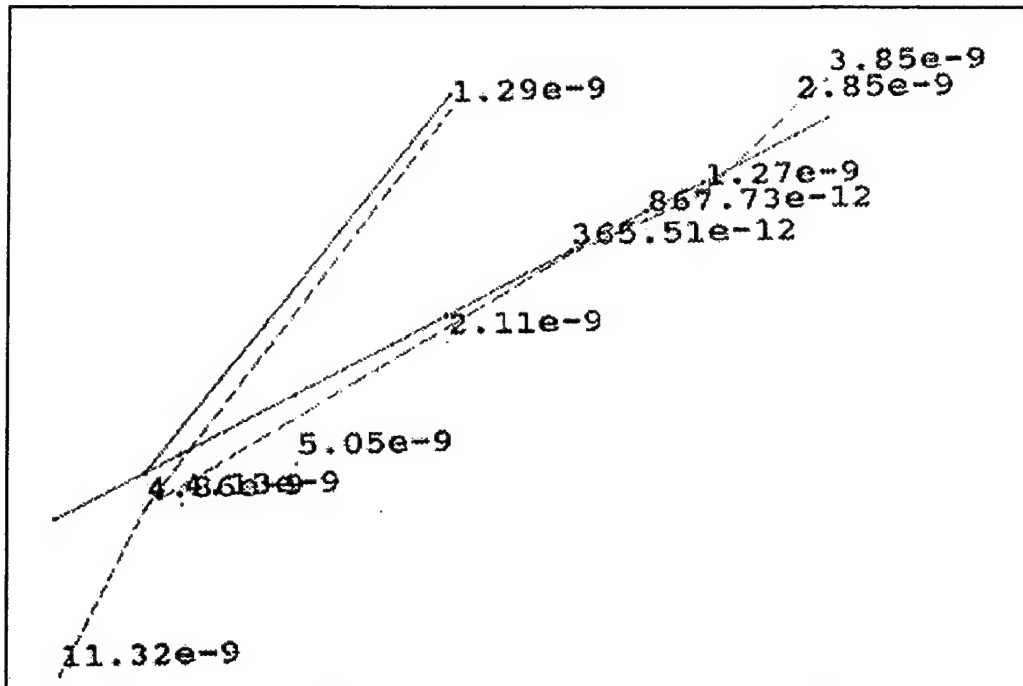


Figure G-4. Configuration 3, First Z-Mode: 28.84 Hz.

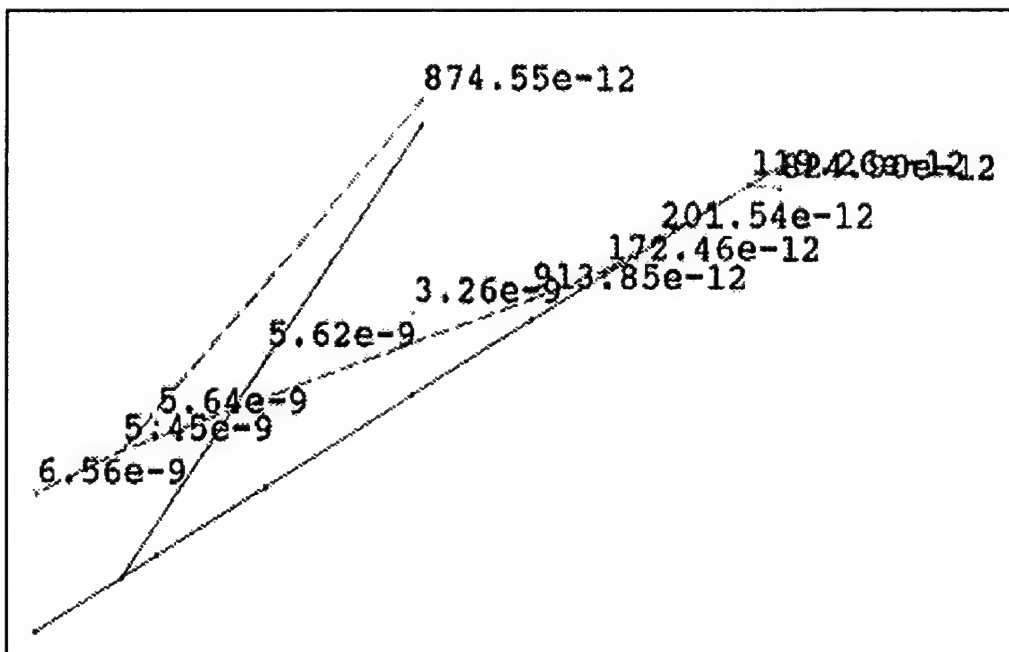


Figure G-5. Configuration 3, Second Z-Mode: 44.69 Hz.

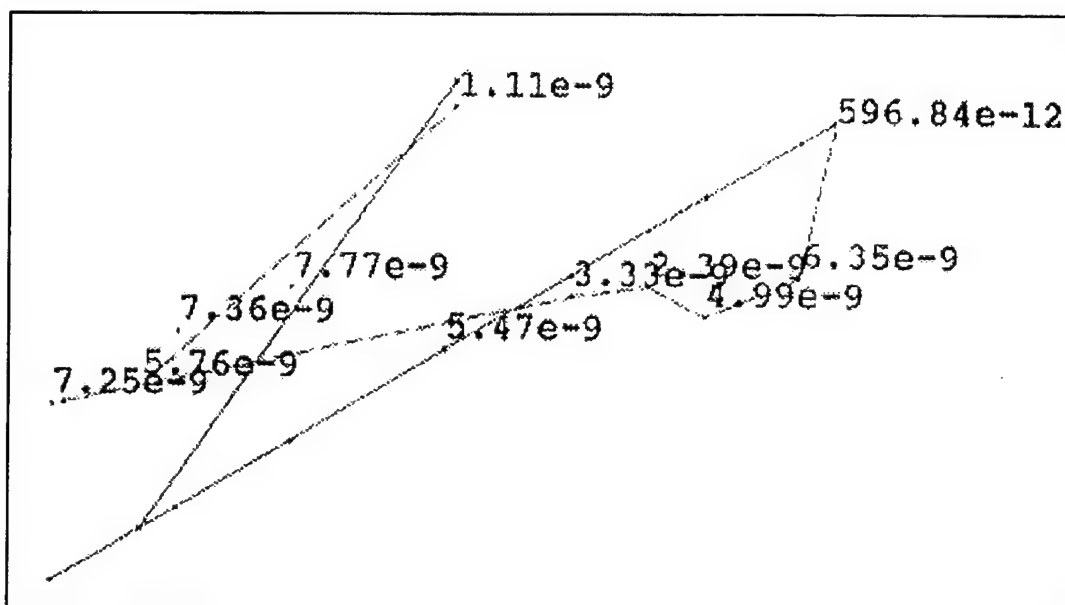


Figure G-6. Configuration 3, Third Z-Mode: 76.87 Hz.

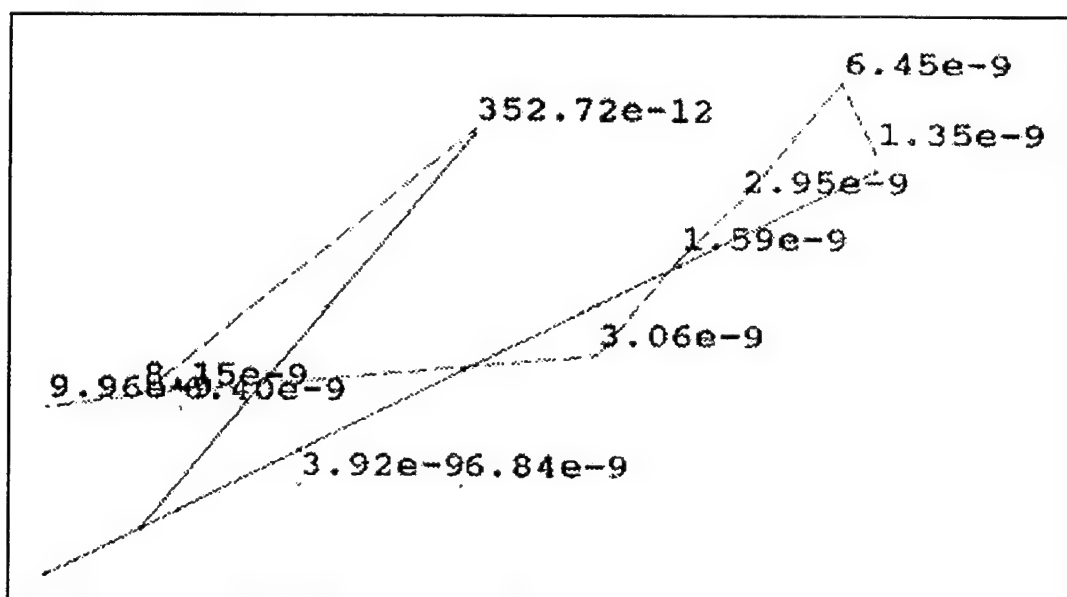


Figure G-7. Configuration 3, Fourth Z-Mode: 101.36 Hz.

Mode	Accelerometer Location	Relative Amplitude	Relative Phase Angle
1	1	3.85e-9	-27.19
	2	2.85e-9	-24.16
	3	1.27e-9	54.24
	4	0.867e-9	64.32
	5	0.365e-9	171.55
	6	1.29e-9	82.37
	7	2.11e-9	87.94
	8	5.05e-9	121.08
	9	4.13e-9	137.81
	10	4.86e-9	168.29
	11	11.32e-9	117.85
2	1	0.824e-9	-176.19
	2	0.119e-9	-104.44
	3	0.201e-9	-66.00
	4	0.172e-9	-47.83
	5	0.913e-9	19.89
	6	0.874e-9	-19.70
	7	3.26e-9	13.98
	8	5.62e-9	16.32
	9	5.64e-9	16.95
	10	5.45e-9	17.05
	11	6.56e-9	24.69
3	1	0.596e-9	-168.62
	2	6.35e-9	-148.34

Table G-1. Amplitudes and phases computed by STARModal for configuration 3, Z-direction.

Mode	Accelerometer Location	Relative Amplitude	Relative Phase Angle
	3	4.99e-9	-129.52
	4	2.39e-9	-104.79
	5	3.33e-9	-41.22
	6	1.11e-9	-97.10
	7	5.47e-9	-22.89
	8	7.77e-9	24.89
	9	7.36e-9	46.13
	10	5.76e-9	67.19
	11	7.25e-9	69.94
4	1	1.35e-9	70.93
	2	6.45e-9	48.75
	3	2.95e-9	78.66
	4	1.59e-9	111.14
	5	3.06e-9	-164.88
	6	0.352e-9	8.22
	7	6.84e-9	-140.50
	8	3.92e-9	-89.21
	9	6.40e-9	9.04
	10	8.15e-9	19.03
	11	9.96e-9	24.86

Table G-1 (cont.).

APPENDIX H. BRUEL AND KJAER TYPE 8001 IMPEDANCE HEAD CALIBRATION CHART

Calibration sheet for the B&K Type 8001 impedance head used to measure the force to
the driving force.

Brüel & Kjær

Reference Sensitivity at 159.2 Hz at 23 °C and including

Accelerometer:

.....	pC/ms ⁻² or	pC/g.....
2,25.....	319.....	319.....

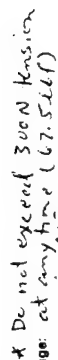
..... 3.08 $\text{mV} \cdot \text{ms}^{-2}$ or 39.2 mV/g .

Maximum Transverse Sensitivity at 30Hz	%
1.8	

Polarity is negative on the center of the accelerometer connector for an acceleration directed from the mounting surface into the body of the impedance head.

$$\bullet \quad 1g \approx 9.807 \text{ ms}^{-2}$$

AC 0058-12



Voltage Sensitivity	3.94	mV/N
---------------------	------	------

Base Strain Sensitivity

Stiffness below Accelerometer: 25×10^7 N

Max. Screw-Down Torque: 0.5 Nm

Physical:
Hazardous surface

10 mm
Material: Titanium & Stainless Steel

Electrical Connector:
Miniature coaxial

Environmental:

Max. Temperature: 260°C or 500°F
Magnetic Sensitivity (50 Hz): < 20 mV/T

Resistance min. 20 000 m Ω at room temperature

1

APPENDIX I. PCB J353B04 ACCELEROMETER CALIBRATION CERTIFICATE

Calibration sheet for the PCB model no. J353B04 series quartz shear mode accelerometer used to measure gun assembly response to sinusoidal excitation. The use of shear mode quartz sensors reduces sensitivity to environmental effects that might bias the results.

Calibration Certificate

Baker Special

Per ISA-RP37.2

Model No. **J353B04**

Serial No. **11850**

PO No. _____ Customer _____

Calibration traceable to NIST thru Project No. **822/253168**

ICP® ACCELEROMETER

with built-in electronics

Calibration procedure is in compliance with MIL-STD-45662A and traceable to NIST.

CALIBRATION DATA

Voltage Sensitivity **9.63** mV/g
 Transverse Sensitivity **1.4** %
 Resonant Frequency **51.5** kHz
 Time Constant **0.8** s
 Output Bias Level **8.6** V

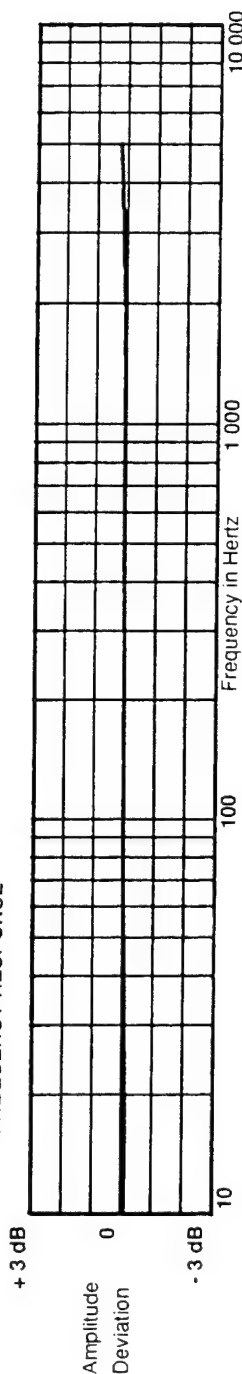
KEY SPECIFICATIONS

Range **500** ± g
 Resolution **0.01** g
 Temp. Range **-65/+250** °F
 METRIC CONVERSIONS:
 ms² = 0.102 g
 °C = 5/9 x (°F - 32)

Reference Freq.

Frequency	Hz	10	15	30	50	100	300	500	1000	3000	5000	
Amplitude Deviation	%	-0.9	-1.1	-1.7	-3.3	0.0	.4	.6	.6	1.5	2.8	

FREQUENCY RESPONSE



PCB

Piezotronics, Inc. 3425 Walden Avenue Depew, NY 14043-2495 USA

716-684-0001

Calibrated by *J. Chadwick*

Date **5/20/94**

CODE CC ENG

APPENDIX J. LIST OF ELEMENTS, MATERIAL AND REAL CONSTANTS FOR M61A1 ANSYS FINITE ELEMENT MODEL

The following page lists the element types, material constants and original real constants used in the finite-element simulation program for the PHALANX gun as created by Michael Hatch in 1993. Note that real constants 5, 13, and 14 are the spring stiffness values discussed in Chapters III and V. See Reference 11 for further details.

GUN MODEL

GUNNMU10 - UPDATED BEARINGS/GEAR UX,UY COUPLING

ET,1,45	3-D SOLID
ET,2,63	SHELL
ET,3,14	SPRING
ET,4,4	BEAM
ET,5,21	MASS
ET,6,16	STRAIGHT PIPE (OD,TKWALL)

MATERIAL 1, STEEL

EX,1,30E6	DENS,1,.000733	NUXY,1,.293
-----------	----------------	-------------

MATERIAL 2, STEEL, MASSLESS FOR FILLING HOLES

EX,2,30E6	DENS,2,0.1E-9	NUXY,1,.293
-----------	---------------	-------------

MATERIAL 3, ALUMINUM

EX,3,10E6	DENS,3,.000259	NUXY,3,.345
-----------	----------------	-------------

R,1,.200	GUN BODY SHELL ELEMENTS
R,2,	GUN BACK SOLID ELEMENTS
R,3,	GUN BEARING OUTER RACES
R,4,	ROTOR SOLID ELEMENTS
R,5,856607	BALL STIFFNESSES, SINGLE ROW OF 18 BALLS
R,6,	INNER RINGS
R,7,	
R,8,	STUB ROTOR SOLID ELEMENTS
R,9,.093	STUB ROTOR SHELLS
R,10,	MID BARREL SOLID
R,11,	MUZZLE CLAMP SOLID
R,12,.093	MUZZLE CLAMP SHELLS
R,13,1.22E6	REAR NEEDLE BEARING, 1 SET AT 120 DEGREES, K = 1.83E6 LB/IN
R,14,442500	BALL JOINT AT REAR, 4 SPRINGS, K = 885000LB/IN
R,15,3222	RECOIL SPRING, EACH SIDE WITH K = 3222 (FROM AVERAGE CURVE STIFFNESS)
R,16,	MASSLESS STUB ROTOR HOLE ELEMENTS
R,17,	MASSLESS MID HOLE ELEMENTS
R,18,2.0,0.6	BARREL END CONSTRAINT PIPE ELEMENTS
R,19,2.0,0.6	BARREL
R,20,1.570,.384	BARREL
R,21,1.220,.209	BARREL
R,22,1.360,.279	BARREL
R,23,1.050,.125	BARREL
R,24,	MUZZLE SUPPORT INNER RING (RACE)
R,25,	MUZZLE OUTER RING/STRUT CONNECTIONS
R,26,	
R,27,	MUZZLE SUPPORT UPPER
R,28,1.25,.125	MUZZLE SUPPORT ARMS (PIPE ELEMENTS)
R,29,	WEBS IN MUZZLE SUPPORT UPPER
R,30,266666	MUZZLE SUPPORT VERTICAL BALL STIFFNESS
R,31,466667	MUZZLE SUPPORT LATERAL BALL STIFFNESSES

APPENDIX K. ANSYS HARMONIC RESPONSE TRANSFER FUNCTION PLOTS FOR Y AND Z DIRECTIONS

The following plots show the transfer functions (displacement versus frequency) for five individual points in both the Y-(horizontal) and Z-(vertical) directions for the unrestrained gun model. These points are in close proximity to the same points used in the experiments. In each case, a one pound force was "applied" at node 5443 ("BRLTIP") in the same direction as the plotted displacement. Figure K-1 shows an isometric view of the gun barrel assembly as seen in ANSYS, showing the location of each point.

Figures K-2 through K-11 show the harmonic responses for each point shown in Figure K-1.

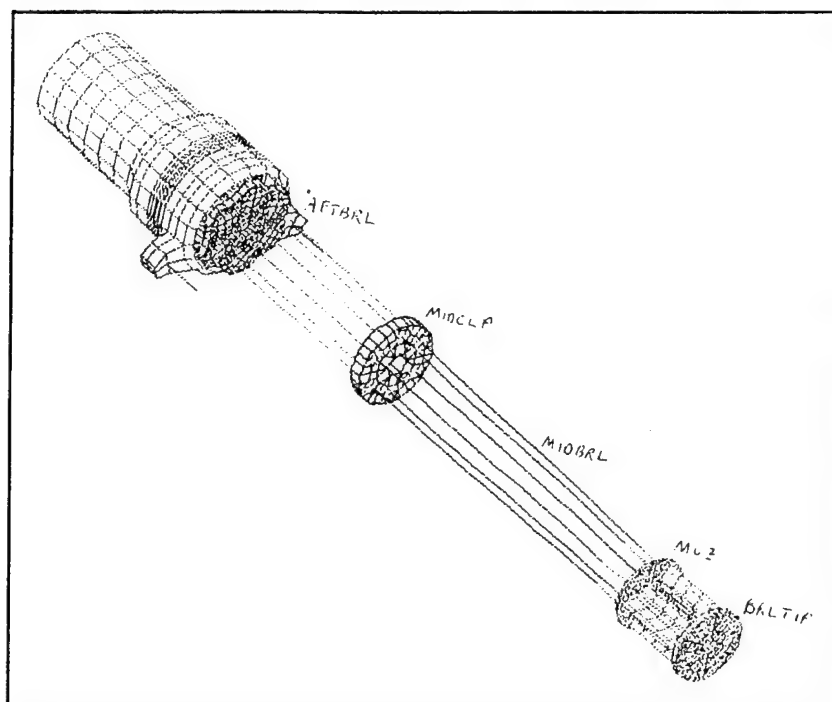


Figure K-1. FEM Measurement Points.

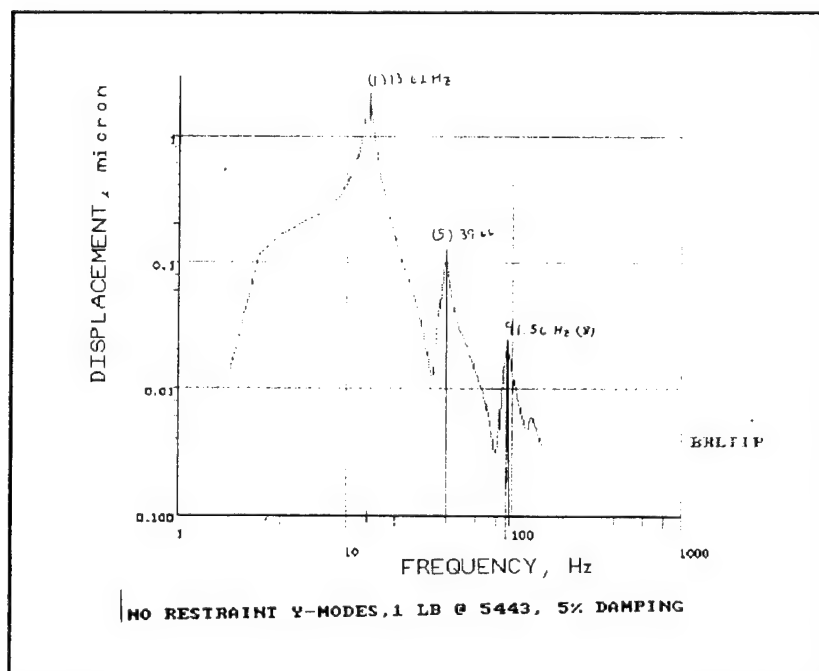


Figure K-2. Y, Barrel-Tip Response.

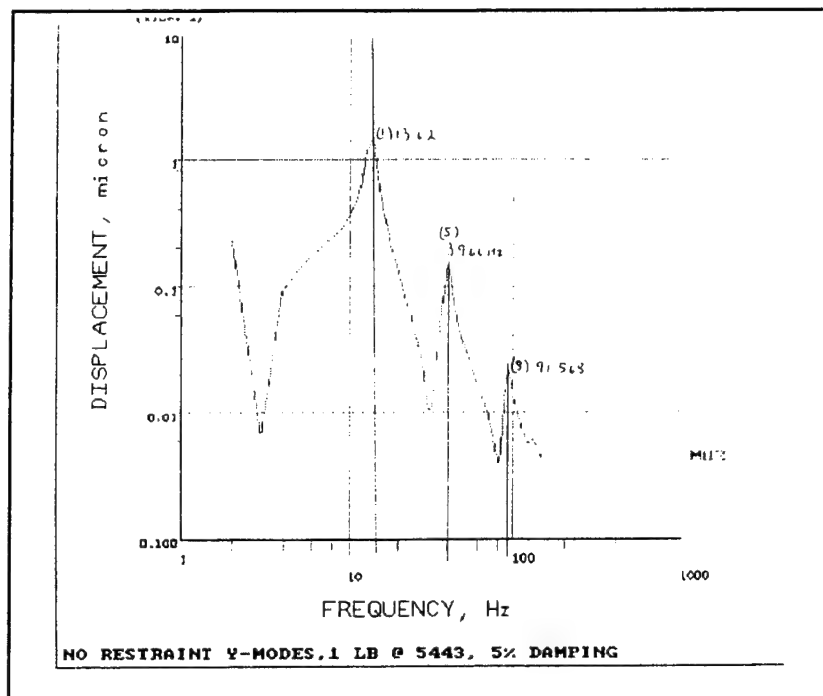


Figure K-3. Y, Rear-of-Muzzle Clamp Response.

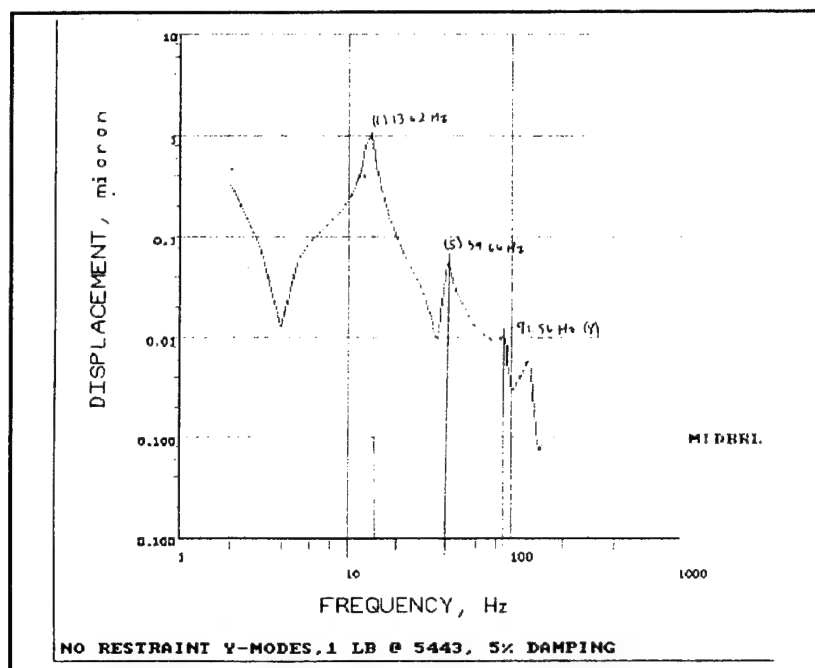


Figure K-4. Y, Mid-Barrel Response.

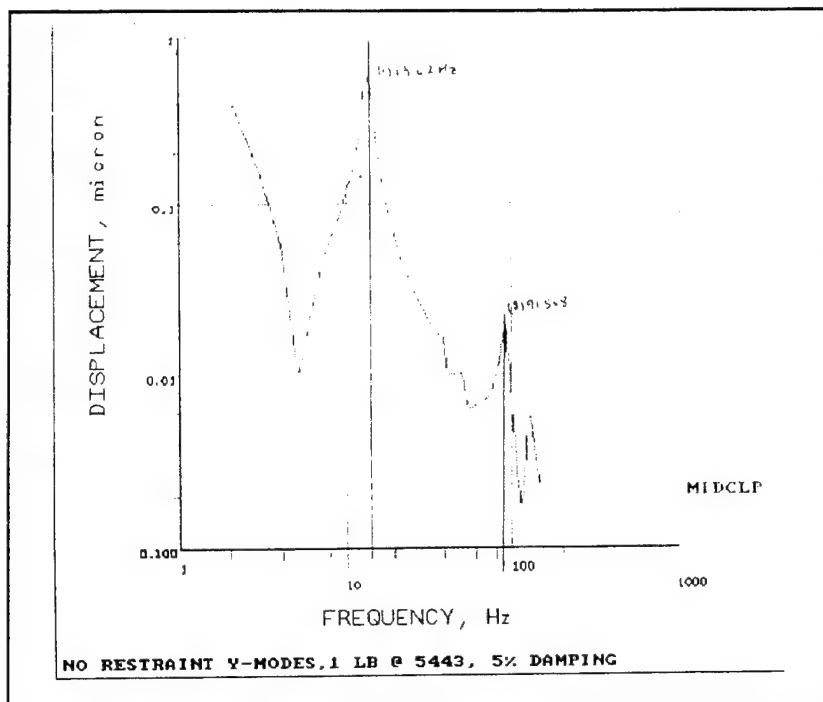


Figure K-5. Z, Barrel-Tip Response.

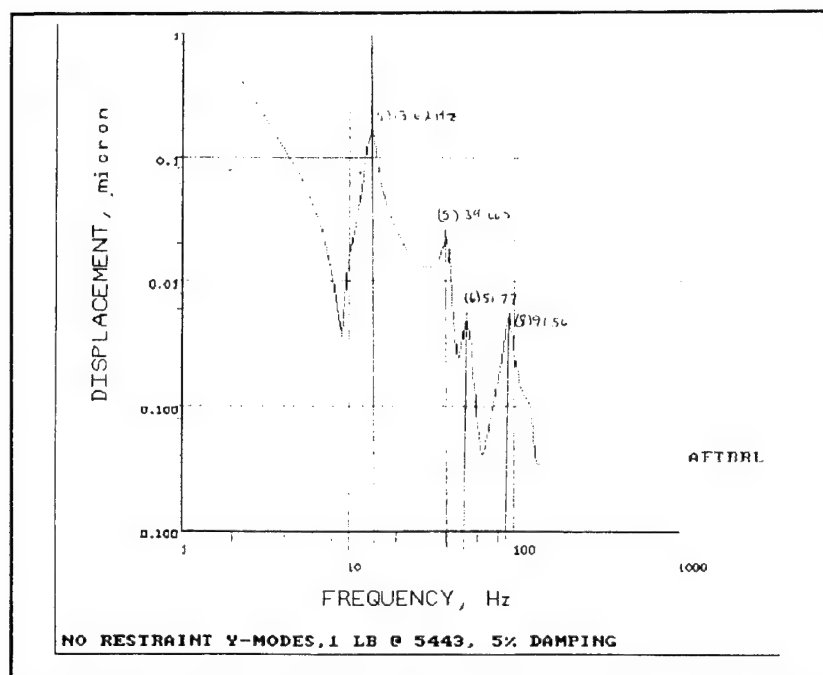


Figure K-6. Z, Rear-of-Muzzle Clamp Response.

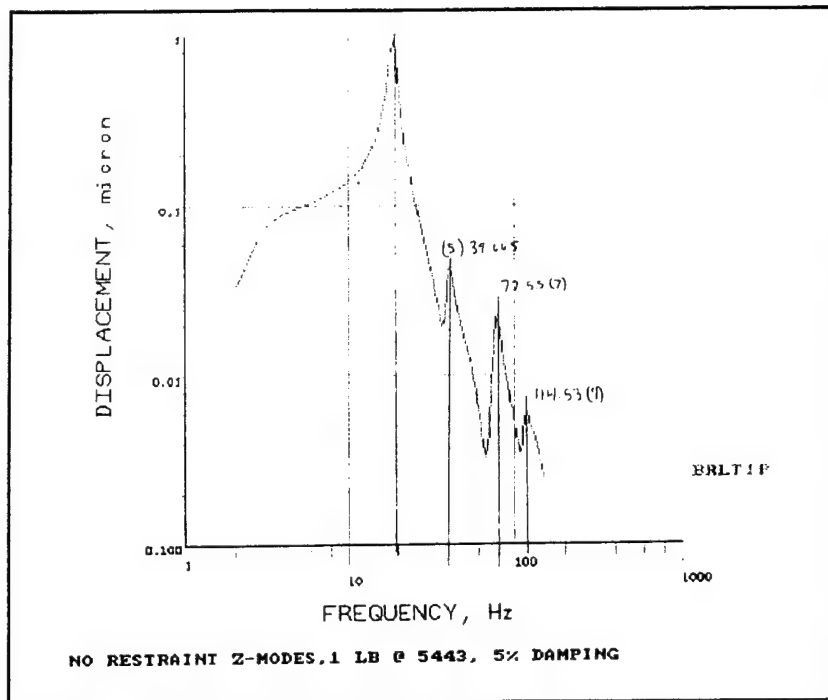


Figure K-7. Z, Barrel-Tip Response.

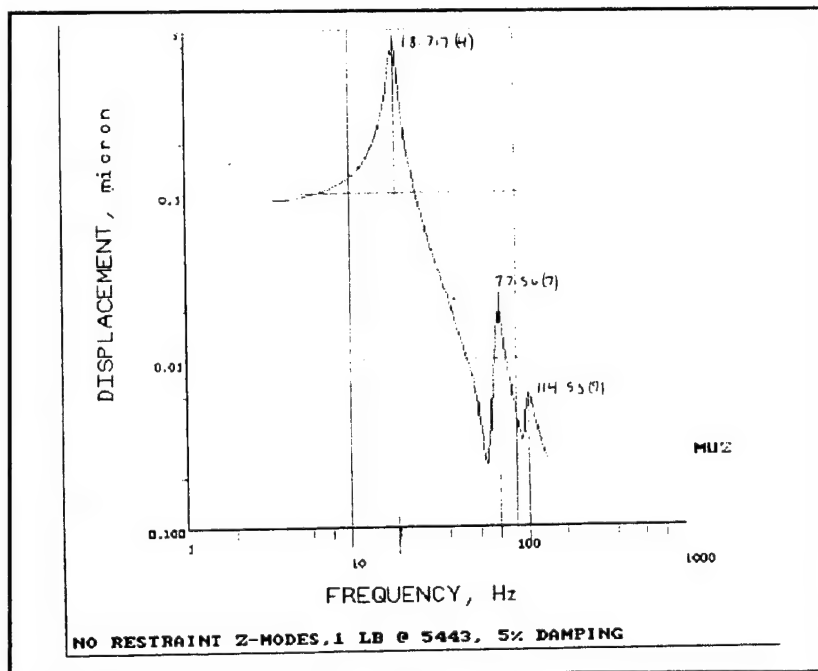


Figure K-8. Z, Rear-of-Muzzle Clamp Response.

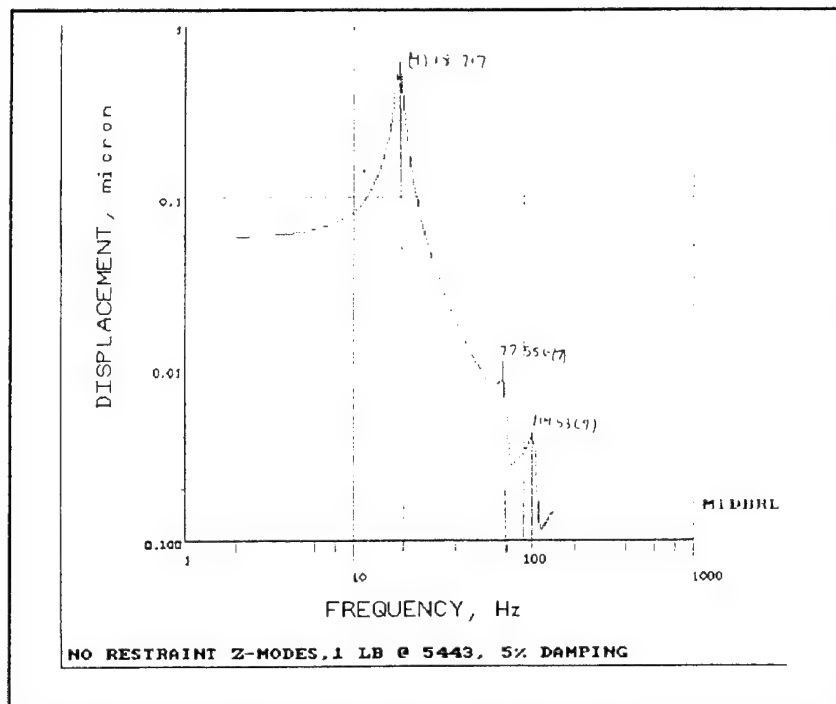


Figure K-9. Z, Mid-Barrel Response.

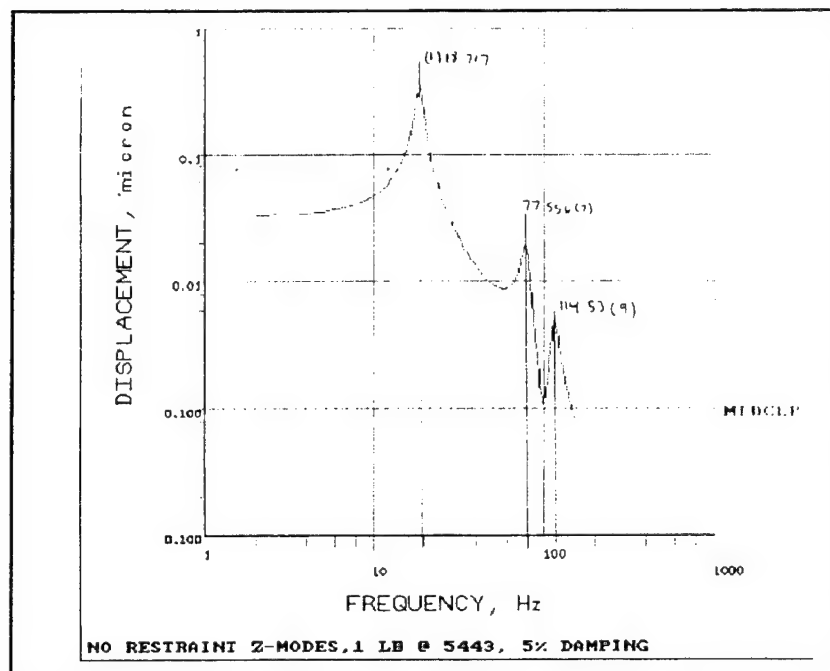


Figure K-10. Z, Mid-Barrel Clamp Response.

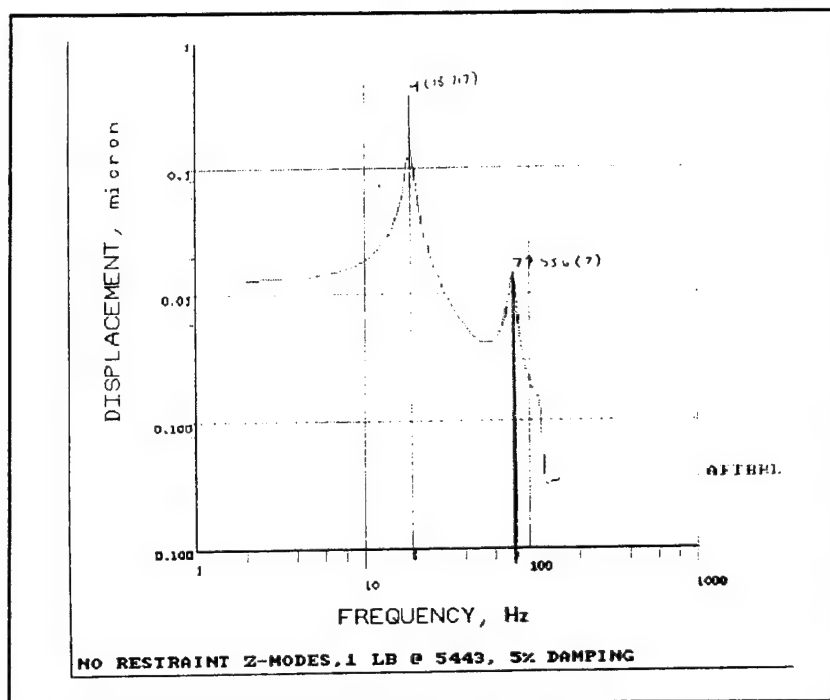


Figure K-11. Z, Rear-of-Barrel Response.

LIST OF REFERENCES

1. Naval Sea Systems Command, *Close-In Weapon System Mk 15 MODS 1 Thru 4 and 6 (PHALANX): Introduction to CIWS*, Naval Sea Systems Command, 1987.
2. Peterschmidt, John C., *Normal Modes of Vibration of the Phalanx Gun*, Naval Postgraduate School Master's Degree Thesis, Monterey, CA, June 1993.
3. Inman, Daniel J., *Engineering Vibrations*, Prentice Hall, 1994.
4. Dossing, Ole, *Structural Testing* (Parts 1 and 2), Bruel and Kjaer, 1988.
5. Hansberry, Robert J., *Modal Analysis of the PHALANX M61A1 Close-in Weapons System*, Naval Postgraduate School Master's Degree Thesis, Monterey, CA, December 1994.
6. APS Dynamics (Acoustic Power Systems), Carlsbad, California, (619) 438-4848.
7. Bruel and Kjaer, Anaheim, California, (714) 978-8066.
8. ENDEVCO, San Juan Capistrano, California, (714) 493-8181.
9. Hewlett-Packard, Palo Alto, California, (415) 968-9200.
10. PCB Piezotronics Inc., Depew, New York, (716) 684-0001.
11. Structural Dynamics Research Corporation, *Model Solution and I-DEAS User's Guide*, Structural Measurement Research Corporation, 1990.
12. ANSYS Incorporated, *Commands Vol II (Rev 5.0)*, ANSYS INC., 1995, (412) 746-3304.
13. AUTODESK, *AUTOCAD Release 12 User's Manual*, AUTODESK, 1995, (800) 225-1301.
14. Borland International Corporation, *BRIEF for DOS and OS2*, Borland International Corp, 1992, (408) 438-5300.
15. Naval Surface Warfare Center, *Installation of MK15 CIWS Muzzle Restraint (ORDALT 166196)*, Naval Surface Warfare Center, 1993.

16. Structural Measurement Systems, *STAR Reference Manual*, Structural Measurement Systems, 1990.
17. ANSYS Incorporated, *Commands Vol II (Rev 4.4a.)*, ANSYS INC., 1995, (412) 746-3304.

INITIAL DISTRIBUTION LIST

- | | |
|--|---|
| 1. Defense Technical Information Center
8725 John J. Kingman Rd., STE 0944
Ft. Belvoir, Virginia 22060-6218 | 2 |
| 2. Library, Code 13
Naval Postgraduate School
Monterey, California 93943-5101 | 2 |
| 3. Professor William B. Colson Code PH/Cw
Chairman, Department of Physics
Naval Postgraduate School
Monterey, California 93943-5000 | 2 |
| 4. Professor Steven R. Baker Code PH/Ba
Department of Physics
Naval Postgraduate School
Monterey, California 93943-5000 | 2 |
| 5. Yuji Wilson
Port Hueneme Division
Naval Surface Warfare Center
Code 4121
Port Hueneme, California 93043 | 1 |
| 6. Mike Hatch
2163 Woodleaf Way
Mountain View, California 94040 | 1 |
| 7. LT Carlos S. Guzman
Condominio Playa Dorada, TH-9
Carolina, Puerto Rico 00979 | 2 |
| 8. LT John Gaffe
Rt. 3, Box 407 Magnolia Terrace
Buena Vista, Georgia 31803 | 2 |

9. LCDR Stuart Borland
PHALANX Program Office, Code G30
Naval Surface Warfare Center
Dahlgren Division
Dahlgren, Virginia 22448-5000

1